MODELLING AND CONTROL OF MAGNETORHEOLOGICAL DAMPERS FOR VEHICLE SUSPENSION SYSTEMS

A thesis submitted to the University of Manchester for the degree of

Doctor of Philosophy

in the Faculty of Engineering and Physical Sciences

2010

HASSAN AHMED METERED

SCHOOL OF MECHANICAL, AEROSPACE AND CIVIL ENGINEERING

Contents

List of Figures

List of Tables

THE UNIVERSITY OF MANCHESTER
FACULTY OF ENGINEERING AND PHYSICAL SCIENCE
SCHOOL OF MECHANICAL, AEROSPACE AND CIVIL ENGINEERING

ABSTRACT

Doctor of Philosophy

MODELLING AND CONTROL OF MAGNETORHEOLOGICAL DAMPERS FOR VEHICLE SUSPENSION SYSTEMS

Hassan Ahmed Ahmed Mohamed Metered

21 July 2010

Magnetorheological (MR) dampers are adaptive devices whose properties can be adjusted through the application of a controlled voltage signal. A semi-active suspension system incorporating MR dampers combines the advantages of both active and passive suspensions. For this reason, there has been a continuous effort to develop control algorithms for MR-damped vehicle suspension systems to meet the requirements of the automotive industry. The overall aims of this thesis are twofold:

- The investigation of non-parametric techniques for the identification of the nonlinear dynamics of an MR damper.
- The implementation of these techniques in the investigation of MR damper control of a vehicle suspension system that makes minimal use of sensors, thereby reducing the implementation cost and increasing system reliability.

The novel contributions of this thesis can be listed as follows:

1- Nonparametric identification modelling of an MR damper using Chebyshev polynomials to identify the damping force from both simulated and experimental data.
2- The neural network identification of both the direct and inverse dynamics of an MR damper through an experimental procedure.
3- The experimental evaluation of a neural network MR damper controller relative to previously proposed controllers.
4- The application of the neural-based damper controller trained through experimental data to a semi-active vehicle suspension system.
5- The development and evaluation of an improved control strategy for a semi-active car seat suspension system using an MR damper.

Simulated and experimental validation data tests show that Chebyshev polynomials can be used to identify the damper force as an approximate function of the displacement, velocity and input voltage. Feed-forward and recurrent neural networks are used to model both the direct and inverse dynamics of MR dampers. It is shown that these neural networks are superior to Chebyshev polynomials and can reliably represent both the direct and inverse dynamic behaviours of MR dampers. The neural network models are shown to be reasonably robust against significant temperature variation. Experimental tests show that an MR damper controller based a recurrent neural network (RNN) model of its inverse dynamics is superior to conventional controllers in achieving a desired damping force, apart from being more cost-effective. This is confirmed by introducing such a controller into a semi-active suspension, in conjunction with an overall system controller based on the sliding mode control algorithm. Control performance criteria are evaluated in the time and frequency domains in order to quantify the suspension effectiveness under bump and random road excitations. A study using the modified Bouc-Wen model for the MR damper, and another study using an actual damper fitted in a hardware-in-the-loop-simulation (HILS), both show that the inverse RNN damper controller potentially gives significantly superior ride comfort and vehicle stability. It is also shown that a similar control strategy is highly effective when used for a semi-active car seat suspension system incorporating an MR damper.

Declaration

No portion of the work referred to in this thesis has been submitted in support of an application for another degree or qualification of this or any other university or other institution of learning.

Copyright

Acknowledgement

I would like to express my sincere gratitude to my supervisor Dr. Philip Bonello for his supervision, guidance, valuable advice, innovative ideas, encouragement, support, endurance, enthusiasm, and dedication throughout this thesis. Also, I would like to express great thanks to Dr. S. O. Oyadiji for his support, helpful advice, valuable discussion and encouragement throughout this work.

I am grateful to thank all the university members for their kindness and continuous support. I owe special thanks to the technician staff for manufacturing the experimental test equipment.

I thank Mr. Bob Brown, electronics technician, for his help and advice in matters relating to electronics and electrical equipment. I am also grateful to Mr. David Mortimer, technical team leader, for his support and assistance during the experimental work.

I would like to extend my special thanks to my wife, T. Hassan, and my children, Ahmed and Judy, for their patience, love and undying support throughout this thesis. This thesis is dedicated to them.

Finally, I wish to acknowledge my parents and family members for their blessing, love, support and belief in me during my life.

CHAPTER 1

Introduction

Magnetorheological (MR) dampers are adaptive or "smart" devices that have been the subject of intensive research into various dynamics applications within civil and automotive engineering. This thesis concerns the modelling and control of an MR damper for use in a vehicle suspension in order to improve ride comfort and vehicle stability. This chapter presents the reader with an introduction to the research conducted in this thesis. A brief background of vehicle suspension system requirements is presented. The aims, objectives and contributions to knowledge of this thesis are then introduced, followed by a summary of the thesis organisation.

1.1 Background

MR fluid dampers are adaptive control devices that have received considerable interest due to their mechanical simplicity, high dynamic range, low power requirements, large force capacity, and robustness. MR fluids respond to an applied

magnetic field with a significant change in rheological behavior. These fluids can reversibly and instantaneously change from a free-flowing liquid to a semi-solid with controllable yield strength when exposed to a magnetic field [1]. MR dampers have been applied over a wide range of vibration control applications: from automobiles [2, 3] to railway vehicles [4] and civil structures such as buildings [5, 6]. This thesis focuses on the application of MR dampers to automobile suspensions.

The design of a better quality suspension system remains an important development goal for vehicle manufacturers. An ideal vehicle suspension system should have the capability to reduce the displacement and acceleration of the vehicle body, maximising ride comfort. It should also aim to minimise the dynamic deflection of the tyre to maintain tyre-terrain contact. Ride comfort and vehicle stability are two conflicting requirements which the suspension's vibration control strategy has to satisfy [7]. A vehicle suspension system basically consists of springs and dampers. The basic function of the spring is to support the static weight of the vehicle body and moderately isolate it from the wheels [8]. Spring selection is based on the weight and ride height of the vehicle. The damper is used to dissipate energy transmitted to the vehicle body from the wheels due to the road profile disturbance [8]. In passive suspension systems, the two elements are fixed at the design stage. The damper selection is affected by the typical trade-off between vehicle stability and ride comfort [7]. A low suspension damping force (soft damper) gives good ride comfort, while a high suspension damping force (hard damper) provides good stability (also referred to as vehicle handling/road holding) [7].

The performance limitations inherent in a passive suspension are overcome through the use of active or semi-active control. Such suspensions have control systems which force them to achieve optimised conditions e.g. by following the dynamic response of some ideal reference system. Active suspensions use active devices (electro-hydraulic actuators) which can be commanded directly to give a desired control force. A semi-active suspension uses dampers that are termed "semi-active" since their force is commanded indirectly through a controlled change in the dampers' properties. This change is effected by a damper controller that receives information from the overall system controller (that in turn estimates the desired damping force).

An MR damper is a semi-active device and a suspension system incorporating such dampers combines the advantages of both active and passive suspensions. It can be nearly as efficient as a fully active suspension in improving ride comfort and is much more economical [9, 10]. It is also safer since, if the control system fails, the semi-active suspension can still work as a passive suspension system. Moreover, most vehicles have the facility to provide the voltage (or current) that is required to generate a continuously controllable variable damping force. Hence, the effective stiffness and damping of the entire suspension system can be continuously adjusted by electronic controls to provide optimum ride comfort and vehicle stability. Semi-active suspension systems using MR dampers have been shown to offer a compromise solution for the conflicting requirements of ride comfort and vehicle stability [11-13]. For all these reasons, there has been a continuous effort to develop control algorithms for MR-damped vehicle suspension systems to meet the requirements of the automotive industry. Such analysis is complicated by the fact

that the MR damper is a nonlinear and hysteretic device [14], as will be discussed in following chapter.

1.2 Aims and Objectives of this thesis

The overall aims of this thesis are twofold:

- The investigation of non-parametric techniques for the identification of the nonlinear dynamics of an MR damper.
- The implementation of these techniques in the investigation of MR damper control of a vehicle suspension system. The investigation is aimed at improving ride comfort and vehicle stability with minimal reliance on the use of sensors, thereby reducing the implementation cost and increasing system reliability.

The identification techniques consider both the "direct" and "inverse" models of the dynamics of the damper. The direct (or "forward") model identifies the damper force for given voltage and damper displacement inputs. The "inverse" damper model identifies the voltage required for given displacement and desired damper force inputs.

To achieve these aims, a series of objectives are specified as follows:

1- To investigate the use of Chebyshev polynomials for the identification of the dynamical behaviour of an MR damper.

2- The neural network identification of both direct and inverse dynamics of an MR damper through an experimental procedure.

3- The experimental evaluation of a neural network MR damper controller relative to the alternative controllers available from the literature.

4- The application of the neural-based damper controller to a semi-active vehicle suspension system.
5- The development and evaluation of an improved control strategy for a semi-active car seat suspension system using an MR damper.

1.3 Contributions to Knowledge

The studies reported in this thesis are intended to provide a deeper insight into the behaviour of MR dampers and their potential application in a vehicle suspension system. The outcomes of this study are expected to accelerate the implementation of these dampers in vehicle suspension systems. The novel contributions of this thesis can be listed as follows:

1- A three dimensional interpolation using Chebyshev orthogonal polynomial functions is applied for studying the dynamical behaviour of an MR damper. The identification and its validation are done with both simulated and experimental data. In the former case the identification and validation data are generated by solving the modified Bouc-Wen model. In the experimental approach, the data are generated through dynamic tests with the damper placed in a tensile testing machine. In either case, validation tests representing a wide range of working conditions of the damper show that the damper force can be approximately identified as a function of the displacement, velocity and input voltage. This explicit functional representation allows a rapid means of reliably estimating the damping force for any desired combination of voltage, amplitude, and frequency of the excitation.

2- Feed-forward and recurrent neural networks are used to model both the direct and inverse dynamics of MR dampers. Training and validation of the proposed neural networks are achieved by using data generated through dynamic tests with the damper mounted in a tensile testing machine. Results show that neural networks are superior to Chebyshev polynomials for modelling the MR damper and are capable of reliably representing both its direct and inverse dynamic behaviours. The effect of the damper's surface temperature on both the direct and inverse dynamics of the damper is investigated, and the neural network models are shown to be reasonably robust against significant temperature variation.

3- The inverse recurrent neural network (RNN) model is introduced as a damper controller and experimentally evaluated against another controllers proposed in the literature. By testing the ability to achieve a given desired damper force signal, it is revealed that the proposed neural-based damper controller offers superior damper control. It also gives the most cost-effective vibration control solution among the controllers investigated.

4- The neural-based MR damper controller is applied in tandem with an overall system controller based on a sliding mode control algorithm within a semi-active vehicle suspension. Control performance criteria are evaluated in the time and frequency domains in order to quantify the suspension effectiveness under bump and random road excitations using the proposed control strategy. Studies using the modified Bouc-Wen model for the MR damper, as well as an actual damper fitted in a hardware-in-the-loop simulation (HILS), both

show that the inverse RNN damper controller offers significantly superior ride comfort and vehicle stability relative to a conventional MR damper controller based on continuous state control. The proposed control strategy indicates that the neural-based damper controller can offer a solution to the conflicting requirements of ride comfort and vehicle stability. Moreover, unlike conventional damper controllers, the inverse RNN controller does not require damper force sensors, thereby reducing the implementation cost and increasing system reliability.

5- Further studies performed using an RNN model of the direct (forward) dynamics of the MR damper show that it is a reliable substitute for HILS for validating multi-damper suspension systems.

6- The above described semi-active control strategy for the vehicle suspension is extended to a semi-active MR-damped car seat suspension. The proposed semi-active seat suspension is compared to a passive seat suspension for prescribed base displacements. Control performance criteria are assessed under different operating conditions, in order to quantify the effectiveness of the proposed semi-active control system. The simulated results show that the use of semi-active control in the seat suspension provides a significant improvement in ride comfort.

1.4 Thesis Organisation

This thesis is not presented in the classical format of a PhD thesis. Rather, it is presented in the *alternative format* with its core context provided in the form of

published/submitted research papers. It should be noted however that, as in the classical format, the alternative format requires that all references at the end of each paper be collected together and grouped in the 'References' Chapter at the end of the thesis.

Chapter 2 gives a comprehensive critical literature review summarising the previous published work in the core areas relevant to this thesis. The first part of this chapter provides brief fundamentals of MR fluids and MR dampers. This is then followed by discussion of parametric and nonparametric modelling techniques for MR dampers. A concise review of MR dampers' controllers is then presented. Finally, previous research related to the semi-active vibration control of vehicle and car seat suspension systems using MR dampers is reviewed.

Chapter 3 contains a summary of the papers included in this thesis, explaining the purpose and contributions of each paper. The following four chapters, Chapter 4 to Chapter 7, are respectively constituted of four published or submitted papers that report the candidate's own work. In Chapter 4, a new approach for studying the dynamical behaviour of an MR damper is introduced. It consists of a three dimensional interpolation using Chebyshev orthogonal polynomial functions to identify the damping force as a function of the displacement, velocity and input voltage. Chapter 5 concerns the experimental identification of the dynamic behaviour of an MR damper using neural networks. Also, the inverse recurrent neural network model is introduced as a damper controller and experimentally evaluated against alternative controllers proposed in the literature. Chapter 6 is an investigation into the use of neural networks for the semi-active control of an MR-

damped vehicle suspension system. Chapter 7 presents a semi-active control strategy for an MR damper used in a car seat suspension.

In chapter 8, conclusions are drawn summarising all salient outcomes and the advantages of the proposed control strategy of this study. Also, recommendations for future work in this research area are listed at the end of chapter 8.

CHAPTER 2

Literature Review

The purpose of this chapter is to present a comprehensive literature review summarising the previous published work relevant to the research aims and objectives introduced in Chapter 1. It starts by giving a short background on the behaviour of magnetorheological (MR) fluids and the design of MR dampers. This is then followed by a review of parametric and nonparametric modelling techniques used to study their dynamical response. Finally, previous research relating to the semi-active vibration control of vehicle and car seat suspension systems using MR dampers is reviewed, focusing on both system and damper controllers.

2.1 Magnetorheological (MR) Fluids

Controllable fluid dampers generally utilise either electrorheological (ER) fluids or MR fluids, whose viscosity properties can be altered dramatically by applying an electric field (ER) or a magnetic field (MR). These fluids were first discovered by

the inventor Willis Winslow, who achieved a US patent regarding these fluids in 1947 [15] and published a scientific article in 1949 [16]. The yield stress of these fluids can be controlled very precisely by changing the field intensity to generate a continuously variable damping force. These fluids have found several successful applications in field of vibration control. This thesis is focussed on MR fluid dampers, which are considered more suitable than ER fluid dampers for automotive applications for the reasons given below.

An MR fluid consists of micro-sized magnetically polarisable particles, such as iron particles, suspended in a carrier liquid such as mineral oil, synthetic oil, water or glycol. A typical MR fluid will contain 20 to 40 percent by volume of relatively pure iron particles around 3 to 10 micron diameter in size. A variety of proprietary additives, similar to those found in commercial lubricants, is commonly added. These additives are intended to discourage gravitational settling and promote particle suspension, and enhance lubricity, modify the viscosity and inhibit wear. MR fluids respond to a magnetic field with a dramatic change in rheological behaviour. Moreover, MR fluids can reversibly and instantaneously change from a free-flowing liquid to a semi-solid within a few milliseconds with controllable yield strength when subjected to a magnetic field [17]. In the absence of an applied field, an MR fluid is reasonably well approximated as a Newtonian liquid – it is free flowing with a consistency similar to motor oil. In this condition, the ferrous particles are in an amorphous state as shown in Fig. 2.1(a). When a magnetic field is applied, the ferrous particles begin to align along the flux path, as shown in Fig. 2.1(b), eventually forming particle chains in the fluid, as shown in Fig. 2.1(c). Such chains resist and restrict fluid movement. As a result, a yield stress develops in the fluid.

The degree of change is related to the strength of the applied magnetic field and it has been shown that this change can occur in less than 1 millisecond [18].

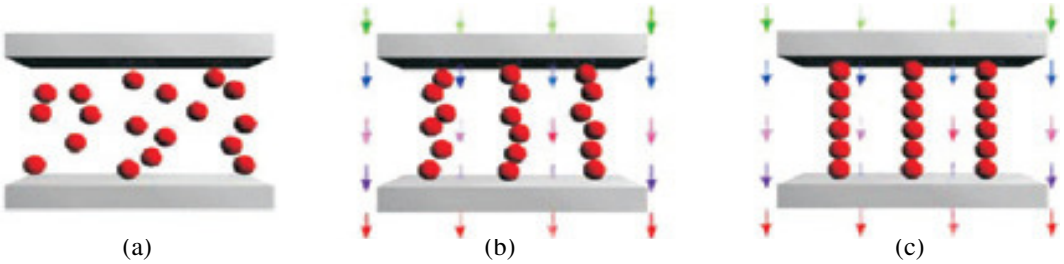

(a) (b) (c)

Fig. 2.1 Activation of MR fluid [18]
(a) No magnetic field applied (b) Magnetic field applied (c) Chains have formed

The controllable yield stress is exploited by MR fluid devices, whose mode of operation is classified according to the way their MR fluid is made to flow. These devices are classified as operating in one of three basic modes, or a combination of these modes: (a) valve mode; (b) direct shear mode; (c) squeeze mode. Diagrams of these basic modes of operation are shown in Fig. 2.2. Examples of valve mode devices include servo-valves, dampers and actuators. Shear mode devices include clutches, brakes, dampers and structural composites. While less well-understood than the other modes, the squeeze mode has been used in some small-amplitude vibration dampers [19].

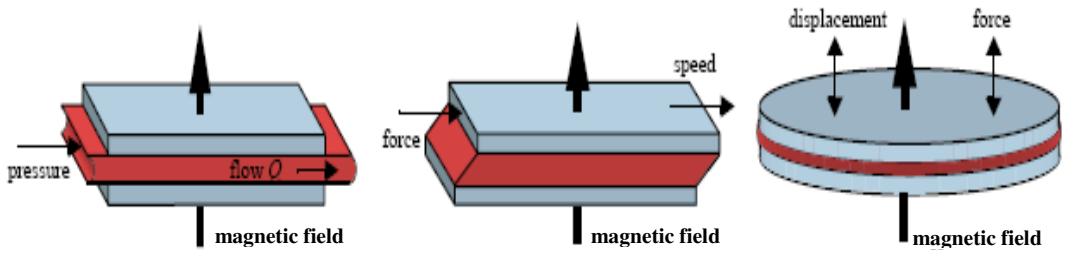

(a) (b) (c)

Fig. 2.2 Basic operating modes for controllable fluid devices [19]
(a) Valve Mode (b) Direct Shear Mode (c) Squeeze Mode

MR fluids are considered to be an attractive alternative to ER fluids for use in controllable fluid dampers [20]. This can be seen in Table 2.1, which compares the physical properties of both MR and ER fluids [21]. In contrast to ER fluids, MR fluids are 20 to 50 times stronger. Furthermore, because the magnetic polarization mechanism is unaffected by temperature, the performance of MR-based devices is relatively insensitive to temperature over a broad temperature range (including the range for automotive use) [22]. In fact, MR fluids can operate at temperatures from - 40 to 150 ^{o}C with only slight variations in the yield stress [1], in contrast to ER fluids (restricted to a range of 10 to 90 ^{o}C). MR fluids are significantly less sensitive to impurities or contaminants such as are commonly encountered during manufacturing and usage [23]. MR technology can provide flexible control capabilities in designs that are far less complicated and more reliable than those based on ER technology [21]. Moreover, as can be seen from Table 2.1, in contrast to ER fluids, MR fluids can be readily operated from a low voltage (*e.g.*, ~12–24V), current-driven power supply outputting only ~1–2 amps.

The advantages of MR technology relative to conventional and electro-mechanical solutions are summarised in [24] as follows:

- Quick response time (less than 10 milliseconds).
- Continuously variable control of damping.
- Simple design of MR devices (few or no moving parts).
- Consistent efficacy across extreme temperature variations.
- High dissipative force that is less dependent on velocity compared to passive dampers.
- Greater energy density.

- Minimal power usage (typically 12V., 1 A. max. current that can fail-safe to battery backup, which can, in turn, fail-safe to passive damping mode).
- Inherent system stability (no active forces generated).

Table 2.1 Properties of MR and ER fluid [21]

Property	MR Fluid	ER Fluid
Max. yield Stress	50 to 100 kPa	2 to 5 kPa
Max. field	~250 kA/m	~4 kV/mm
Plastic viscosity,	0.1 to 1.0 Pa.s	0.1 to 1.0 Pa.s
Operable temperature range	-40 to 150 °C	+10 to 90 °C
Stability	unaffected by most impurities	cannot tolerate impurities
Response time	ms	ms
Density	3 to 4 g/cm^3	1 to 2 g/cm^3
Dynamic Viscosity/Yield Stress	5e-11 s/Pa	5e-8 s/Pa
Max. energy density	0.1 J/cm^3	0.001 J/cm^3
Power supply (typical)	2 to 25 V & 1 to 2 A	2000 to 5000 V & 1 to 10 mA

The above advantages have accelerated research, development and application of MR fluid devices. To date, several MR fluid devices have been developed for commercial use by the LORD Corporation [24]. Currently, thousands of vehicles using MR fluid technology are in operation, and more than 100,000 MR dampers and brakes are in use [24]. MR fluid rotary brakes are smooth-acting, proportional brakes which are more compact and require substantially less power than competing systems. MR fluid vibration dampers for real-time, semi-active control of damping have been used in numerous industrial applications [18]. Most major motor manufacturers have already started to apply MR dampers in suspension systems, and some are near to fruition. These include Cadillac, Ferrari and Honda, to name but a few [24]. Moreover, the capability of MR dampers to produce a large damping force has motivated research into their potential use for controlling railway vehicles' suspension systems [4].

2.2 MR Fluid Dampers

MR dampers typically consist of a piston, magnetic coils, accumulator, bearing, seal, and damper reservoir filled with MR fluid [24]. Figure 2.3 shows a Lord RD-1005-3 MR fluid damper [24], which is used in this study. In this damper, as the piston rod enters the housing, MR fluid flows from the high pressure chamber to the low pressure chamber through orifices in the piston head. The accumulator contains a compressed gas (usually nitrogen) and its piston provides a slightly moveable barrier between the MR fluid and the gas. The accumulator serves three purposes: (i) it provides a degree of softening by providing an extra allowance for the volume changes that occur when the piston rod enters the housing; (ii) it accommodates thermal expansion of the fluid; (iii) it prevents cavitation in the MR fluid during piston movements. The magnetic field generated in the activation regions by the magnetic coils changes the characteristics of the MR fluid as discussed in the previous section. Consequently, the magnitude of the magnetic coils' input current determines the physical characteristics of the MR damper. The maximum force that an MR damper can deliver depends on the properties of the MR fluid, its flow pattern, and the size of the damper [24].

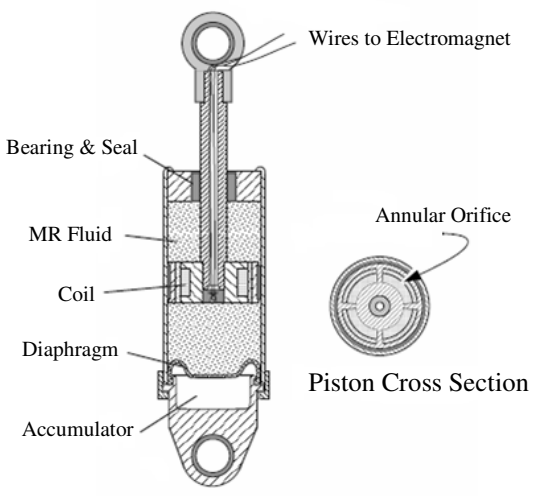

Fig. 2.3 Cross-section of typical MR fluid damper [24]

There are two major types of MR fluid dampers used in vehicle suspensions: mono-tube, and twin tube. Mono-tube MR fluid dampers have only one reservoir and accumulator as shown in Fig. 2.4 which is commonly used in car seat suspension [25]. A twin tube MR damper has two fluid reservoirs, one inside the other as illustrated in Fig. 2.5 that is commonly used in vehicle suspension [26]. This type of damper has inner and outer tubes. The inner tube guides the piston, in exactly the same way as in the mono-tube damper. The volume enclosed by the inner tube is the inner reservoir. The volume that is confined by the space between the inner and the outer tubes is the outer reservoir. The inner reservoir is filled with MR fluid so that no air pockets exist. An outer reservoir that is partially filled with MR fluid serves as an accumulator by accommodating changes in volume due to piston movement.

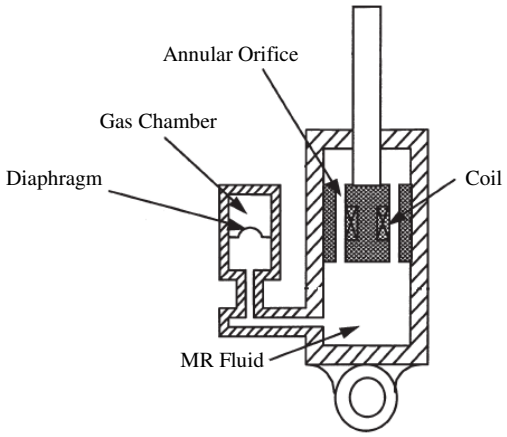

Fig. 2.4 Mono-tube MR damper [25]

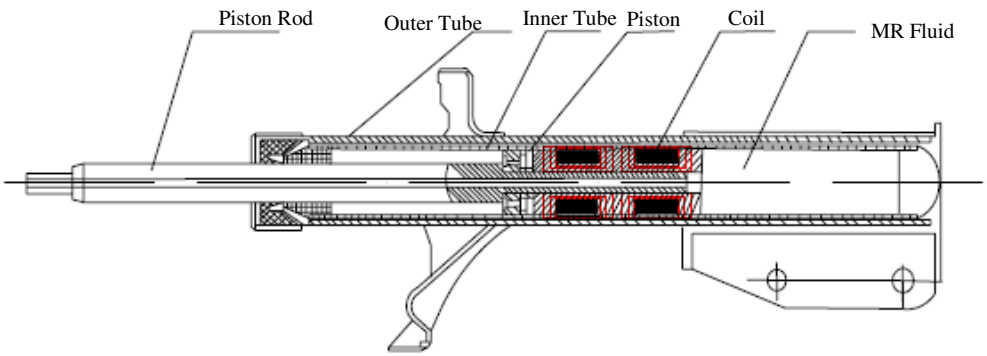

Fig. 2.5 Schematic configuration of the twin tube MR damper without accumulator [26]

In other designs [11] the outer reservoir is completely filled and separated by a diaphragm from a gas filled accumulator as shown in Fig. 2.6.

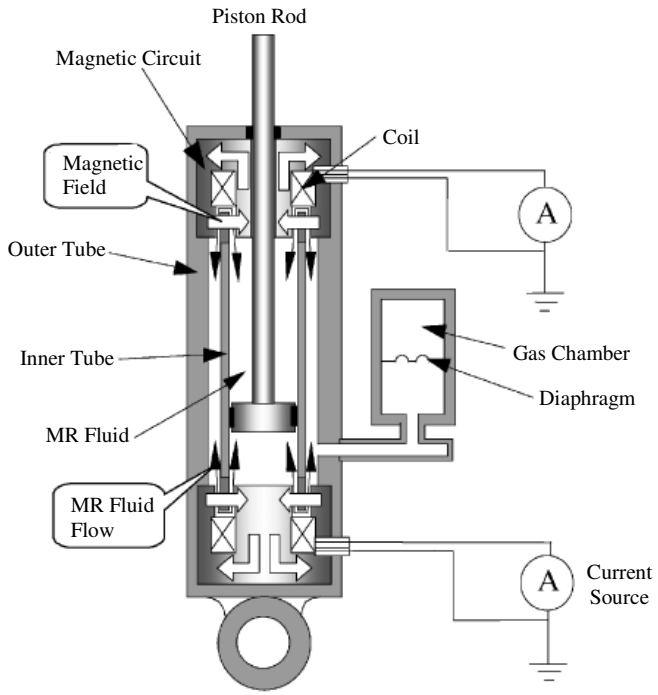

Fig. 2.6 Schematic illustration of the twin tube MR damper with accumulator [11]

2.3 Modelling of MR Fluid Damper

The MR damper is a nonlinear and hysteretic device. By "nonlinear" is meant that the output is a nonlinear function of the inputs. In the case of the forward (or direct) dynamics, the output is the force and the inputs are the electrical input (voltage or current applied to the electromagnet) and the mechanical input (displacement of one end of the damper relative to the other end, and/or the corresponding velocity, and/or acceleration). In the case of the inverse dynamics, the output would be the voltage or current required to generate a desired force for given mechanical input. By "hysteretic" is meant that the output is dependent not just on the instantaneous values of the inputs, but also on the history of the output [27] i.e. such a system has "memory".

The aim of this section is to summarise a number of the models commonly used to identify the nonlinear hysteretic dynamical behaviour of MR fluid dampers. Such identification techniques are based on either on a parametric model or a non-parametric model.

2.3.1 Parametric Models

Parametric models require assumptions regarding the structure of the mechanical model that simulates the behaviour [23]. Such models are based on mechanical idealization involving representation by an arrangement of springs and viscous dashpots [14, 28-30]. The parameters of these elements are determined for a given damper through curve fitting of experimental results.

A number of mathematical models have been published to simulate the behaviour of MR dampers. The most basic model is a Bingham viscoplastic model illustrated in Fig.2.7, which was introduced firstly to study the dynamical behaviour of ER dampers [28] and then used for MR dampers in [14]. Compared with the experiment results, this model does not exhibit the nonlinear force-velocity response when the acceleration and the velocity have opposite signs and the magnitude of the velocity is small [14]. Moreover, this model gives a one-to-one mapping between force and velocity [14]. Hence, it cannot provide a force-velocity hysteresis loop. While this model may be adequate for response analysis, it is not good for the control analysis [14]. The Bouc-Wen model, shown in Fig. 2.8, is extensively used to model hysteresis in systems [29]. It is an extremely versatile model that is able to emulate a variety of hysteretic behaviours. When applied to the MR damper it is found to yield a force-velocity hysteresis loop. However, it was shown in [14] that this loop still

did not match the experimental results adequately in those regions where the acceleration and velocity had opposite signs and the magnitude of the velocity was small [14]. In order to overcome this latter problem, a modified Bouc-Wen model was proposed firstly in [14], Fig. 2.9. This modifies the Bouc-Wen representation through the introduction of an extra internal degree of freedom [14]. This model was shown to yield a force-velocity hysteresis loop that closely matched the experimental measurements [14] so that it is used in this thesis.

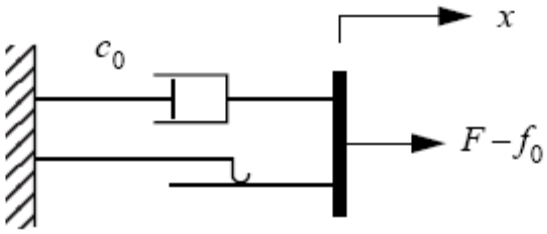

Fig. 2.7 Bingham Model [28]

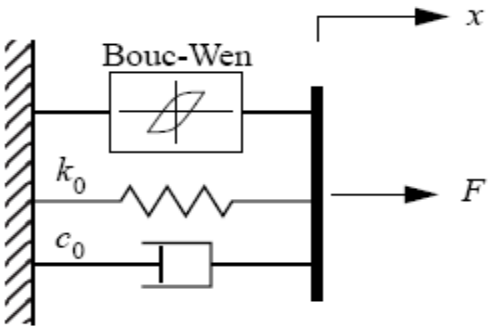

Fig. 2.8 Bouc-Wen Model [29]

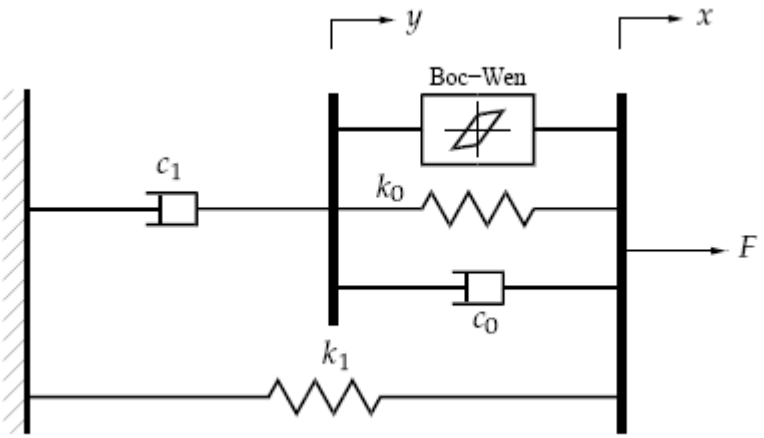

Fig. 2.9 Modified Bouc-Wen Model [14]

Once a parametric model is selected, the values of system parameters are determined in such a way as to minimise the error between experimental data and the simulation from the model. In [14], for the modified Bouc-Wen model, a least-squares output-error method was employed, in conjunction with a constrained nonlinear optimisation, to update the 14 model parameters required to model the MR damper. The optimization was performed using the sequential quadratic programming algorithm available in MATLAB. The experimental validation [14] showed that the modified Bouc-Wen model is able to accurately predict the response of a typical MR damper over a wide range of operating conditions under various input voltage levels.

Instead of least-squares, the modified Bouc-Wen parameters can be determined using a computationally efficient Genetic Algorithm (GA), as done in [31] using experimental data from a Lord RD-1001-4 MR damper [24]. The experimental validation of the model based on these new parameters showed that it was able to accurately predict the dynamical behaviour of the MR damper, including the hysteresis loop. The GA was also used in [30] to determine the parameters of an improved version of the original Bouc-Wen model. The model considered the effect of non-symmetrical hysteresis which was not taken into account in the original Bouc-Wen model. Termination of the algorithm was determined through a statistical test by modelling the progress of the identification error as an exponential distribution with a specified level of decision confidence. The validation results proved that the Bouc-Wen model is able to represent non-symmetric hysteresis using GA.

It is noted that hysteresis in the Bouc-Wen and modified Bouc-Wen model is accounted for through the use of an "evolutionary variable" [14] that is represented by a first order differential equation. Additionally, to account for the effect of variable applied voltage, another first order differential equation is introduced. In the case of the modified Bouc-Wen model, an additional first order differential equation is required to account for the extra internal degree of freedom introduced into the model. Hence, to calculate the force for given time histories of displacement and voltage it is necessary to solve a set of (two or three) first order differential equations. It is also important to note that all the parametric models proposed are only suitable for the direct (or forward) dynamic modelling of the MR damper.

2.3.2 Non-parametric Models

Unlike parametric models, non-parametric models do not make any assumptions on the underlying input/output relationship of the system being modelled. An elevated amount of input/output data has to be used to identify the system, enabling the subsequent reliable prediction of the system's response to arbitrary inputs within the range of the training data. Non-parametric models can be used for modelling both the direct and the inverse dynamics of an MR damper. Since ER dampers exhibit similar dynamic behaviour to MR dampers, a few of the non-parametric methods described here have been used on ER dampers rather than MR dampers. However, they are equally applicable to the latter.

Proposed non-parametric models can be classified as follows:

- Interpolation techniques [32-37]:
    - Simple polynomial model [32];

- Non-parametric linearised data modelling [33];
- Restoring force surface techniques (e.g. Chebyshev polynomial interpolation) [34-37].

- Neural-based methods:
  - Neural networks [23, 38-42];
  - Adaptive neuro-fuzzy inference system (ANFIS) [43].

A model expressing the force as a six-degree polynomial function of velocity, with current-dependent coefficients, was introduced to study the forward dynamical behaviour of MR damper [32]. This approach was formulated based on experimental results. To account for the force-velocity hysteresis loop, two regimes were considered: one for positive acceleration, the other for negative acceleration. The predicted results of this model showed that the model adequately predicts the non-linear force-velocity hysteresis loop of the MR damper. However, the model was not tested under conditions of fluctuating voltage/current.

A Non-Parametric Linearised Data Driven (NPLDD) approach was presented to study the forward dynamical behaviour of an MR damper in [33]. This model again considered two separate regimes, respectively corresponding to positive and negative accelerations of the damper. For each regime, experimental data relating to the force-velocity hysteresis loop were mapped into a look-up table for a set of input voltage signals. As can be expected, the predicted results from this model agreed well with the measured force-velocity loops.

A more sophisticated interpolation alternative to the methods described above is offered by the Restoring Force Surface technique. This was first introduced in [34]

and has so far been used only on ER fluid dampers [35-37]. In [35], a Chebyshev polynomial fit was used to approximate the force generated by an ER fluid damper. For fixed electric field strength (and fixed excitation frequency) the restoring force of the ER damper was predicted by an analytical function constructed by two dimensional (2D) orthogonal Chebyshev polynomials fits. An extension of the previous curve fitting method to three dimensions (3D) was done by Gavin et al. [36]. These researchers related the restoring force of an ER fluid damper to the displacement, velocity, and the electric field strength. Further use of Chebyshev polynomials was made in [37] for the identification and comparison of the dynamical behaviours of conventional and ER fluid dampers. It is noted that one of the novel contributions of the present thesis, listed in Section 1.3, is the application of the Restoring Force Method to MR dampers.

The advantage of the above-described polynomial interpolation techniques is that they offer an explicit functional representation of the output variable in terms of the instantaneous values of the inputs. This is in contrast to the Bouc-Wen/modified Bouc-Wen models, which require time histories of the input variables to produce a prediction of the damper force. However, this means that these polynomial techniques are memory-less and so are *equivalent nonlinear models* in the case of hysteretic systems [27]. Hence, despite being capable of yielding a force-velocity hysteresis loop, the functional representation of force in terms of displacement, velocity and electric field strength in [36] is still a single-valued function in terms of these three variables (i.e. can yield only one possible force value for a given combination of displacement, velocity and electric field). Similarly, the functional representation in [32], referred to earlier, can only yield one possible force value for

a given combination of velocity, acceleration and current. Hence, such interpolation schemes are not strictly hysteretic in the true sense of the word.

Neural-based methods offer an alternative non-parametric approach that can allow memory into the model. They are also equally tractable to both forward and inverse modelling. As stated previously, inverse modelling involves the prediction of the voltage signal (applied to the damper's electromagnet) that will produce a desired damper force signal when the damper is subjected to a given time history of the relative displacement across its ends. Neural networks (NNs) are able to approximate any complicated multi-input/multi-output continuous function. NNs used for modelling MR dampers are typically multilayer networks with either perceptron or sigmoid transfer function neurons e.g. [23, 38-41]. Radial basis function networks have also been used to a lesser extent [42].

The multi-layer networks in [23, 38-41] were used to identify both the forward (direct) [23, 38, 39] and inverse [23, 39-41] dynamics of MR fluid dampers. For both forward and inverse models, the NN architecture could be either "feed-forward" (FNN) [23, 38-40] or "recurrent" (RNN) [23, 41]. Due to hysteretic effects of the MR damper, the output variable of the mapping (i.e. force, in case of the direct problem, or voltage, in case of the inverse problem), suitably delayed, was included with the inputs to the neural network. This gave memory to the system. In the case of the FNN, this extra input was the *actual* value of the output variable (i.e. the value that truly corresponds to the other input variables) and so was taken not from the network output but from some other independent source of information (e.g. a force sensor on the damper in the case of the direct problem). In the case of the RNN, this

extra input was taken from the output of the network itself. For the direct problem, the trained RNN had the advantage of not requiring a force sensor, although it was slightly less precise than the FNN [23]. For the inverse problem, the RNN would be the only useful approach in practice since the FNN would require real-time knowledge of the correct desired voltage (to include with the other inputs) - this of course would not be possible unless one has previously solved the direct form of the same problem.

The works in [38, 39] used optimisation algorithms including "optimal brain surgeon strategies" to prune the weights of the network and optimise their values. The Gauss-Newton based Levenberg-Marquardt optimisation algorithm was selected as the training method for the networks in [23, 38-41], due to its rapid convergence and robustness.

An evolving radial basis function (RBF) neural network was presented to emulate the forward and inverse dynamic behaviours of an MR damper in [42]. It had a structure of four input neurons and one output neuron to predict the damper force and input voltage of MR dampers. This model was developed using a genetic algorithm to select the network centres and widths. The validation results showed that the evolving RBF networks can simulate both forward and inverse dynamic behaviours of the MR damper satisfactorily.

An alternative non-parametric model of MR dampers in the form of a Takagi-Sugeno-Kang fuzzy inference system (ANFIS) was presented [43]. In this model, 27 nonlinear premise parameters and 96 linear consequent parameters were determined

to describe the dynamical behaviour of MR dampers. The validation results of ANFIS model showed an acceptable representation of the MR damper's behaviour while significantly reducing numerical computations.

It is important to note that, as far as the author is aware, in all neural-based methods in the literature e.g. [23, 38-43], the networks have been trained and validated through simulated data (generated from the numerical solution of the modified Bouc-Wen model [14]) rather than measured data. One of the novel contributions of the present thesis is the construction of neural networks from experimental data (contribution no. 2 listed in Section 1.3).

2.4 Semi-active Vibration control of Vehicle Suspension Systems

This section starts by considering fundamental issues relating to the construction, operation and design requirements of vehicle suspension systems. It then reviews the previous work related to the control strategy used in both damper and system controllers for semi-active vibration control of a vehicle suspension system.

2.4.1 Vehicle suspension system overview

The vehicle suspension system is the support device between the vehicle body and its wheels. It basically consists of a spring and damper mounted in parallel between the wheel and the vehicle body (Fig. 2.10). The spring supports the weight of the body ("sprung mass") and moderately isolates it from the wheel ("unsprung mass"). The spring allows the wheel to move relative to the car body when the wheel is

subjected to excitation from the road profile as the vehicle moves along the road. The potential energy stored in the spring is transformed into kinetic energy of the body which is dissipated by the damper [44].

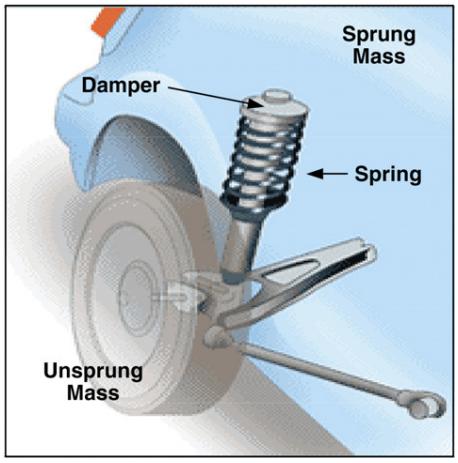

Fig. 2.10 Automotive suspension system [44]

Ride comfort and vehicle stability (also referred to as vehicle handling/road holding) are the two main goals of a vehicle suspension system. Comfort is provided by isolating the vehicle's body from road disturbances, thereby minimising the body displacement and acceleration. Good stability is achieved by keeping the car body from rolling and pitching excessively, and maintaining a sufficient traction force between the tyre and the road surface. The latter is ensured by maintaining a sufficient normal contact force between tyre and ground, which means minimising the dynamic deflection of the tyre. Comfort and stability are conflicting requirements and the suspension design typically involves a compromise solution [7]. The importance of the damper to ride comfort and stability was investigated in [37, 45]. With regards to ride comfort, the damper is required to be relatively soft in order to dissipate the road shock energy well. On the other hand, hard dampers are appropriate for good vehicle stability. In luxury sedan cars, the suspension is usually

designed with an emphasis on comfort (soft damping), but the result is a vehicle that rolls and pitches while driving and during turning and braking. In sports cars, the emphasis is on stability (hard damping), so the suspension is designed to reduce roll and pitch and maintain good traction, at the expense of comfort. Developing improved methods to improve vehicle comfort and stability within the available suspension working space has always been one of the major challenges in vehicle design.

There are three main categorizations of suspension systems: passive, active, and semi-active. Passive suspension systems using conventional oil dampers are simple, reliable and cheap. The tuning of the conventional passive dampers involves the physical adjustment of their valves. The setting is fixed during their lifetime, so they are not able to operate satisfactorily in a broad range of road states. This problem is overcome by active or semi-active suspension systems. Moreover, the control strategy of these systems can be devised to optimise both ride comfort and vehicle stability [8]. The majority of research into such systems has been done on the basis of a quarter-vehicle suspension model (e.g. [2, 10]). This model will also form the basis of the research of this thesis. With reference to the quarter-vehicle model in Fig. 2.11, the ride comfort is quantified by the root-mean-square (RMS) or peak to peak acceleration of the sprung mass, and the vehicle stability is quantified by the RMS or peak to peak dynamic tyre load.

Active and semi-active suspensions have control systems which force the system to achieve optimised conditions. Active suspensions use active devices (electro-hydraulic actuators) which can be commanded directly to give a desired control force

that is calculated by the system controller. Compared with the conventional passive system, an active suspension can offer high control performance over a wide frequency range. However, it is not cost-effective for commercial application since it requires a high power supply, many sensors, and servo-valves.

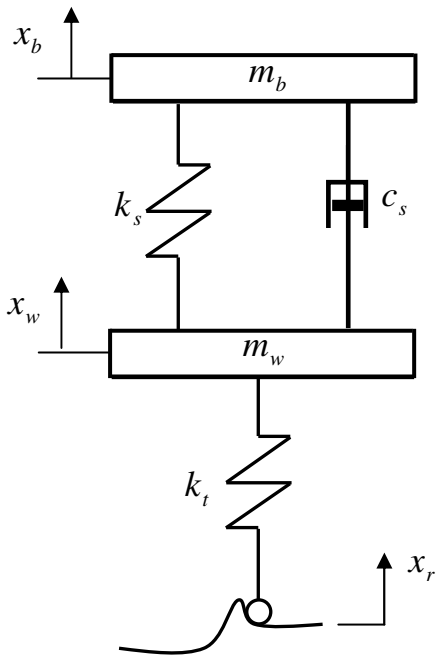

Fig. 2.11 Quarter vehicle suspension model

A semi-active suspension uses semi-active dampers whose force is commanded indirectly through a controlled change in the dampers' properties. This change is effected by a damper controller that receives information from the system controller. A semi-active suspension combines the advantages of both active and passive suspensions. It can be nearly as efficient as a fully active suspension in improving ride comfort and stability and is much more economical [9, 10]. It is also safer since if the control system fails, the semi-active suspension can still work as a passive suspension system.

MR dampers have been shown to be effective semi-active dampers that can satisfy the requirements of ride comfort and vehicle stability [11]. Moreover, an MR damper is an effectively fail-safe device from an electronic perspective. If any fault happened in the system, the MR damper still works as a passive damper within definite performance characteristics, depending on the off-state case of the MR damper [46].

2.4.2 Semi-active vehicle suspension using MR fluid dampers

A semi-active or active system forces the system dynamics to achieve optimised conditions. In the case of a semi-active suspension system incorporating MR damper, this necessitates two nested controllers [2, 23]. A system controller computes the desired damping force for given system conditions [2, 23]. Since the MR damper is a semi-active device, it is the applied voltage, rather than the desired force, that can be commanded directly. Hence, a second controller (the damper controller) is required to command the damper to produce the desired force [2, 23]. The effectiveness of the damper controller depends on its ability to deal with the nonlinear hysteretic nature of the device. The following subsections deal respectively with the damper and system controllers.

2.4.2.1 MR damper controllers

Some methods for controlling the electrical input to the MR damper are based on the simplistic Bingham Model, which is known to be inadequate for MR control purposes [14]. For example, in [11] this model was used to express the damper force as $F_d = k_a x + c_f \dot{x} + P_{MR}$ where x is the relative displacement across the damper ends, k_a is the stiffness of the accumulator, c_f is the viscosity of the carrier fluid

and P_{MR} is a controllable part that is independent of velocity and only dependent on current. This formula therefore neglects nonlinearity with respect to mechanical inputs, as well as force-velocity hysteresis. A theoretical formula that relates P_{MR} to the current was then used in [11] to calculate the current required for P_{MR} to have a desired value. In [47], the Bingham Model was only approximately followed since the current was raised or switched off in an attempt to increase or decrease the P_{MR} according to its desired value, without comparative force feedback. Hence, neither of the methods in [11, 47] can correctly track a desired force signal. This thesis will focus on MR damper control algorithms that are not based on simplified theoretical assumptions and are specifically intended to command the MR damper to track a desired force signal. From the literature, there are five such algorithms:

- Heaviside Step Function (HSF) control [3, 5];
- Signum Function Method (SFM) [48];
- Continuous State Control (CSC) [2, 49, 50];
- Inverse polynomial control [32, 51];
- Inverse recurrent neural network (RNN) control [23, 41].

HSF control was introduced in [5] and applied to a vehicle suspension system in [3]. It uses an "on-off" control algorithm, where the applied voltage is either 0 or maximum. The SFM is an improvement on this algorithm, which, under certain conditions, permits the applied damper voltage to switch between discrete voltage levels below the maximum [48]. This algorithm was used to command an MR damper used in a semi-active suspension system of a train [4]. In both these controllers, the command voltage signal is discontinuous. Allowing the voltage

signal to be continuous ensures more effective control, lower power requirement and extended service life of the damper [23].

The CSC algorithm allows the command of a continuous voltage signal. CSC was introduced in [49] for an ER damper first and then was used in [2, 50] for an MR damper, although no comparison was made in either [50] or [2] with alternative control strategies.

The above three types of damper controller (HSF, SFM and CSC) need to be fed with a measurement of actual damper force from a force sensor. This sensor needs to be in series with each MR fluid damper for a multi-damper system, thereby reducing system reliability and increasing its cost. The other two damper controllers listed above (inverse polynomial, inverse RNN) do not require a force sensor.

As mentioned in Section 2.3.2, a model expressing the force as a six-degree polynomial function of velocity, with current-dependent coefficients, was introduced in [32] to study the forward dynamical behaviour of MR damper. This model is invertible, so it is possible to calculate the input current for given velocity and desired force. This controller is rather simplistic and has only been validated experimentally for tracking a desired force in the form of a simple sinusoid [32]. It was subsequently used in a simulation of a quarter-vehicle suspension model [51]. In that work, the inverse polynomial controller did not operate on an actual damper or an advanced numerical model like the modified Bouc-Wen. Instead, it appears to have operated on the forward model of the damper based on the same polynomial

from which the controller was derived. Hence, not surprisingly, it gave good control performance.

A more sophisticated method of commanding a continuous voltage signal without needing a force sensor is through a recurrent neural network (RNN) of the inverse dynamics of the MR damper [23]. This controller uses a measure of the relative displacement across the damper, which is already available from the sensors used by the system controller. Until now, this controller has not been experimentally evaluated against the established MR damper controllers (HSF, SFM, and CSC). In fact, it has only been compared in simulation to the HSF method [23]. Moreover, although the inverse RNN controller has been applied to simulations of single and multi-degree-of-freedom systems, it has not been applied to vehicle suspension systems until now. These gaps in knowledge are addressed in this thesis through contributions nos. 3 and 4 listed in Section 1.3.

2.4.2.2 System Controller

The system controller computes the desired force required from the MR damper in order to achieve optimised conditions for the system shown in Fig. 2.11. A large number of system controller algorithms have been developed and these can be broadly classified according to the control strategy used to optimise the system conditions:

- Direct optimisation of the state variables:
    - H∞ control [51, 52];
    - Linear-Quadratic-Gaussian (LQG) control [3, 4];

- Neural Network (NN) system control [53];
- Robust control [54].

- Forcing the system to emulate the behaviour of some idealised system:
  - Skyhook model and its variants [9, 11, 47, 55, 56];
  - Model-reference sliding mode control [2, 50].

In H∞ control, the controller is formulated by expressing a mathematical optimisation problem and finding the controller gain. This strategy has been used in [51, 52] to control a vehicle suspension system using MR dampers. A static output feedback H∞ controller, that employed the measured suspension deflection and body velocity as feedback signals for semi-active quarter vehicle suspension, was designed [51] using a genetic algorithm. This controller was validated using numerical simulation under random excitation in the time domain. The theoretical results showed that the semi-active suspension system incorporating an MR damper controlled using static output feedback H∞ controller achieved good ride comfort and vehicle stability.

In [52], an H∞ controller with inherent robustness against system uncertainties was developed to handle variations in the vehicle body mass. It was applied to a full-car mathematical model [52] to study the dynamical behaviour of vehicle suspension system using Hardware in the Loop Simulation (HILS) for simulated bump and random road excitations. The results showed that both ride comfort and vehicle stability can be noticeably improved in both time and frequency domains by using MR dampers.

Due to their non-linear mapping and learning ability, neural networks (NN) are popular methods for designing robust, adaptive and intelligent control systems. An adaptive system controller was designed using a NN method to control a semi-active suspension system incorporating an MR damper based on a quarter vehicle model [53]. This algorithm consisted of two sub-controllers: a NN identifier and a NN controller. The former works as a system controller in the semi-active system and computes the back propagation error for the NN controller. This algorithm was examined through both theoretical and experimental results. These results showed the superiority of this control strategy against the passive system in both the time and frequency domains.

LQG control is another concept for optimal control strategy that has been used for vehicle suspensions with MR dampers. It has been applied in [3, 4] to study the simulated dynamical behaviour of a half vehicle model including seat dynamics and a full train suspension system, 6 and 9 degrees-of-freedom (DOFs) respectively. The LQG controller was the combination of a Kalman filter and a Linear-Quadratic-Regulator (LQR). The control technique was based on control theory with optimal state-feedback control gain that was calculated from the solution of the algebraic Riccati equation. Simulations in [3, 4] showed that the use of MR dampers with this control strategy offered superior performance of the vehicle suspension system relative to a passive one. It is noted however that the performance of LQG depends on the selection of weighting matrices for the vector of regulated responses and control forces. When the cost function weighting matrices is changed, the response of the system can be greatly changed and the values in the weighting matrices are often determined by trial and error [57].

Robust control techniques have become a common concept in control engineering systems because real systems depend on external disturbance and measurement noise. Also, there are always some differences between the mathematical model used for plant design and the real system. Robust inverse dynamics control strategy was investigated [54] to control a half vehicle suspension system including seat dynamics, comprising 6 DOFs, using two MR dampers. The main objective of the controller was to force the vertical and pitch motions of the chassis to zero. A feedback control mechanism was established to achieve this design objective. The simulation results confirmed that a good performance of vehicle suspension system was achieved, especially with regard to vertical and rotational displacements.

Rather than calculating the desired damper force on the basis of direct optimisation of the state variables, an alternative strategy would be to calculate the force such that the actual system approximately follows the behaviour of an ideal system. In the classic skyhook control [9, 47, 55] the ideal system is shown in 2.12(a). It is seen from Fig. 2.12(a) that the MR damper in Fig. 2.11 is required to behave like a fictitious damper attached at one end to the sprung mass and at the other end to a fixed point in the sky.

The experimental results in [47] indicated that such control reduced the transmissibility of the sprung mass (ratio of amplitude of sprung mass displacement to input displacement excitation). In [47], the skyhook control was also applied to the unsprung mass, in which the ideal system is Fig. 2.12(b). In this case it was referred to as “ground-hook” control. It was found to reduce the transmissibility of the unsprung mass. A hybrid of skyhook and ground-hook was also applied in [47],

as in the ideal system in Fig. 2.12(c). This was shown to guarantee a semi-active control strategy that can be slowly adjusted to the driving and vehicle situations for better stability and comfort.

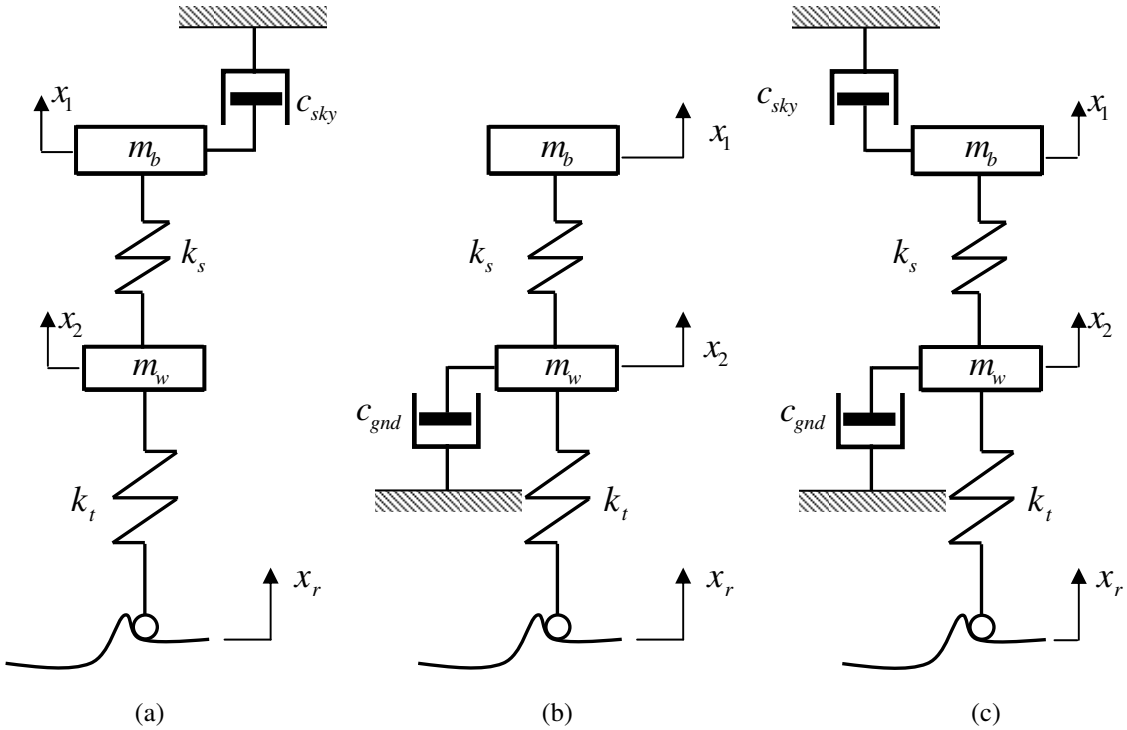

Fig. 2.12 Ideal systems for skyhook control [47]
(a) Skyhook (b) Ground-hook (c) Combined

The absolute velocity is impractical to measure for a running vehicle but the acceleration of the sprung mass can be measured easily [55]. Hence, a modified version of the skyhook was introduced in [55]. This was based on the measurement of the absolute vertical acceleration of the vehicle body rather than the absolute velocity. Both analytical and experimental results confirmed that the modified sky-hook control method appreciably reduced the root mean-square values of both the acceleration and relative displacement of the sprung mass. Another implementation of skyhook and ground-hook was made in [56]. In this case, the desired MR damper force was computed by applying fuzzy logic rules based on skyhook and ground-

hook principles. Fuzzy logic emulates human intelligence in learning and decision making by using linguistic variables. In [56] a fuzzy logic system controller was implemented in an MR-damped quarter-vehicle model of a real mini-bus. The fuzzy inputs were the sprung mass velocity, the unsprung mass velocity, and the relative velocity, while the desired damping force was its output. The dynamical behaviour of the MR suspension system was evaluated by road testing. The test results showed that the vibration levels of the sprung and unsprung masses were reduced significantly.

Since the MR damper is not an actuator but a semi-active device, the classic models in Fig. 2.12 are only approximately achieved with MR dampers. The MR damper can be made to approximately behave like the skyhook damper in Fig. 2.12(a) if its force is very low for $\dot{x}_1(\dot{x}_1 - \dot{x}_2) \leq 0$ and equal to $G\dot{x}_1$ for $\dot{x}_1(\dot{x}_1 - \dot{x}_2) > 0$, where G is some gain [47]. As discussed in Section 2.4.2.1, in both [11, 47] the damper force F_d was assumed to follow the Bingham Model where $F_d = k_a x + c_f \dot{x} + P_{MR}$ and $x = x_1 - x_2$ in Fig. 2.12 and P_{MR} is the controllable part that is independent of velocity and dependent only on current. This model was already described as inadequate for control purposes in Section 2.4.2.1. More importantly, the system control was applied in [11, 47] to P_{MR} and not to F_d i.e.

$$P_{MR} = G\dot{x}_1 \quad for \quad \dot{x}_1(\dot{x}_1 - \dot{x}_2) > 0 \quad and \quad P_{MR} = 0 \quad for \quad \dot{x}_1(\dot{x}_1 - \dot{x}_2) \leq 0$$

Hence, with such a control strategy there would be a passive damping component $c_f(\dot{x}_1 - \dot{x}_2)$ that would tend to increase the absolute velocity $\dot{x}_1$ of the sprung mass when $\dot{x}_1(\dot{x}_1 - \dot{x}_2) \leq 0$. The addition of such a passive damping component between

the sprung and unsprung masses of Fig. 2.12(a) results in a non-ideal skyhook system [2].

It is possible to emulate an ideal skyhook system though the use of model-reference sliding mode control. Such an algorithm provides a very powerful method of forcing the system to emulate the behaviour of any chosen reference system e.g. ideal skyhook or non-ideal skyhook [2, 50]. Moreover, this algorithm can handle uncertainties in the sprung mass due to variations in loading conditions. This algorithm was first applied in [50] to a single-degree-of-freedom model of an MR-damped vehicle suspension with loading uncertainty. This was then extended in [2] to an MR-damped quarter-vehicle suspension system like the one in Fig. 2.11. The reference models used in [2] are shown in Fig. 2.13.

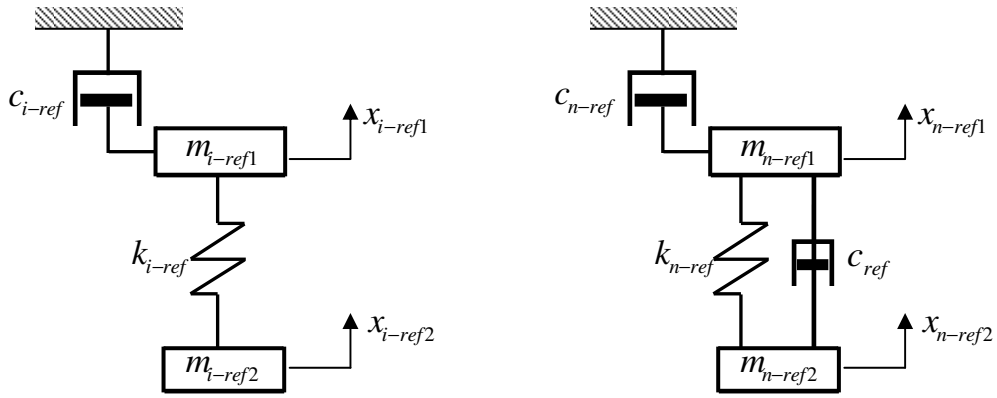

Fig. 2.13 Reference models for sliding mode control [2]
(a) Ideal skyhook reference model (b) Non-ideal skyhook reference model

The value of the sprung mass of the reference model is made equal to the nominal value of the sprung mass of the actual system in Fig. 2.11. However, the other parameters in Fig. 2.13 can take different values. The displacement of the unsprung mass of the reference model is set to be identical to that of the unsprung mass of the

actual system. The sliding mode control algorithm calculates the force required from the MR damper such that the displacements of the sprung masses of the reference and actual systems are as close to each other as possible. The results in [2] showed that the controlled system using ideal skyhook as a reference model is the more efficient for suppressing the vibration of the quarter vehicle model. CS control was used in [2] to realise the force desired from the MR damper (Section 2.4.2.1). The simulation results were done in both the time and frequency domains using bump and random road excitations. Moreover, HILS with sinusoidal road excitation was used to illustrate the practical implementation of the control strategy. The results obtained from [2] confirmed that the ride comfort can be significantly improved in both time and frequency domains by using MR dampers.

Of all the system controller algorithms proposed in the literature and discussed in this sub-section, the author has opted for the above-described model-reference sliding mode control algorithm. The reasons for this are its proven effectiveness, its ease of implementation, and its robustness in handling uncertainties in sprung mass due to loading variations. In Chapter 6 this system controller is used in conjunction with an inverse RNN MR damper controller for the semi-active control of a quarter vehicle suspension model, as per novel contribution no.4 listed in Section 1.3.

2.5 Car seat suspension system using MR damper

Car seat suspension systems have a major role in offering the vehicle's driver and passengers with an adequate level of comfort. This section reviews literature concerning research into the semi-active control of car seat suspensions.

A literature review revealed only 4 papers where the use of an MR damper in a seat suspension has been investigated [25, 58-60]. The works in [25, 58, 59] all used a cylindrical MRF-132LA seat damper manufactured by Lord Corporation [24] and controlled using the skyhook scheme.

In [25], the seat suspension was modelled as base-excited 2 DOF system, as shown in Fig 2.14, where the upper mass, stiffness and damping are the rider's properties. The lower mass and spring are respectively the mass and stiffness of the seat. The MR damper is shown circled in Fig 2.14. A skyhook controller was used in a closed-loop control manner to reduce the vibration level at the driver's seat. A test-rig was built to study the impact of the MR damper and the skyhook control strategy on the ride comfort. Seat displacement and acceleration were measured to evaluate the performance in both the time and frequency domains. Additionally, a commercial truck model incorporating the above semi-active seat suspension model was established and its vibration control performance was evaluated using the HILS technique. The experimental results confirmed that the ride comfort can be considerably improved by using MR dampers in seat suspension.

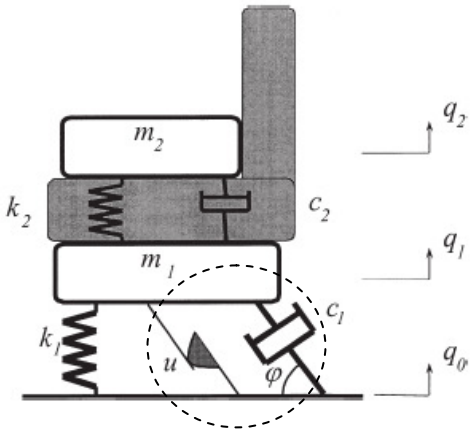

Fig 2.14 Car seat suspension model used in [25]

The seat suspension in [58] was regarded as a base-excited single-degree-of-freedom (SDOF) system, as shown in Fig. 2.15. The seat suspension system was evaluated experimentally to assess the improvement in the ride quality and the riders' health benefit in comparison with a conventional passive seat. In the experiments, a person was sitting on a controlled seat suspension excited by a hydraulic shaker system. Three control schemes were studied: skyhook, continuous skyhook and relative displacement control. Among them, the continuous skyhook was found to give the best performance for bump and random road condition excitations.

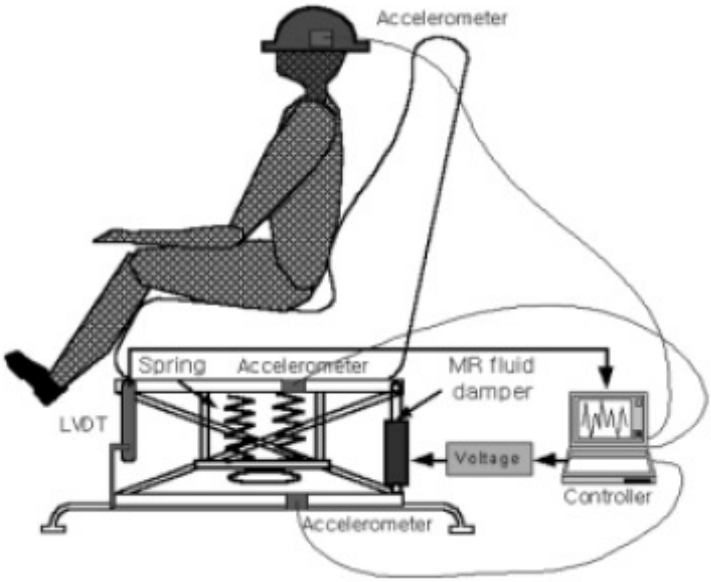

Fig. 2.15 Seat suspension considered in [58]

A full "cab over engine" commercial vehicle model equipped with semi-active ER dampers for the vehicle suspension and an MR damper for the seat suspension was proposed in [59] and shown in Fig. 2.16. The seat suspension itself was modelled as a base-excited SDOF system and its efficacy for vibration reduction was investigated through HILS using skyhook control theory. The skyhook controller gain was calculated for each damper and realised via HILS. The results showed that the MR damper significantly reduced the seat vertical displacement and acceleration under a

simulated road bump test. Also, it was found that, for a simulated random road test, the power spectrum densities of the displacement and acceleration at the vehicle driver's seat were considerably reduced.

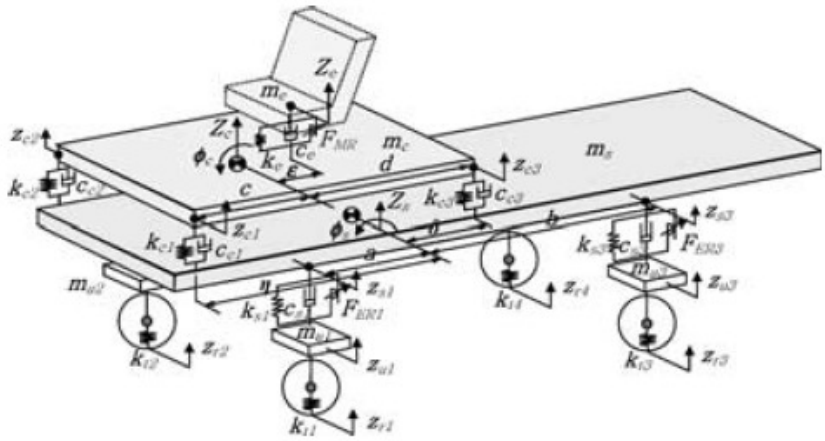

Fig. 2.16 Mechanical model of the full-vehicle system, cab over engine, featuring ER primary dampers and MR seat damper [59]

The control implementation in the above described works [58, 59] was not quite appropriate for the semi-active and nonlinear hysteretic nature of the MR damper. In [25, 59] the current required to produce the skyhook damper force was calculated on the basis of the simplified Bingham model, as discussed in Section 2.4.2.1. Moreover, this resulted in non-ideal skyhook conditions, as discussed in Section 2.4.2.2. In [58], the MR damper force was assumed to be a linear function of the velocity and an empirical relation was established between the approximate damping coefficient of the MR damper and the applied current.

A more appropriate approach would be to use a semi-active control scheme that would enable the MR damper to accurately track the desired control force. Such a control scheme comprises two nested controllers: a system controller and a damper controller, as discussed in Section 2.4.2. To date, such semi-active control systems

have been mainly used in seat suspensions containing an electrorheological damper e.g. [61, 62]. It is noted that a different type of adaptive control of a seat MR damper has been used recently [60]. In this work, a base-excited SDOF system with MR damper was analysed theoretically. A non-parametric model was established, relating the damper force with the current and the relative velocity across the damper. The current fed to the damper coil was updated in such a way as to minimise a performance index (chosen to be the square of the instantaneous absolute acceleration of the seat). The controller adaptation was examined using a chirp input that swept from very low frequencies to frequencies higher than the resonant frequency of the seat suspension system. The numerical results showed that the ride comfort can be significantly improved using such an adaptive controller compared with passive dampers. However, the researchers in [60] have recognised the computational burden imposed by this method on micro-controllers for real world implementation and gave suggestions for simplifying the non-parametric model used for the MR damper.

The above literature review shows that there is a need for an improved, easy-to-implement semi-active control strategy for an MR-damped car seat suspension. This would comprise of two nested controllers, as described for the vehicle suspension in Section 2.4.2. This motivates novel contribution no.6 in the list of Section 1.3.

2.6 Summary

This chapter has presented a comprehensive critical literature review on MR dampers and their use in vehicle suspensions. It started by giving a short background on the behaviour of MR fluids and the design of MR dampers. This was

then followed by a review of parametric and nonparametric modelling techniques used to study their dynamical response. Previous research relating to the semi-active vibration control of vehicle suspensions using MR dampers was then reviewed, focussing on the system and damper controllers. Finally, research into the use of MR dampers in car seat suspension systems was discussed. The shortcomings and gaps in the research were highlighted at various stages in this review in order to explain the motivation for the various novel contributions listed in Section 1.3.

CHAPTER 3

Research Publications

This thesis is written in an *alternative format*, in which the research methodologies and findings are introduced in the form of published and submitted papers. In this chapter, an outline of the research carried out in this study is provided. This is followed by the abstract of each paper, together with a statement of the authors' contribution.

3.1 Research outline

As stated in Section 1.2, the overall aims of this thesis are twofold:

- The investigation of non-parametric techniques for the identification of the nonlinear dynamics of an MR damper.
- The implementation of these techniques in the investigation of MR damper control of a vehicle suspension system. The investigation is aimed at improving

ride comfort and vehicle stability with minimal reliance on the use of sensors, thereby reducing the implementation cost and increasing system reliability.

The specific objectives to achieve these aims were listed in Section 1.2. These five objectives form the themes of this thesis. Following these objectives, a summary of the research conducted is presented in the remainder of this section.

A new model for studying the dynamical behaviour of an MR damper is introduced. It involves a three dimensional interpolation using Chebyshev orthogonal polynomial functions to identify the damping force as a function of the displacement, velocity and input voltage. The identification and its validation are done in both simulation and experimentation. In the former case the data are generated by solving the modified Bouc-Wen model. In the experimental approach, the data are generated through dynamic tests with the damper mounted on a tensile testing machine.

The experimental identification of the dynamic behaviour of an MR damper through neural networks is introduced. Feed-forward and recurrent neural networks are used to model both the direct and inverse dynamics of the damper. Training and validation of the proposed neural networks are performed using the data generated through dynamic tests with the damper mounted on a tensile testing machine. The effect of the cylinder's surface temperature on both the direct and inverse dynamics of the damper is studied. The inverse recurrent neural network model is introduced as a damper controller and experimentally evaluated against alternative controllers proposed in the literature.

The neural-based MR damper controller is then introduced for use in conjunction with the system controller of a semi-active vehicle suspension. A mathematical model of a semi-active quarter-vehicle suspension using an MR damper is derived. The system controller is based on model-reference sliding mode control. The performance criteria are: the suspension working space (SWS); vertical body acceleration (BA); dynamic tyre load (DTL). These performance criteria are evaluated in the time and frequency domains in order to quantify the suspension effectiveness under bump and random road disturbance. These studies are performed using two alternative means of providing the damper force in the model: (a) a modified Bouc-Wen model; (b) an actual damper fitted in a hardware-in-the-loop simulation (HILS). The former method is used to study bump excitation where the large damper deflections could not be achieved by HILS. The latter method is used to illustrate the practical implementation of the control strategy. In either case the damper controller was based on an experimentally trained RNN network of the inverse dynamics of the damper. Further studies are performed using an experimental RNN model of the forward dynamics of the MR damper as a substitute for HILS.

An improved semi-active control strategy for an MR damper used in a car seat suspension is demonstrated in this study. The seat suspension system is approximated by base-excited single degree of freedom system. The proposed semi-active seat suspension is compared with a passive seat suspension for prescribed base displacements. These inputs are representative of the vibration of the sprung mass of a passive or semi-active quarter-vehicle suspension under bump or random-profile road disturbance. Performance criteria such as seat travel distance and seat

acceleration are evaluated in time and frequency domains, in order to quantify the effectiveness of proposed semi-active control system.

The outcomes of the above described research were summarised in Section 1.3 (Contributions to Knowledge).

3.2 Outline of published/submitted papers included

The papers are included as separate chapters (Chapters 4-7) with appropriate re-formatting. In total, four published papers are included. These comprise three journal papers and one refereed conference paper. Each paper has been peer reviewed by two or three experts. Three journal papers and the refereed conference paper have been published. All papers are co-authored by myself, Dr. Philip Bonello, and Dr. S Olutunde Oyadiji. The work in these papers was carried out solely by myself under the supervision of Dr. Philip Bonello. As the first author, I contributed the major ideas and contents of all papers.

With regard to the five objectives listed in Section 1.2, these papers are listed as follows:

- Objective no. 1:
    - Metered, H., Bonello, P., & Oyadiji, S. O. Nonparametric identification modeling of magnetorheological damper using Chebyshev polynomials fits. *SAE International Journal of Passenger Cars - Mechanical Systems*, 2009, Vol. 2 (1), pp. 1125-1135

- Objective nos. 2, 3:
    - Metered, H., Bonello, P., and Oyadiji, S. O. The experimental identification of magnetorheological dampers and evaluation of their controllers. *Mechanical Systems and Signal Processing*, 2010, Vol. 24 (4), pp. 976-994

- Objective no. 4:
    - Metered, H., Bonello, P., & Oyadiji, S. O., An investigation into the use of neural networks for the semi-active control of a magnetorheologically damped vehicle suspension. *Proceedings of the Institution of Mechanical Engineers, Part D: Journal of Automobile Engineering*, 2010, Vol. 224 (7), 829-848

- Objective no. 5:
    - Metered, H., Bonello, P., & Oyadiji, S. O. Vibration control of a seat suspension system using magnetorheological damper. ASME International Design Engineering Technical Conferences & Computers and Information in Engineering Conference, San Diego, California, USA (paper no. DETC2009-86081), 30 August - 2 September 2009.

The following sub-sections contain the abstracts of these papers.

3.2.1 Nonparametric Identification Modeling of Magnetorheological Damper using Chebyshev Polynomials Fits [63]

Authors: Hassan Metered, Philip Bonello and S Olutunde Oyadiji

Published in: SAE International Journal of passenger cars: Mechanical systems, 2009, Vol. 2, No. (1), pp 1125-1135.

The magnetorheological (MR) damper is one of the most promising new devices for vehicle vibration suppression because it has many advantages such as mechanical simplicity, high dynamic range, low power requirements, large force capacity and robustness. The damper offers a compromise solution for the two conflicting requirements of ride comfort and vehicle handling. In this paper, a new approach for studying the dynamical behavior of an MR damper is presented. It consists of a three dimensional interpolation using Chebyshev orthogonal polynomial functions to identify the damping force as a function of the displacement, velocity and input voltage. The identification and its validation are done in both simulation and experimentation. In the former case the data are generated by solving the modified Bouc-Wen model. In the experimental approach, the data are generated through dynamic tests with the damper mounted on a tensile testing machine. In either case, validation data sets representing a wide range of working conditions of the damper show that the use of Chebyshev interpolation to predict the damping force for known displacement, velocity and voltage is reasonably accurate.

3.2.2 The Experimental Identification of Magnetorheological Dampers and Evaluation of their Controllers [64]

Authors: Hassan Metered, Philip Bonello and S Olutunde Oyadiji

Published in: Mechanical System and Signal Processing, 2010, Vol. 24 (4), pp. 976-994

Magnetorheological (MR) fluid dampers are semi-active control devices that have been applied over a wide range of practical vibration control applications. This paper concerns the experimental identification of the dynamic behaviour of an MR damper and the use of the identified parameters in the control of such a damper. Feed-forward and recurrent neural networks are used to model both the direct and inverse dynamics of the damper. Training and validation of the proposed neural networks are achieved by using the data generated through dynamic tests with the damper mounted on a tensile testing machine. The validation test results clearly show that the proposed neural networks can reliably represent both the direct and inverse dynamic behaviours of an MR damper. The effect of the cylinder's surface temperature on both the direct and inverse dynamics of the damper is studied, and the neural network model is shown to be reasonably robust against significant temperature variation. The inverse recurrent neural network model is introduced as a damper controller and experimentally evaluated against alternative controllers proposed in the literature. The results reveal that the neural-based damper controller offers superior damper control. This observation and the added advantages of low power requirement, extended service life of the damper and the minimal use of sensors, indicate that a neural-based damper controller potentially offers the most cost-effective vibration control solution among the controllers investigated.

3.2.3 An investigation into the use of neural networks for the semi-active control of a magnetorheologically damped vehicle suspension [65]

Authors: Hassan Metered, Philip Bonello and S Olutunde Oyadiji

Published in: Proceedings of the Institution of Mechanical Engineers, Part D: Journal of Automobile Engineering, 2010, Volume: 224 (7), pp 829–848.

Neural networks are highly useful for the modelling and control of magneto-rheological (MR) dampers. A damper controller based on a recurrent neural network (RNN) of the inverse dynamics of an MR damper potentially offers significant advantages over conventional controllers in terms of reliability and cost through the minimal use of sensors. This paper introduces a neural-based MR damper controller for use in conjunction with the system controller of a semi-active vehicle suspension. A mathematical model of a semi-active quarter-vehicle suspension using an MR damper is derived. Control performance criteria are evaluated in the time and frequency domains in order to quantify the suspension effectiveness under bump and random road disturbance. Studies using the modified Bouc-Wen model for the MR damper as well as an actual damper fitted in a hardware-in-the-loop simulation (HILS) both showed that the inverse RNN damper controller potentially offers significantly superior ride comfort and vehicle stability over a conventional MR damper controller based on continuous state (CS) control. The neural controller produces a smoother and lower input voltage to the MR damper coil, respectively ensuring extended damper life and lower power requirement. Further studies performed using an RNN model of the forward dynamics of the MR damper showed that it is a reliable substitute for HILS for validating multi-damper control applications.

3.2.4 Vibration control of a seat suspension system using Magnetorheological damper [66]

Authors: Hassan Metered, Philip Bonello and S Olutunde Oyadiji

Published in: ASME 2009 International Design Engineering Technical Conferences & Computers and Information in Engineering Conference, San Diego, CA, USA. 30 Aug. – 2 Sep. 2009. ASME Paper No. DETC 2009-86081.

A car seat's suspension system is critical to the ride comfort experience of a vehicle's driver and passengers. The use of a magnetorheological (MR) damper in a seat suspension system has been shown to offer significant benefits in this regard. In most research on seat MR dampers the control implementation was not quite appropriate for the semi-active and nonlinear hysteretic nature of the MR damper. This paper introduces a more suitable semi-active control strategy for an MR damper used in a seat suspension, enabling more effective control. The proposed control system comprises a system controller that computes the desired damping force using a sliding mode control algorithm, and a neural-based damper controller that provides a direct estimation of the command voltage that is required to track the desired damping force. The seat suspension system is approximated by a base-excited single degree of freedom system. The proposed semi-active seat suspension is compared to a passive seat suspension for prescribed base displacements. These inputs are representative of the vibration of the sprung mass of a passive or semi-active quarter-vehicle suspension under bump or random-profile road disturbance. Control performance criteria such as seat travel distance and seat acceleration are evaluated in time and frequency domains, in order to quantify the effectiveness of proposed semi-active control system. The simulated results reveal that the use of semi-active control in the seat suspension provides a significant improvement in ride comfort.

CHAPTER 4

Nonparametric Identification Modeling of Magnetorheological Damper using Chebyshev Polynomials Fits

Authors:

Hassan Metered, Philip Bonello and S Olutunde Oyadiji

Reformatted version of paper published in:

SAE International Journal of passenger cars: Mechanical systems, 2009, Volume: 2 (1), pp 1125-1135.

Abstract

The magnetorheological (MR) damper is one of the most promising new devices for vehicle vibration suppression because it has many advantages such as mechanical

simplicity, high dynamic range, low power requirements, large force capacity and robustness. The damper offers a compromise solution for the two conflicting requirements of ride comfort and vehicle handling.

In this paper, a new approach for studying the dynamical behavior of an MR damper is presented. It consists of a three dimensional interpolation using Chebyshev orthogonal polynomial functions to identify the damping force as a function of the displacement, velocity and input voltage. The identification and its validation are done in both simulation and experimentation. In the former case the data are generated by solving the modified Bouc-Wen model. In the experimental approach, the data are generated through dynamic tests with the damper mounted on a tensile testing machine. In either case, validation data sets representing a wide range of working conditions of the damper show that the use of Chebyshev interpolation to predict the damping force for known displacement, velocity and voltage is reasonably accurate.

4.1 Introduction

Magnetorheological (MR) dampers are semi-active control devices that have received considerable interest in recent years due to their mechanical simplicity, high dynamic range, low power requirements, large force capacity and robustness. They are useful devices for vibration control in many applications such as civil, aerospace and vehicle engineering. MR fluids respond to a magnetic field with a dramatic change in rheological behavior. These fluids can reversibly and instantaneously

change from a free-flowing liquid to a semi-solid with controllable yield strength when exposed to a magnetic field [1].

Identification techniques for modeling the dynamic behavior of MR dampers can be broadly classified into two categories: parametric and non-parametric identification techniques. Parametric models are based on mechanical idealization involving representation by an arrangement of springs and viscous dashpots [14, 50, 67, 68, 69]. The most recent parametric model is the modified Bouc–Wen model [14]. This is a semi-empirical relationship in which 14 parameters are determined for a given damper through curve fitting of experimental results.

Unlike parametric models, non-parametric models do not make any assumptions on the underlying input-output relationship of the system being modeled. Consequently an elevated amount of input/output data is used to identify the system, enabling the subsequent prediction of the system's response to arbitrary inputs. Proposed models in this category are based on neural networks, neuro-fuzzy modeling, and Restoring Force Surface techniques (e.g. Chebyshev polynomial interpolation).

So far, the nonparametric techniques used for identifying MR dampers have involved neural networks and neuro fuzzy models. In [23, 38] a feed forward neural network and recurrent neural network were used. The training of the network depends on the input and output data sets obtained from experimental results or from a mathematical simulation of the MR fluid dampers. The modeling of MR fluid dampers with an adaptive neuro-fuzzy inference system (ANFIS) was proposed in [43].

An alternative non-parametric identification approach is through the Restoring Force Surface method, specifically the Chebyshev polynomial fitting. The advantage of this method is that it offers an explicit functional representation of the output variable (damping force in this case), in terms of the instantaneous values of the inputs. This is in contrast to the Bouc-Wen parametric approach and the neural network approach, which require time histories of the input variables to produce a prediction of the force.

Up to now, the Restoring Force Surface method has only been used on electrorheological (ER) dampers. In [35], a Chebyshev polynomial fit was used to approximate the force generated by an ER test device. For fixed electric field strength (and fixed excitation frequency) the restoring force of the ER damper was predicted by an analytical function constructed by two dimensional (2D) orthogonal Chebyshev polynomials fits. An extension of the previous curve fitting method to three dimensions (3D) was done by [36]. They related the restoring force of an ER fluid damper to the displacement, the velocity, and the electric field strength.

In the present paper, Chebyshev orthogonal polynomials fits are applied for the first time for the non-parametric identification modeling of MR fluid dampers. The damping force will be expressed as a function of the displacement, velocity and input voltage. This functional representation could then be used to predict the damping force for different operating conditions, under any desired combination of voltage, amplitude, and frequency of the excitation signals, within the limits of the interpolation. It should be noted that in this research the MR damper force is regarded as independent of temperature. In fact in [14] it is observed that this

assumption is reasonable over a broad temperature range (–40 to 150 ^{o}C). The identification and its validation will be done for both simulated data (from the modified Bouc–Wen model) and experimental data.

The experimental setup is described in the next section, which is followed by a brief background to the modified Bouc-Wen model. The Chebyshev polynomial fitting procedure and the results obtained are then presented.

4.2 MR fluid damper and test setup

An MR damper typically consists of a piston rod, electromagnet, accumulator, bearing, seal, and damper cylinder filled with MR fluid (Fig. 4.1). The magnetic field generated by the electromagnet changes the characteristics of the MR fluid, which consists of small magnetic particles in a fluid base. Consequently, the strength of the electromagnet's input current determines the physical characteristics of the MR dampers. The damper used in this research is the Lord RD-1005-3.

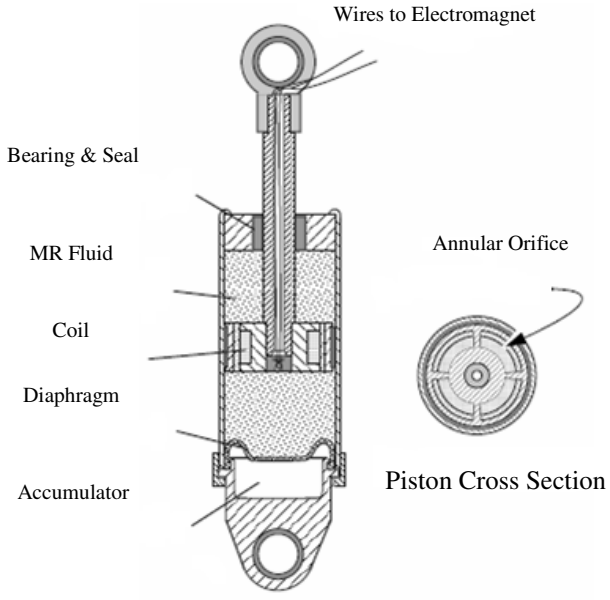

Fig. 4.1 Small scale MR fluid damper

Continuously variable damping is controlled by the increase in yield strength of the MR fluid in response to magnetic field strength. In this damper, MR fluid flows from a high pressure chamber to a low pressure chamber through an orifice in the piston head. The damper is 209 mm long in its extended position, and the main cylinder is 38 mm in diameter. The main cylinder houses the piston, the magnetic circuit, an accumulator, and 50 ml of MR fluid. The damper has a ± 52 mm stroke. The magnetic field, which is perpendicular to the fluid flow, is generated by a small electromagnet in the piston head. Forces of up to 3 kN can be generated with this device.

The MR damper was tested by using the Electro-Servo Hydraulic (ESH) tensile testing machine, as shown in Fig. 4.2(a). The schematic diagram of the test setup is illustrated in Fig. 4.2(b). The ESH test machine has an upper and lower head with grippers that can grasp the dampers in the proper place. The upper head is attached to the hydraulic cylinder that can move up, down and take an external signal. The lower head incorporates a load cell allowing the operator to measure the force applied to the MR damper. The MR damper is first mounted in its position by the grippers; preliminary tests are then conducted to measure the response of the damper under various operating conditions. In each test, the hydraulic actuator drives the upper head, while the lower head is held fixed, according to data sets displayed in Table 4.2.

An LVDT sensor was integrated with the test machine to measure the displacement of the damper. Also, an OPTIPACT speed sensor was installed to measure the damper piston velocity. The damping force, displacement, and velocity are measured

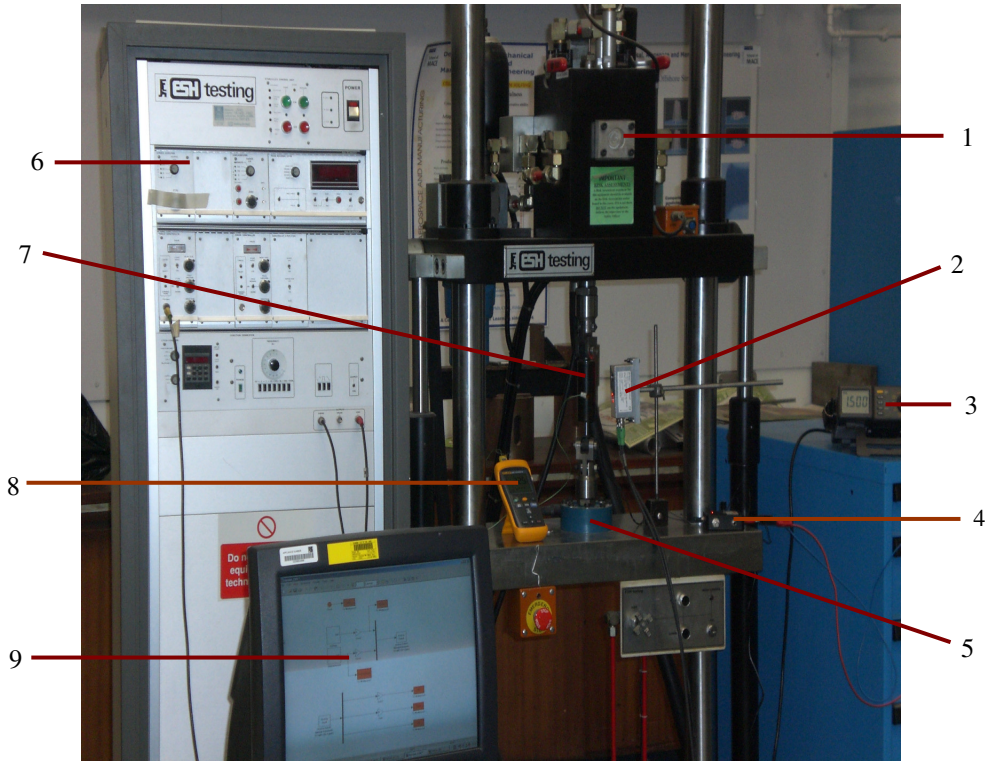

(a)

1- Hydraulic actuator **2- Velocity sensor** **3- Voltmeter** **4- Current driver**
5- Load cell **6- ESH Control panel** **7- MR damper** **8- Thermometer**
9- Computer **10- Moving head** **11- Fixed head** **12- Data acquisition card**
13- Power supply **14- Voltage signal** **15- Velocity signal**
16- Force signal **17- LVDT signal** **18- Displacement signal**

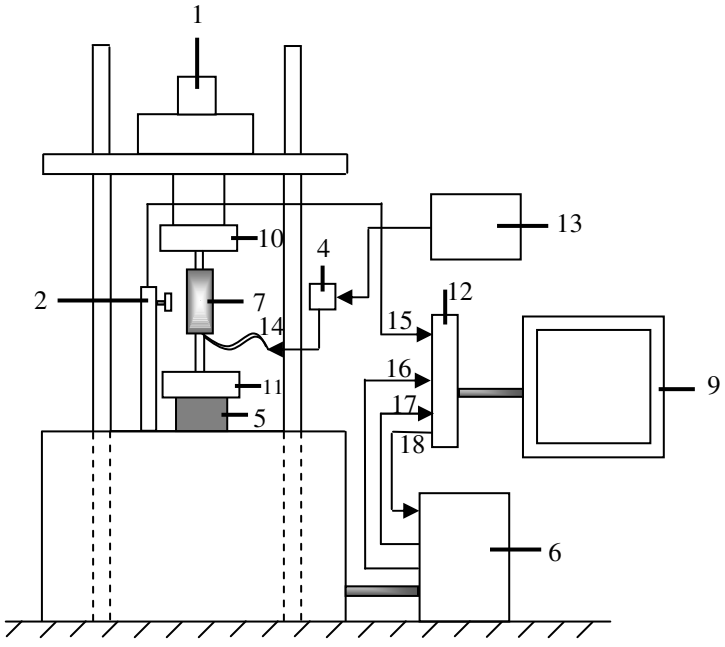

(b)

Fig. 4.2 Experimental Setup and ESH Machine
(a) Photo (b) Schematic Diagram

and fed through a data acquisition card to a PC computer. The current excitation was provided by a DC power supply and a thermocouple was also fixed on the damper body to assure that the test is accomplished within the range of 32 ± 10 ^{o}C.

4.3 The Modified Bouc-Wen Model

The mechanical idealization based on the modified Bouc-Wen model is illustrated in Fig. 4.3 [14]. The phenomenological model is governed by the following equations:

$$F = c_1\dot{y} + k_1(x - x_0) \tag{4.1}$$

$$\dot{y} = \frac{1}{c_0 + c_1}\{\alpha z + c_0\dot{x} + k_0(x - y)\} \tag{4.2}$$

$$\dot{z} = -\gamma|\dot{x} - \dot{y}||z|^{n-1}z - \beta(\dot{x} - \dot{y})|z|^{n} + \delta(\dot{x} - \dot{y}) \tag{4.3}$$

$$\alpha = \alpha(u) = \alpha_a + \alpha_b u \tag{4.4}$$

$$c_1 = c_1(u) = c_{1a} + c_{1b}u \tag{4.5}$$

$$c_0 = c_0(u) = c_{0a} + c_{0b}u \tag{4.6}$$

$$\dot{u} = -\eta(u - v) \tag{4.7}$$

In the above equations, x and F are the displacement and the force generated by the MR fluid damper respectively. y is the "internal displacement" of the MR fluid damper model, it is noted that this is a fictitious variable and does not correspond to an actual physical displacement. z is an evolutionary variable that accounts for the hysteresis effect, as discussed at the end of section 2.3.1. The variable u in the first order filter equation (4.7) is introduced to account for the effect of the command

voltage v sent to the current driver and η is the gain filter. The accumulator stiffness is represented by k_1; the viscous damping observed at large and low velocities are represented by c_0 and c_1, respectively. k_0 is present to control the stiffness at large velocities; x_0 is used to account for the effect of the accumulator. α is the scaling value for the modified Bouc–Wen model. The scale and shape of the hysteresis loop can be adjusted by γ, β, A and n.

A total of 14 model parameters [50], which are given in Table 4.1, are obtained to characterize the MR fluid damper using experimental data and a constrained nonlinear optimization algorithm. The modified Bouc-Wen model is the most popular model for studying the dynamic behavior of MR dampers theoretically. It is used in various engineering systems with different control strategies to implement the MR damper and study system performance.

Table 4.1 Parameters for the model of MR fluid damper [50]

PARAMETER	VALUE	PARAMETER	VALUE
c_{0a}	784 Nsm^{-1}	α_a	12441 Nm^{-1}
c_{0b}	1803 $NsV^{-1}m^{-1}$	α_b	38430 $NV^{-1}m^{-1}$
k_0	3610 Nm^{-1}	γ	136320 m^{-2}
c_{1a}	14649 Nsm^{-1}	β	2059020 m^{-2}
c_{1b}	34622 $NsV^{-1}m^{-1}$	A	58
k_1	840 Nm^{-1}	n	2
x_0	0.0245 m	η	190 s^{-1}

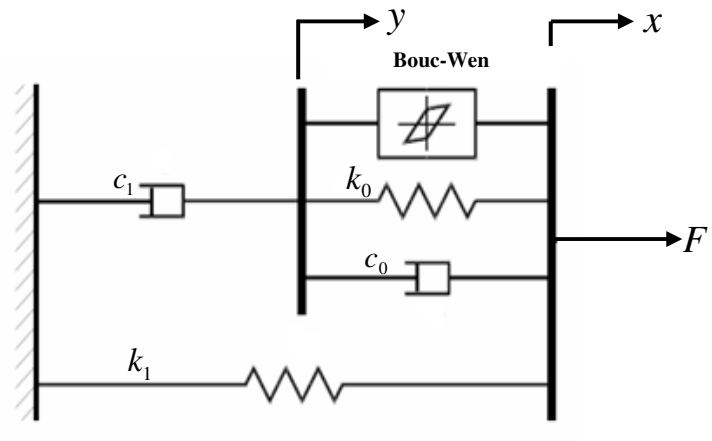

Fig. 4.3 Modified Bouc-Wen Model [14]

4.4 Chebyshev Polynomials Fits

As a function of three variables, the damping force can be approximated as triple series involving variables x, $\dot{x}$ and v.

$$F(x,\dot{x},v) \approx \hat{F}(x,\dot{x},v) = \sum_{k,l,z=0}^{K,L,Z} C_{klz} T_k(\tilde{x}) T_l(\tilde{\dot{x}}) T_z(\tilde{v}) \tag{4.8}$$

where C_{klz} are constants, T_k, T_l, T_z constitute the polynomial basis over which the force is projected and K, L, and Z are the polynomials' truncation orders. The coefficients C_{klz} can be determined by invoking the orthogonality properties of the chosen polynomials. The use of the Chebyshev polynomials makes the integrals required to evaluate these coefficients quite straightforward. These polynomials are given by:

$$T_n(\xi) = \cos(n \arccos(\xi)) \tag{4.9}$$

where $-1 \le \xi \le 1$ $n = 0,1,2,.....$

and satisfy the following weighted orthogonality property:

$$\int_{-1}^{1} w(\xi)T_n(\xi)T_m(\xi)d\xi = \begin{Bmatrix} 0 \\ \pi/2 \\ \pi \end{Bmatrix} \begin{matrix} n \neq m \\ n = m \neq 0 \\ n = m = 0 \end{matrix} \tag{4.10}$$

where $w(\xi) = (1-\xi^2)^{-1/2}$ is the weighting function. Note that this orthogonality property applies only when ξ is within the interval [-1, 1]. Therefore, the variables x, $\dot{x}$ and v have to be normalized, using the change of coordinates,

$$\eta = \frac{2x - x_{\max} - x_{\min}}{x_{\max} - x_{\min}};$$

$$\omega = \frac{2\dot{x} - \dot{x}_{\max} - \dot{x}_{\min}}{\dot{x}_{\max} - \dot{x}_{\min}}; \tag{4.11}$$

$$\psi = \frac{2v - v_{\max} - v_{\min}}{v_{\max} - v_{\min}}$$

The damping force fit is performed over data generated from not only numerically solving the modified Bouc-Wen model but also experimental dynamic results with an ESH test machine. Thus, the normalization limits $x_{\min}, x_{\max}, \dot{x}_{\min}, \dot{x}_{\max}$, $v_{\min}$, and $v_{\max}$ are defined beforehand. Obviously, these limits depend on the mechanical system in which the damping force is incorporated. Hence, in order to avoid incorrect evaluations of the damping force, the normalization limits should be set so that a wide range of instantaneous motions is covered. Using the Chebyshev polynomials as defined by Eq. 4.9 when estimating the damping force, one would better use the form

$$T_n(\xi) = \xi^n - \binom{n}{2}\xi^{n-2}\left(1-\xi^2\right) + \binom{n}{4}\xi^{n-4}\left(1-\xi^2\right)^2 - \ldots\ldots \tag{4.12}$$

Some particular Chebyshev polynomials derived from this formula are presented in the appendix A. It was observed during numerical tests that the use of Eq. (4.12) permits a certain level of extrapolation without distorting the values of the damping force. The presence of the arc-cosine in Eq. 4.9 prevents the normalized variables from exceeding the limit values of 1 and -1, thus preventing the possibility of extrapolation if this equation is employed [70].

The coefficients C_{klz} are obtained as follows. Consider the integral

$$A_{i,j,s} = \int_{-1}^{1}\int_{-1}^{1}\int_{-1}^{1} \hat{F}(\eta,\omega,\psi)T_i(\eta)T_j(\omega)T_s(\psi)w(\eta)w(\omega)w(\psi)d\eta d\omega d\psi \tag{4.13}$$

The substitution of the term $\hat{F}(\eta,\omega,\psi)$ by Eq. (4.8) yields

$$\begin{aligned} A_{i,j,s} = & \int_{-1}^{1}\int_{-1}^{1}\int_{-1}^{1} C_{0,0,0}T_0(\eta)T_i(\eta)T_0(\psi) \\ & * T_j(\omega)T_0(\psi)T_s(\psi) * w(\eta)w(\omega)w(\psi)d\eta d\omega d\psi \\ & + \int_{-1}^{1}\int_{-1}^{1}\int_{-1}^{1}\sum_{k=1}^{K}\sum_{l=1}^{L}\sum_{z=1}^{Z} C_{k,l,z} * T_k(\eta)T_i(\eta)T_l(\psi) \\ & * T_j(\eta)T_z(\omega)T_s(\psi) * w(\eta)w(\omega)w(\psi)d\eta d\omega d\psi \end{aligned} \tag{4.14}$$

Utilizing the orthogonality property, Eq. 4.10, it follows

$$A_{0,0,0} = \pi^3 C_{0,0,0} \quad \text{for} \quad i,j,s = 0 \tag{4.15a}$$

$$A_{i,j,s} = \sum_{k=1}^{K}\sum_{l=1}^{L}\sum_{z=1}^{Z} C_{k,l,z}(\pi/2)^3\delta_{ik}\delta_{jl}\delta_{sz} = (\pi/2)^3 C_{i,j,s} \quad \text{for} \quad i,j,s \neq 0 \tag{4.15b}$$

where δ_{ik} is the Kronecker delta. From Eqs. (4.13), (4.14), (4.15a), and (4.15b), the following general expression can be derived for the coefficients C_{klz}:

$$C_{k,l,z} = \frac{8}{(1+\delta_{k0})(1+\delta_{l0})(1+\delta_{z0})\pi^3} \int_{-1}^{1}\int_{-1}^{1}\int_{-1}^{1} \hat{F}(\eta,\omega,\psi) \tag{4.16}$$

$$* T_k(\eta) T_l(\omega) T_z(\psi) w(\eta) w(\omega) w(\psi) d\eta d\omega d\psi$$

These integrals can be performed by the Gauss-Chebyshev quadrature method. The coordinates of the points used in the integration ('grid points') are defined by:

$$\eta_i = \cos\left(\frac{2i-1}{2Q_\eta}\pi\right) \quad i = 1,2,....,Q_\eta$$

$$\omega_j = \cos\left(\frac{2j-1}{2Q_\omega}\pi\right) \quad j = 1,2,....,Q_\omega \tag{4.17}$$

$$\psi_s = \cos\left(\frac{2s-1}{2Q_\psi}\pi\right) \quad s = 1,2,....,Q_\psi$$

The evaluation of the Chebyshev polynomials and the weighting function at the quadrature points in the integral (4.16) yields

$$C_{k,l,z} = \frac{8}{(1+\delta_{k0})(1+\delta_{l0})(1+\delta_{z0})Q_\eta Q_\omega Q_\psi}$$

$$* \sum_{i=1}^{Q_\eta}\sum_{j=1}^{Q\omega}\sum_{s=1}^{Q\psi} \hat{F}(\eta_i,\omega_j,\psi_s) \cos\left(\frac{2i-1}{2Q_\eta}k\pi\right) \tag{4.18}$$

$$* \cos\left(\frac{2j-1}{2Q_\omega}l\pi\right) * \cos\left(\frac{2s-1}{2Q_\psi}z\pi\right)$$

The determination of the coefficients C_{klz} from the above expression requires the values of the damper force at the grid points i.e. $\hat{F}(\eta_i, \omega_j, \psi_s)$. These are found as follows. For the voltage corresponding to each particular ψ_s, $s = 1,2,....,Q_\psi$, a surface can be constructed showing the force as a function of displacement and velocity. Using the 2D-interpolation function *griddata* available in MATLAB, one can determine the $Q_\eta \times Q_\omega$ grid forces on the constant voltage surface corresponding to each ψ_s i.e. $\hat{F}(\eta_i, \omega_j, \psi_s)$, $i = 1,2,....,Q_\eta$, $j = 1,2,....,Q_\omega$.

4.5 Results: Identification from Bouc-Wen

Prior to performing the 3D interpolation, a 2D interpolation of the damper force as a function of displacement and velocity for a fixed voltage of 1.5V was performed. The purpose of this was to determine the best way to generate the above described constant voltage surfaces. Such a surface could be generated in two alternative ways: (i) by "weaving" the surface from the results obtained from a series of tests conducted with prescribed sinusoidal displacement signals, all at the same frequency but of different amplitudes, as per data set 1 of Table 4.2; (ii) by "weaving" the surface from the results obtained from a series of tests conducted with prescribed sinusoidal displacement signals, all at the same amplitude but at different frequencies, as per data set 2 of Table 4.2

Figure 4.4 shows the generated surface plot produced by the modified Bouc-Wen model according to method of data set 1 of Table 4.2, the forces at the grid points

being indicated by circles. These were used to calculate the 20×20 coefficients. The 2D-interpolation with 20×20 terms was then validated against the modified Bouc-Wen results for the validation data set 1 of Table 4.3 with A = 0.007 m. Figure 4.5 demonstrates good agreement between Chebyshev and Bouc-Wen, thus indicating that the proposed technique is able to predict the hysteresis force of the MR fluid damper accurately and efficiently.

Table 4.2 Definition of data sets for constant voltage surface generation

Set	Displacement (m)	Voltage (V)	Time Span (s)	Kind of Fit
1	A sin(4πt)[a]	1.5	2	2D
2	sin(2kπt)[b]	1.5	2	2D
3	A sin(4πt)[a]	V[c]	2	3D

[a] A = (0.02 : 0.02 : 1)*10^{-2} m

[b] k = (0.2 : 0.2 : 10) Hz

[c] V = (0.5 : 0.5 : 5) V

Table 4.3 Definition of validation sets

Set	Displacement (m)	Voltage (V)	Time Span (s)	Kind of Fit
1	A sin(4πt)	1.5	2	2D
2	sin(2kπt)	1.5	2	2D
3	A sin(4πt)	V	2	3D
4	A sin(4πt)	2+2sin(2kπt)	2	3D
5	A sin(4πt)	GWN[d] + E	2	3D

[d] Gaussian white noise (frequency: 0-2 Hz; amplitude: $\pm$ 2 V)

In addition to the graphical evidence of the effectiveness of the proposed model, a quantitative analysis of the errors for the validation point has been examined. The normalized errors between the Chebyshev prediction and Bouc-Wen simulation can be effectively expressed. According to Fig. 4.5(a), the root mean square values of the simulated and predicted forces are 544.33 and 532.23 respectively. This difference of approximately 2.22% is acceptable.

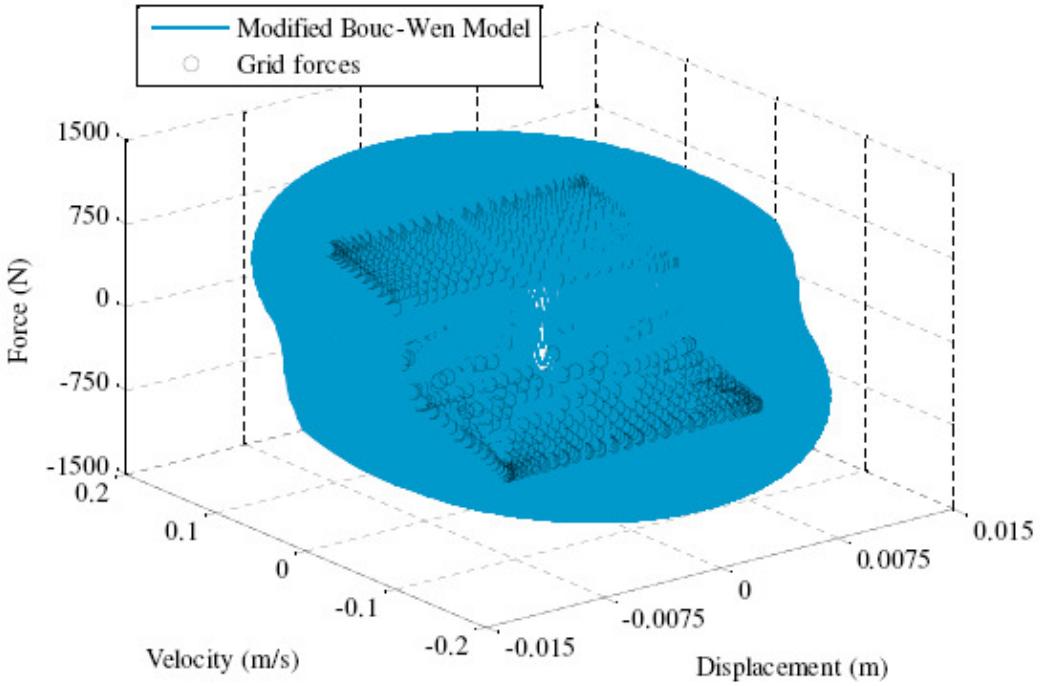

Fig. 4.4 Surface plot of damping force generated by modified Bouc-Wen according to data set 1

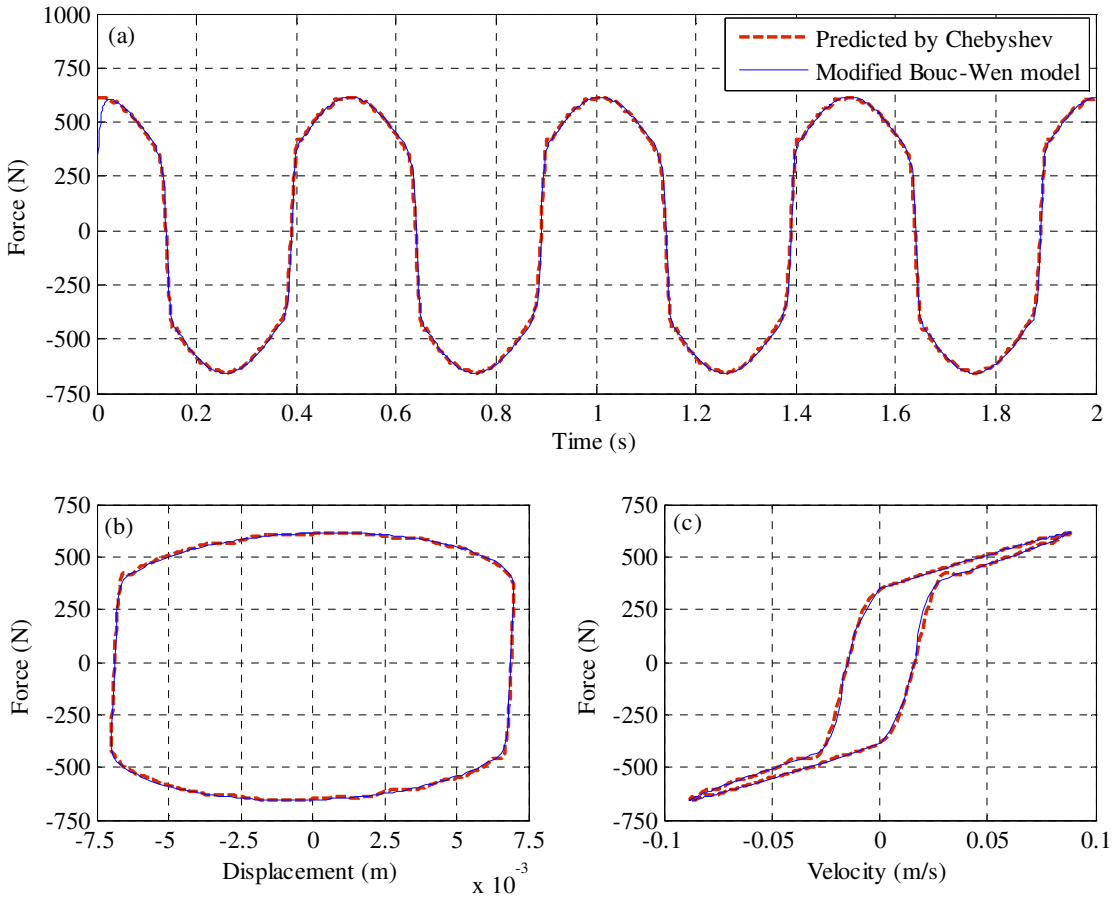

Fig. 4.5 Validation of interpolation procedure derived from surface plot in Fig. 4.4
(a) Force (b) Force-displacement loop (c) Force-velocity loop

Figure 4.6 shows the surface plot at 1.5 V generated according to the method of data set 2 of Table 4.2. The grid points on this surface were used to calculate the 20×20 coefficients. The 2D-interpolation with 20×20 terms was then validated against the modified Bouc-Wen results for the validation data set 2 of Table 4.3 with k=3 Hz, as shown in Fig. 4.7. From Figs. 4.5 and 4.7, it is clearly seen that the Chebyshev polynomials fit predicts the behaviour of the damper accurately and it is unaffected by the way the surface plot used to derive the interpolation coefficients is generated, whether by amplitude variation or frequency variation. Figures 4.5 and 4.7 indicate that the results obtained by the amplitude variation method are slightly more accurate than the frequency variation method. Hence, the former method will be used for the 3D-interpolation, as indicated by data set 3 of Table 4.2.

For the 3D-interpolation, in Eqs. (4.17 and 4.18), $Q_\eta,\ Q_\omega,\ Q_\psi = 20, 20, 10$ respectively, so 10 constant voltage surfaces were generated by the modified Bouc-Wen model, each surface at different input voltage corresponding to ψ_s, $s = 1,2,....,Q_\psi$. Figures 4.8(a, b, and c) show a sample surface plots (3 from 10) at 0.5, 2.5, and 4.5 input voltages respectively.

From these surfaces, the $20\times20\times10$ interpolation coefficients were determined. The 3D-interpolation with $20\times20\times10$ terms was then validated against the modified Bouc-Wen results for the validation data set 3 of Table 4.3 with A = 0.008 m, V = 3 V, as shown in Fig. 4.9. It is noted that the loop crossover at the corners of the hysteresis loop (Fig. 4.9 c) is merely a mathematical artefact introduced by the Chebyshev interpolation and may not be related to any physical behaviour.

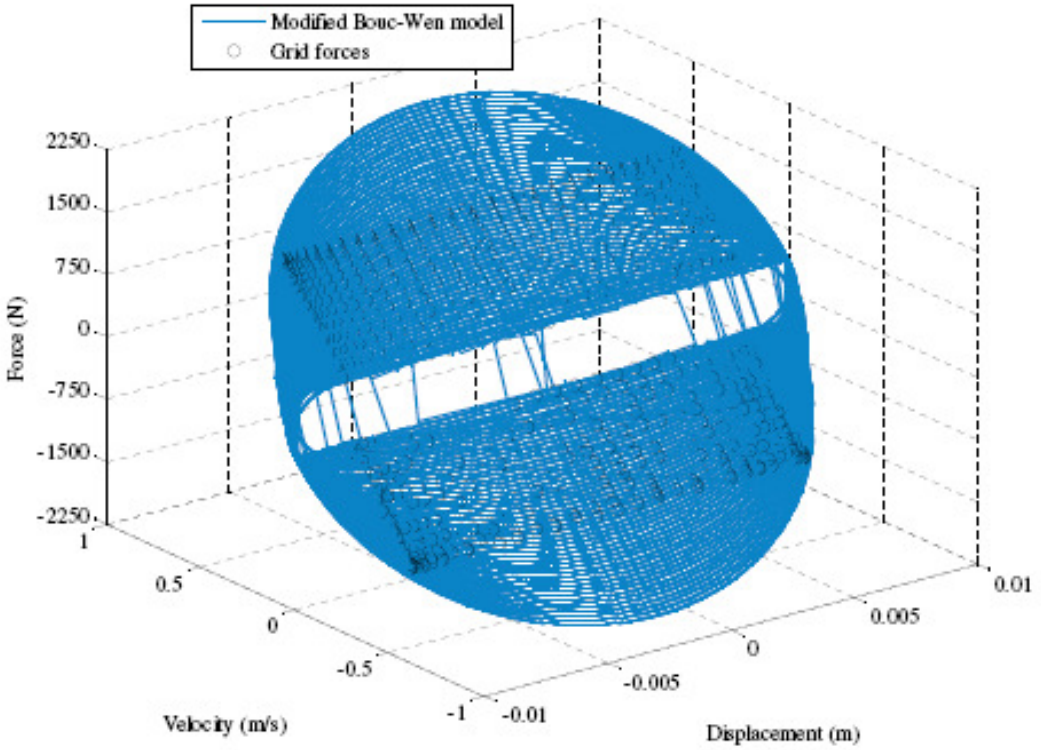

Fig. 4.6 Surface plot of damping force generated by modified Bouc-Wen according to data set 2

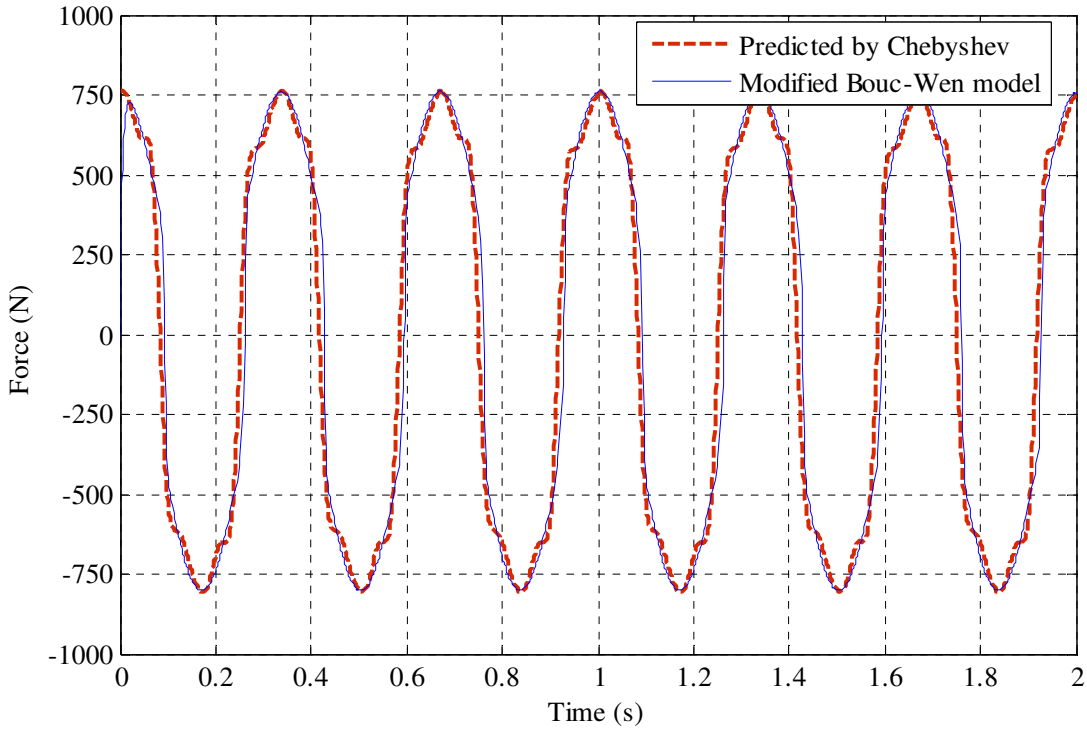

Fig. 4.7 Validation of interpolation procedure derived from surface plot in Fig. 4.6

Further validation of the 3D-interpolation was sought for the conditions of set 4 and set 5 of Table 4.3. Set 4 used a sinusoidal signal for both displacement and input voltage. A comparison between the modified Bouc-Wen model and the prediction by Chebyshev polynomials fit for this set with A = 0.01 m, k = 2 Hz is shown in Fig. 4.10. Validation set 5 of Table 4.3 used a sinusoidal displacement and a Gaussian white noise input voltage signals. Figure 4.11 shows a comparison between the modified Bouc-Wen model and the prediction by Chebyshev polynomials fit with A = 0.008 m, E = 2.5 V. It is shown that the results generated by the proposed model are in good agreement with the theoretical behavior based on the modified Bouc-Wen model.

4.6 Results: Identification from Experiment

A similar study of the MR fluid damper based on the experimental response, obtained by using ESH testing machine, was done to validate the Chebyshev interpolation. The surface plots required for identification were generated by driving the machine according to the different data sets defined in Table 4.2. Figure 4.12 illustrates the generated surface plot produced by driving the ESH testing machine according to data set 1 and the forces at the grid points are illustrated by circles. These grid forces were used to calculate the interpolation coefficients. A comparison between the prediction by Chebyshev polynomials fits with 18×18 terms and the experimental behavior of the MR damper for validation set 1 of Table 4.3 with A = 0.007 m is shown in Fig. 4.13. The examination of Fig. 4.13 reveals that a good agreement exists between the experiments and predicted results according to validation set 1.

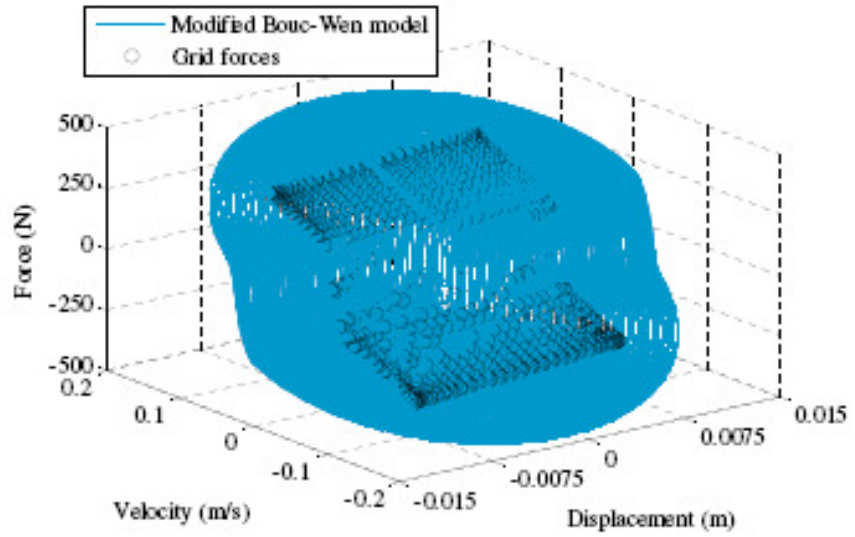

(a) at V = 0.5 V.

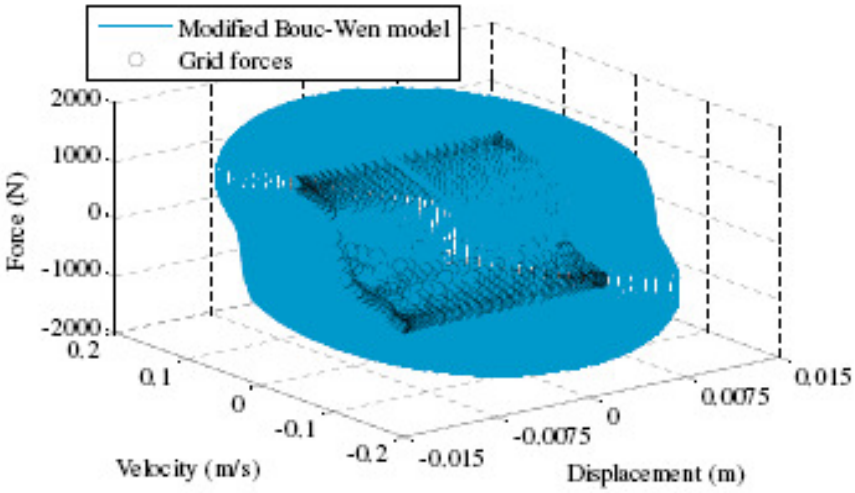

(b) at V = 2.5 V.

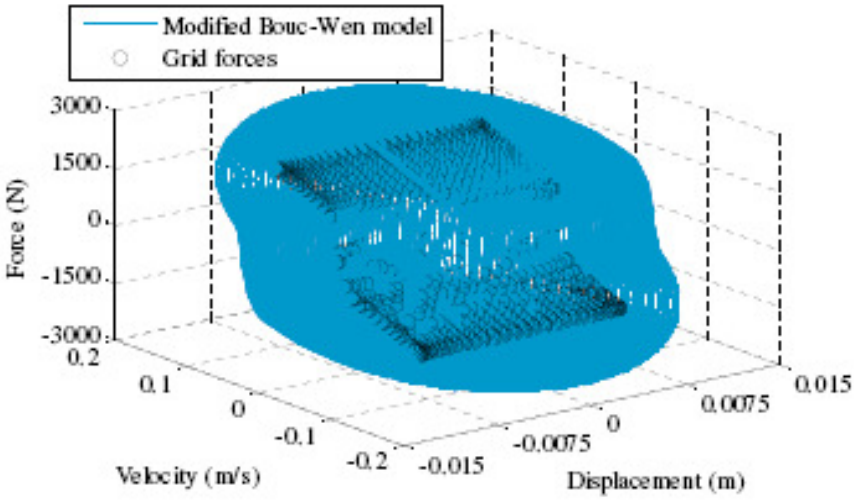

(c) at V = 4.5 V.

Fig. 4.8 Surface plots of damping force generated by modified Bouc-Wen according to set 3

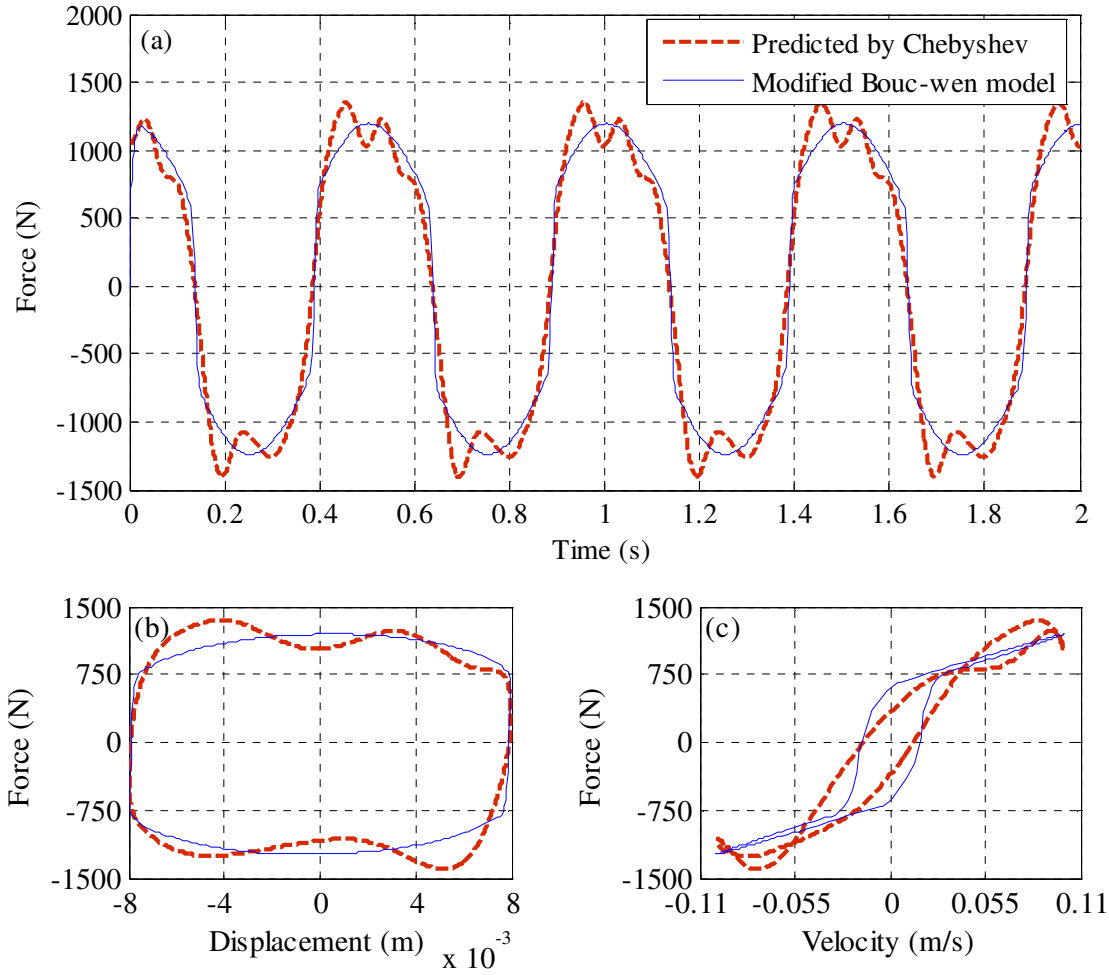

Fig. 4.9 Validation of interpolation procedure derived from surface plot in Fig. 4.8
(a) Force (b) Force-displacement loop (c) Force-velocity loop

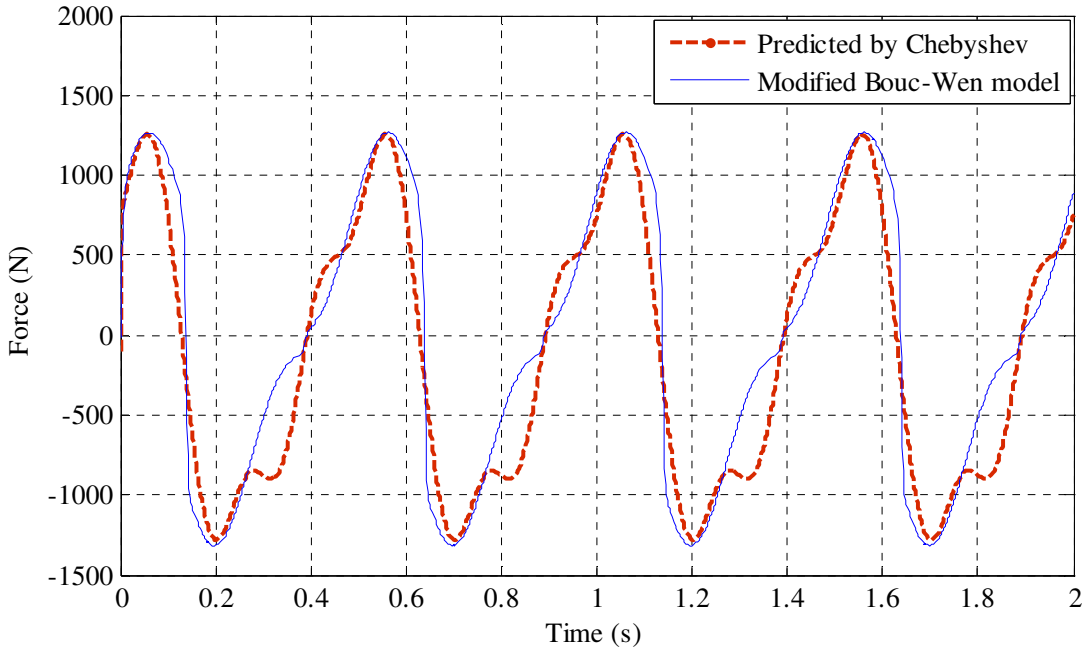

Fig. 4.10 Validation of interpolation procedure according to set 4 of Table 4.3

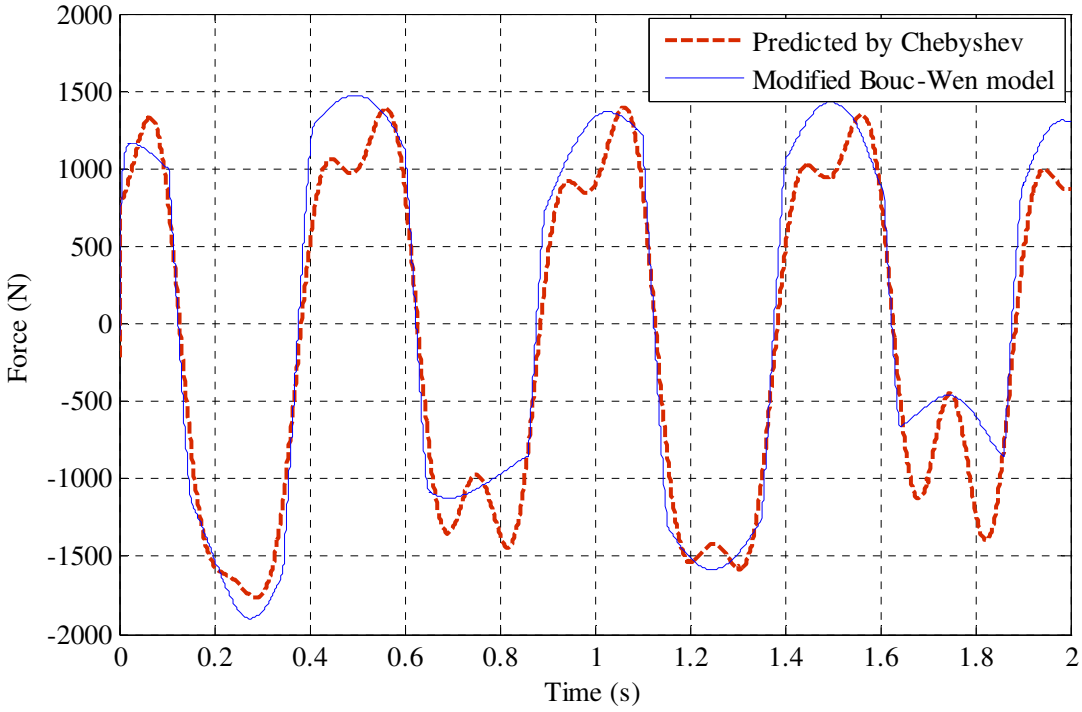

Fig. 4.11 Validation of interpolation procedure according to set 5 of Table 4.3

Figure 4.14 shows an experimental surface plot generated according to the method data set 2 of Table 4.2. A comparison between the prediction by the Chebyshev polynomials fits with 18×18 terms and the experimental response of the MR damper for validation set 1 of Table 4.3 with k = 2Hz is shown in Fig. 4.15. Comparison of Fig. 4.15 with Fig. 4.13 again shows that the constant frequency/variable amplitude method for generation of the constant voltage surface produces slightly better results than the variable frequency/constant amplitude method.

The surfaces required for the 3D-fit were produced as per data set 3 of Table 4.2. Figures 4.16(a, b, and c) show some sample surface plots (3 from 10) at 0.5, 2.5, and 4.5 input voltages. From these surfaces, the $20\times20\times10$ interpolation coefficients were determined. Figure 4.17 shows the predicted results obtained using Chebyshev

polynomials fits (18×18×8 terms) with the experimental behaviour for the validation set 3 of Table 4.3 with A = 0.008 m, V = 3 V.

Further validation was again obtained as per data set 4 and set 5 of Table 4.3. Figure 4.18 compares the experimental response for data set 4 with A = 0.003 m, k = 2 Hz and the Chebyshev polynomials fit prediction (18×18×8 terms). Figure 4.19 shows a comparison between the experimental behaviour and the prediction by Chebyshev polynomials fit for data set 5 with A = 0.0025 m, E = 2 V. In both cases there is reasonably good agreement between the predicted and experimental results.

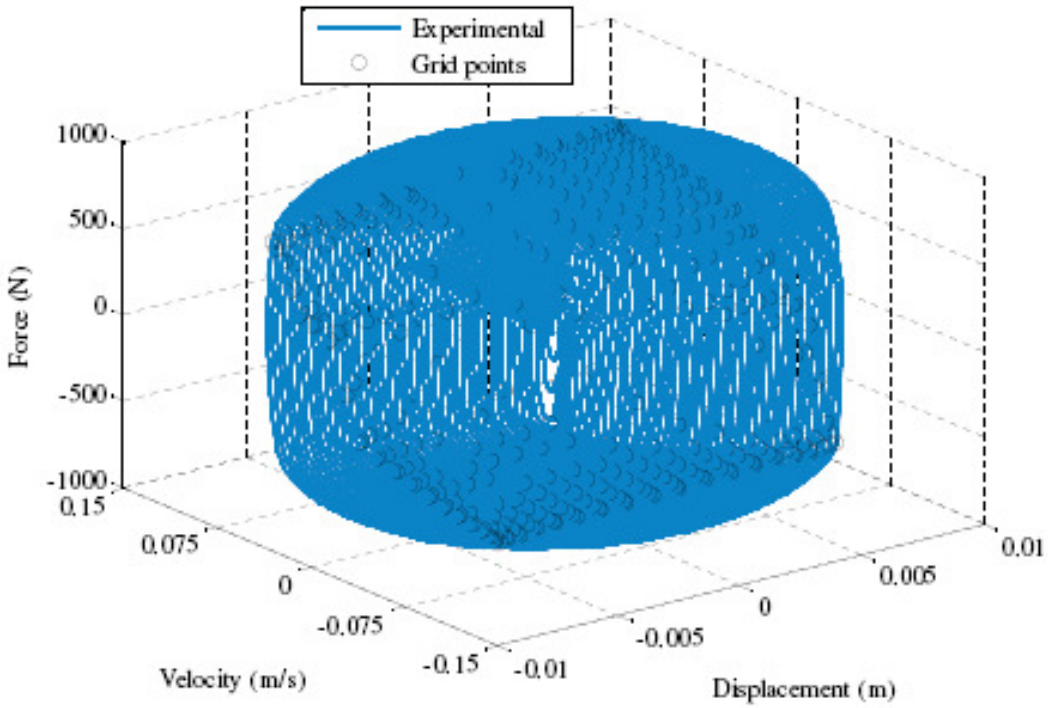

Fig. 4.12 Surface plots of damping force generated by ESH testing machine according to set 1

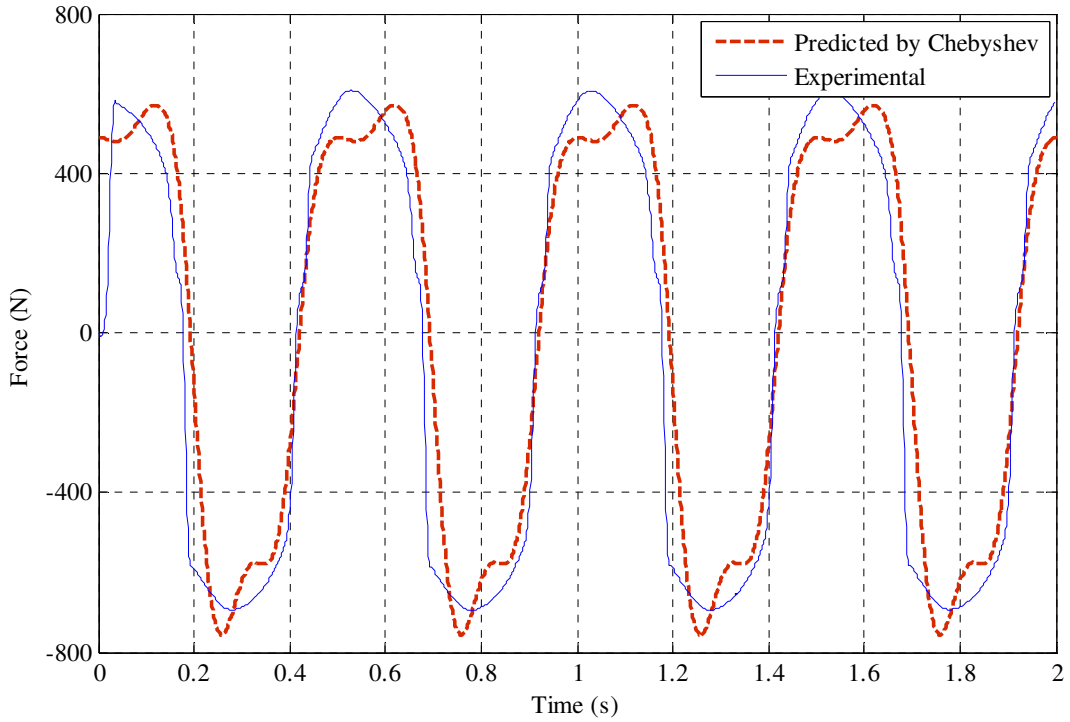

Fig. 4.13 Validation of interpolation procedure derived from surface plot in Fig. 4.12

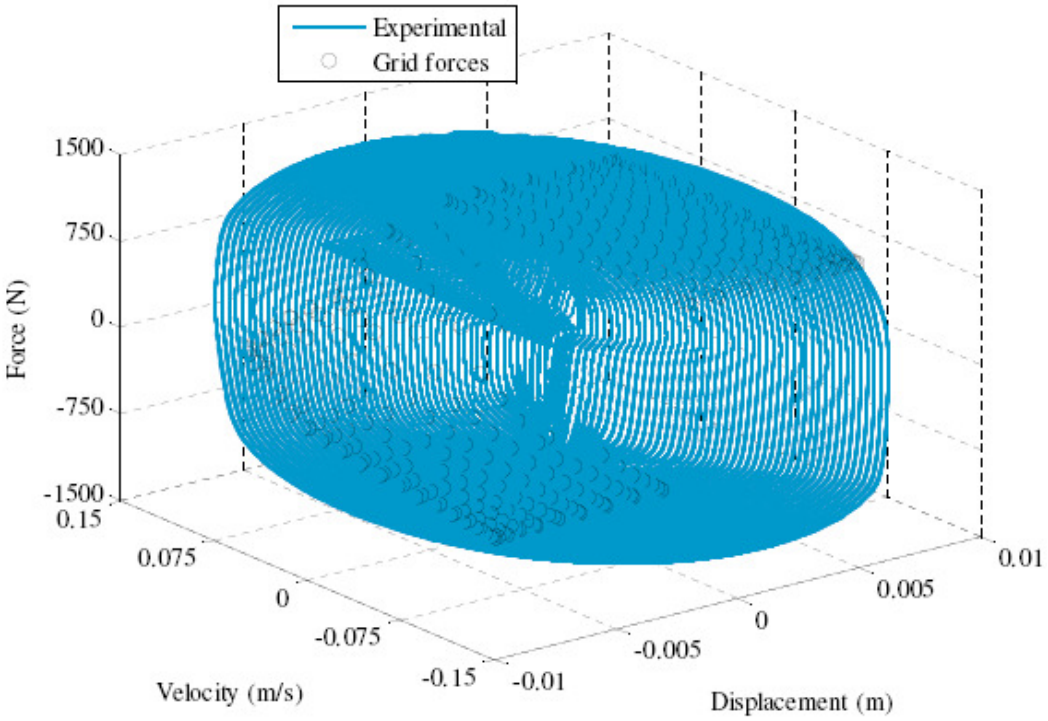

Fig. 4.14 Surface plots of damping force generated by ESH testing machine according to set 2

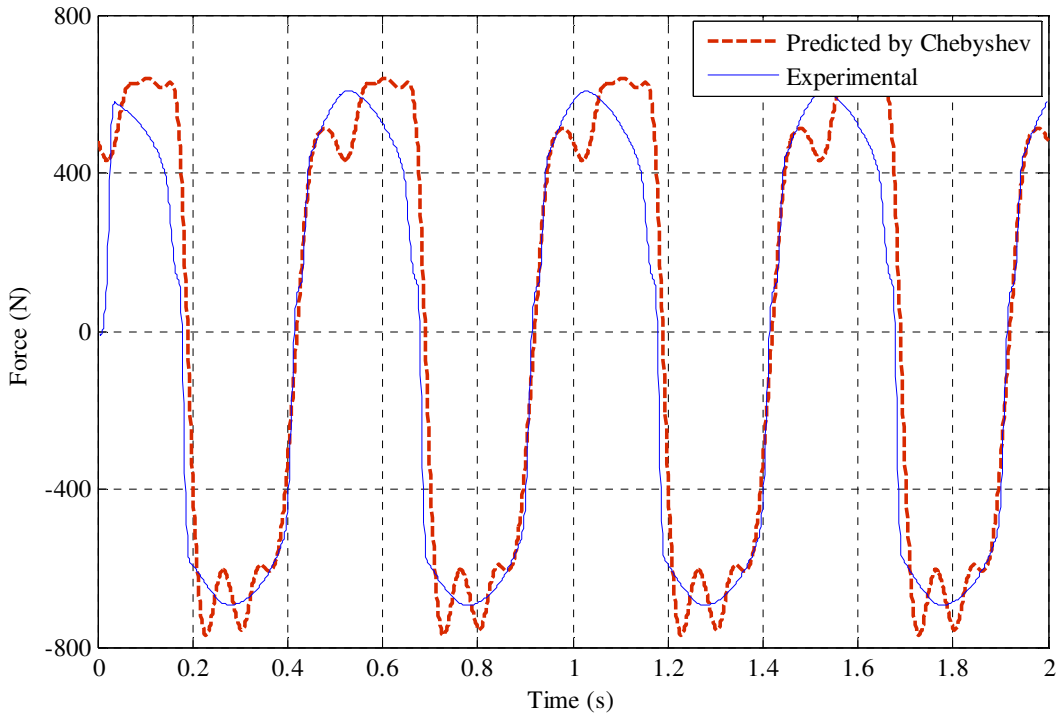

Fig. 4.15 Validation of interpolation procedure derived from surface plot in Fig. 4.14

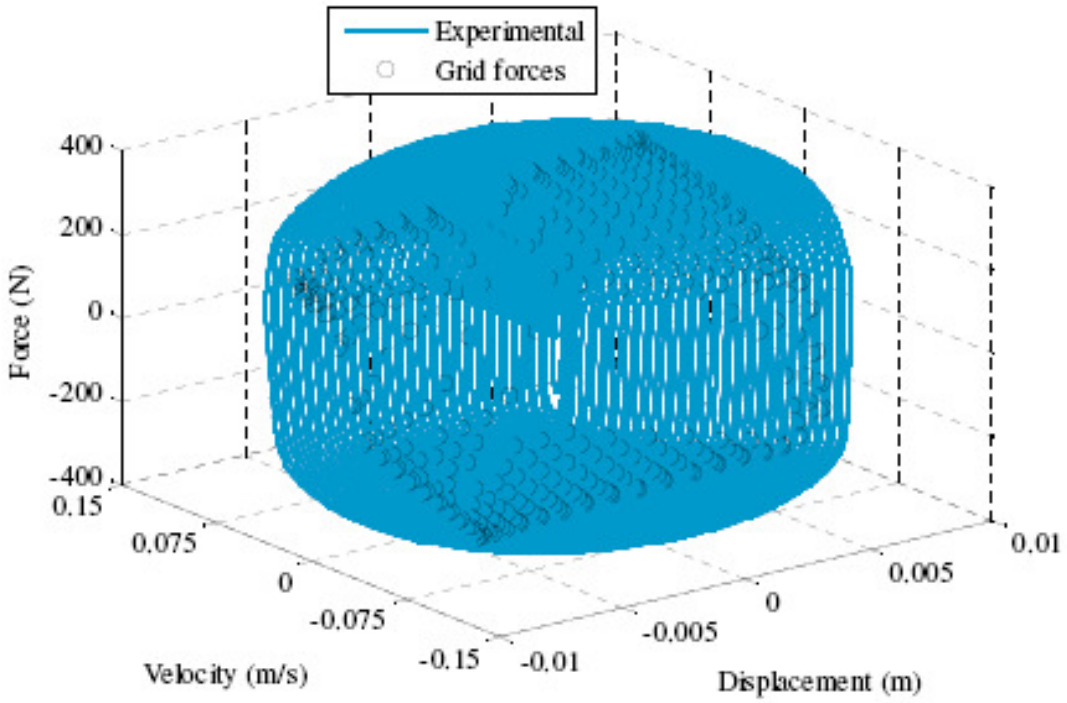

(a) at V = 0.5 V.

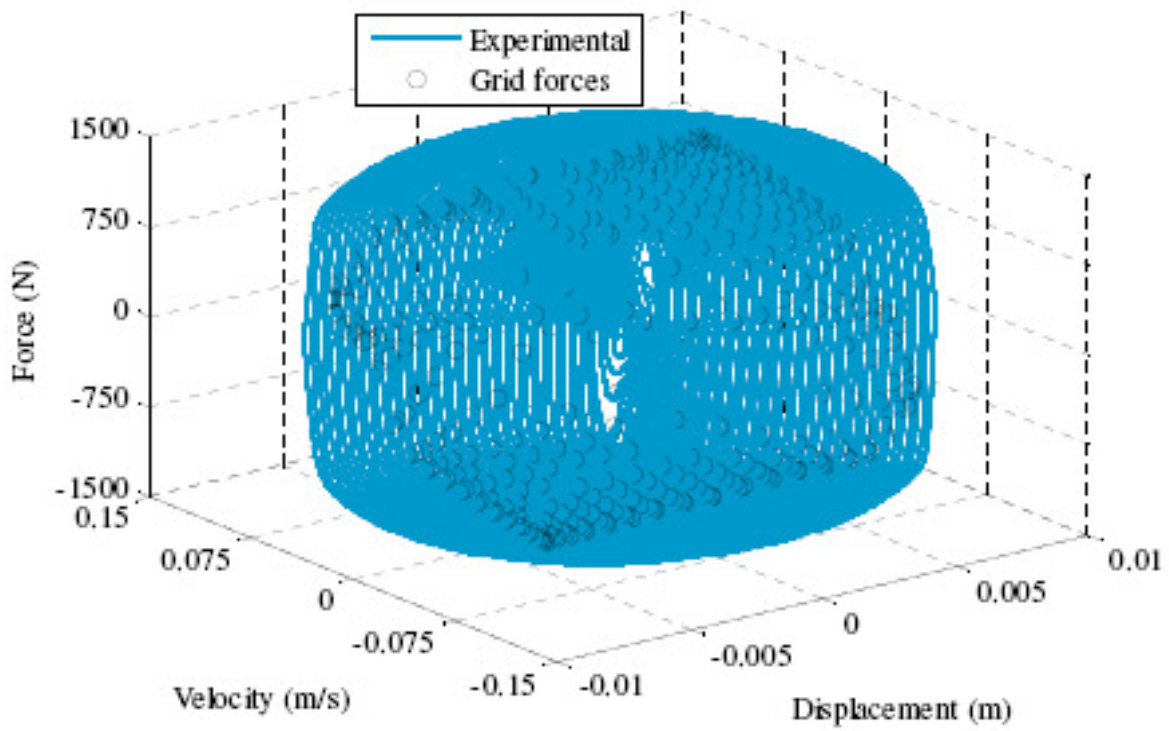

(b) at V = 2.5 V.

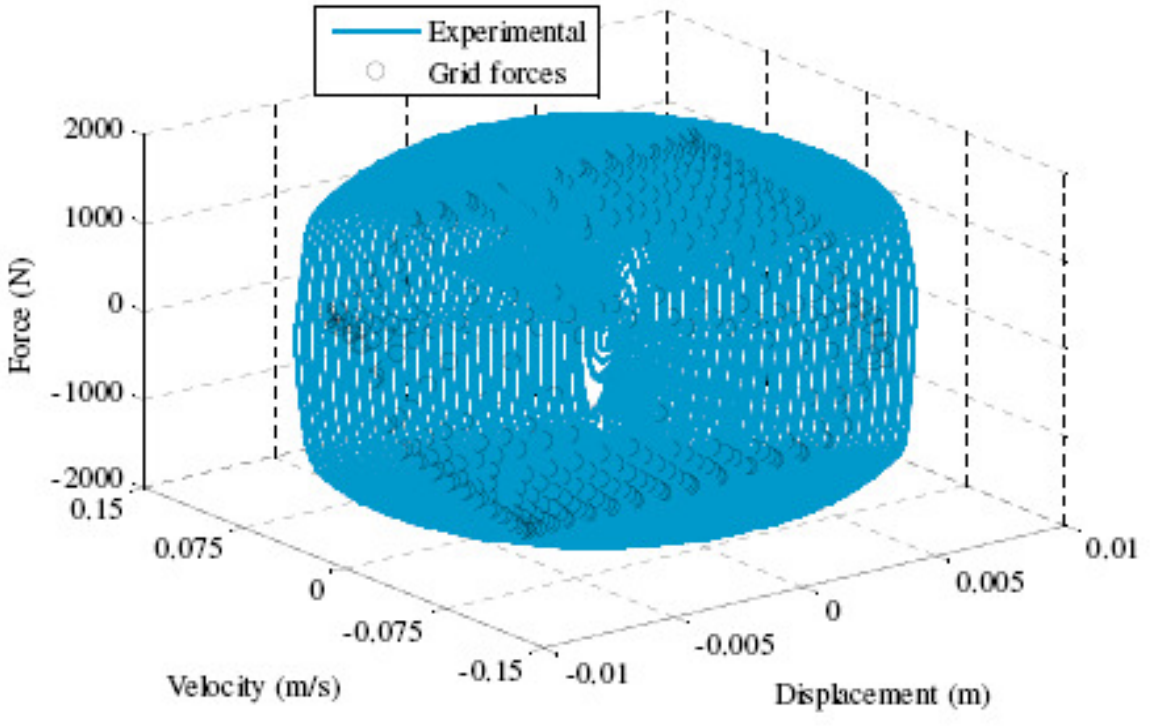

(c) at V = 4.5 V.

Fig. 4.16 Surface plots of damping force generated by ESH testing machine according to set 3

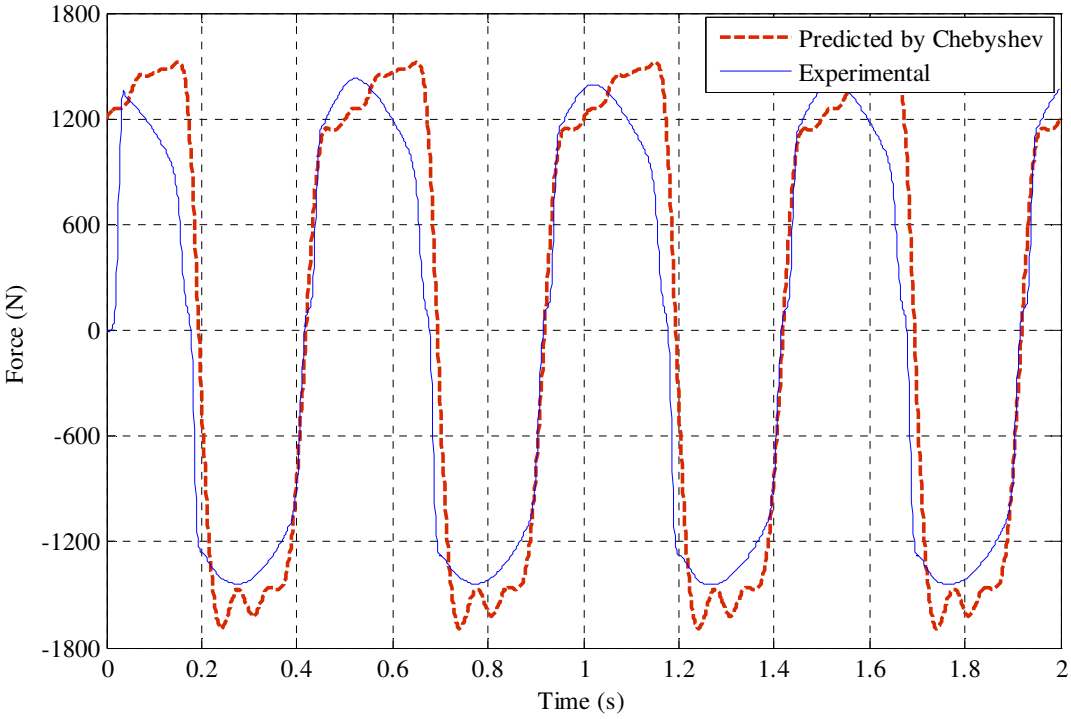

Fig. 4.17 Validation of interpolation procedure derived from surface plot in Fig. 4.16

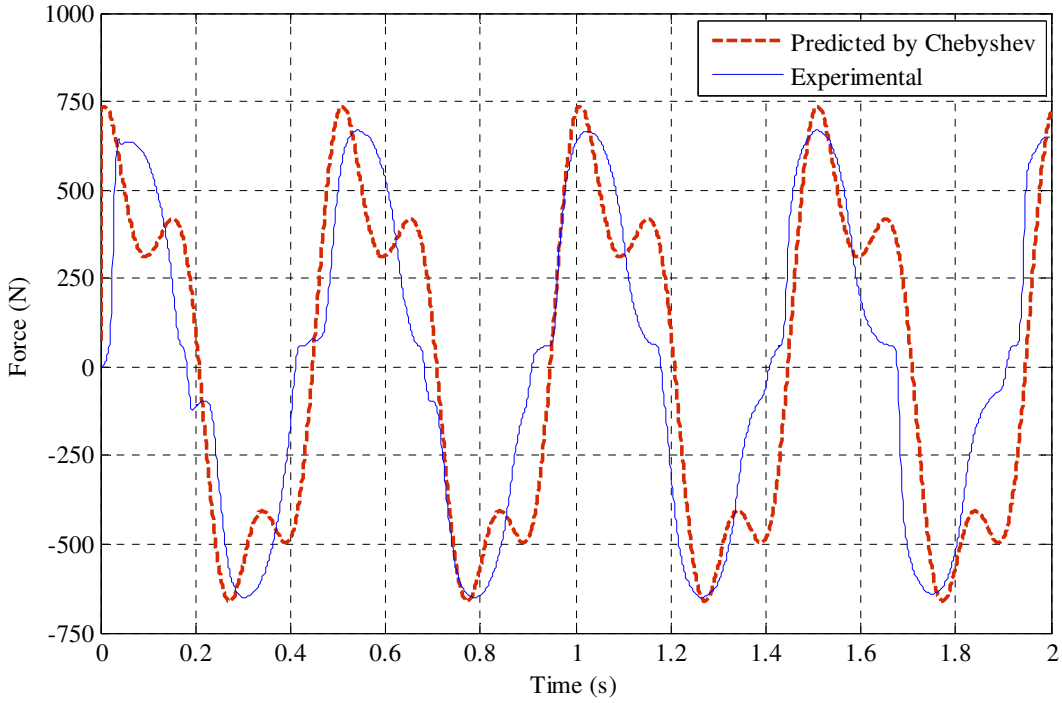

Fig. 4.18 Validation of interpolation procedure according to set 4 of Table 4.3

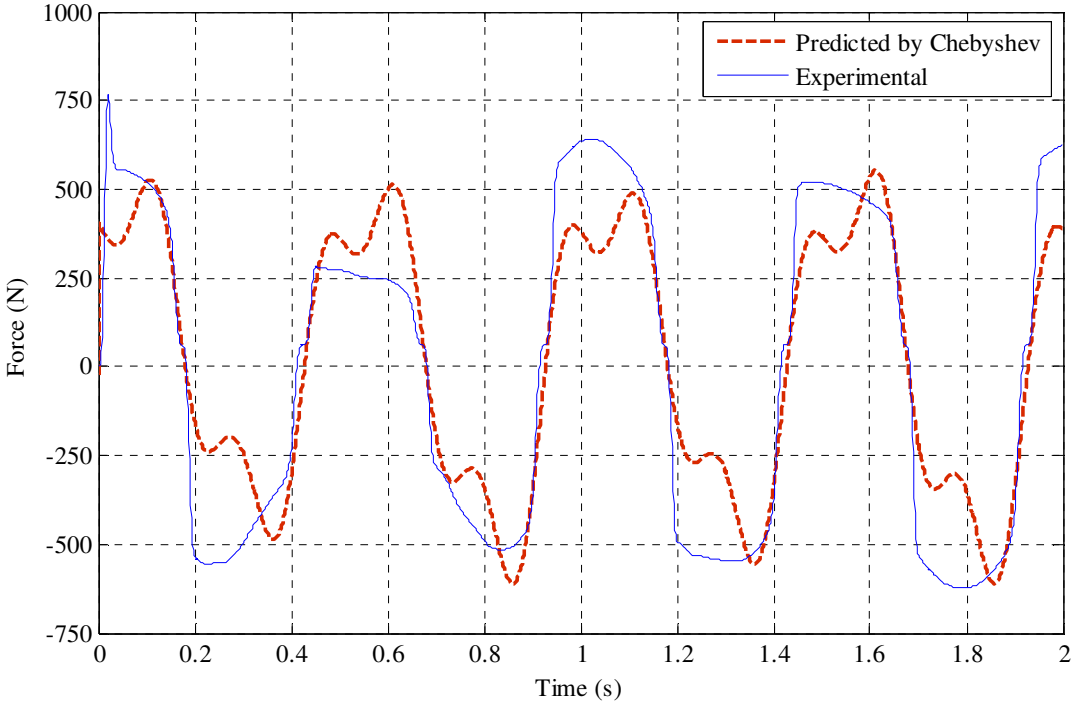

Fig. 4.19 Validation of interpolation procedure according to set 5 of Table 4.3

4.7 Conclusions

In this paper, a non-parametric identification technique based on Chebyshev interpolation has, for the first time, been applied to a Magnetorheological (MR) damper. The technique allows an explicit representation of the MR damper force in terms of the instantaneous values of input displacement, velocity, and voltage. The results obtained by Chebyshev interpolation of the MR damper were presented for different operating conditions. These results showed favorable agreement with those obtained by both the modified Bouc-Wen model and by experimental testing. The proposed technique has therefore been shown to be a fast and reliable system identification method, able to estimate the damping force under any desired combination of voltage, amplitude, and frequency of the excitation.

4.8 Definitions

Symbol	Meaning
F	Damping force
x	Displacement
$\dot{x}$	Velocity
v	Command voltage
u	Output of a first order filter
y	Internal displacement
k_1	Accumulator stiffness
k_0	Stiffness at large velocity
c_1	Viscous damping at low velocity
c_0	Viscous damping at large velocity
x_0	Accumulator effect
α	Scaling value for the Bouc–Wen model
γ, β, A, n	Scale and shape of the hysteresis loop
$F(x, \dot{x}, v)$	Damping force as a function of displacement, velocity, and input voltage
$\hat{F}(x, \dot{x}, v)$	Predicted force as a function of displacement, velocity, and input voltage
C_{klz}	Chebyshev coefficients
T_k, T_l, T_z	Polynomial basis
K, L, Z	Polynomials truncation orders
w	Weighting function
ξ	Factor for orthogonality property
$\hat{F}(\eta, \omega, \psi)$	Damping force at the quadrature points
δ_{ik}	Kronecker delta
Q_η	Number of quadrature points
A	Displacement Amplitude
k	Frequency
GWN	Gaussian white noise

4.9 Comment*

The proven approximate explicit functional representation of force (in terms of instantaneous displacement, velocity and voltage) allows a rapid means of estimating the damping force for any desired combination of voltage, amplitude and frequency of the excitation. However, it was found rather difficult to use a similar technique for the inverse dynamic model of the MR damper. The inverse model is necessary for MR damper control since it outputs the voltage required for a desired force under given mechanical inputs. The following chapter shows that the inverse model is easily identified through neural networks. Moreover, it is also important to note that the above-described representation is an *equivalent nonlinear model* of the direct (forward) dynamics since it has no memory, as discussed in section 2.3.2. The following chapter uses validation tests similar to this chapter and it will be evident from the results that neural networks (that incorporate memory) are superior to the Chebyshev approach even for the direct model. For these reasons, the author opted to use a neural network model of the MR damper, instead of Chebyshev representation, for the remainder of his research.

* Not part of paper.

CHAPTER 5

The Experimental Identification of Magneto-rheological Dampers and Evaluation of their Controllers

Authors:

Hassan Metered, Philip Bonello and S Olutunde Oyadiji

Reformatted version of paper published in:

Mechanical systems and signal processing, 2010, Volume: 24 (4), pp 976–994.

Abstract

Magnetorheological (MR) fluid dampers are semi-active control devices that have been applied over a wide range of practical vibration control applications. This paper concerns the experimental identification of the dynamic behaviour of an MR

damper and the use of the identified parameters in the control of such a damper. Feed-forward and recurrent neural networks are used to model both the direct and inverse dynamics of the damper. Training and validation of the proposed neural networks are achieved by using the data generated through dynamic tests with the damper mounted on a tensile testing machine. The validation test results clearly show that the proposed neural networks can reliably represent both the direct and inverse dynamic behaviours of an MR damper. The effect of the cylinder's surface temperature on both the direct and inverse dynamics of the damper is studied, and the neural network model is shown to be reasonably robust against significant temperature variation. The inverse recurrent neural network model is introduced as a damper controller and experimentally evaluated against alternative controllers proposed in the literature. The results reveal that the neural-based damper controller offers superior damper control. This observation and the added advantages of low power requirement, extended service life of the damper and the minimal use of sensors, indicate that a neural-based damper controller potentially offers the most cost-effective vibration control solution among the controllers investigated.

Key Words: Magnetorheological damper; Damper controller; Semi-active control; Neural network

5.1 Introduction

Magnetorheological (MR) fluid dampers are semi-active control devices that have received considerable interest due to their mechanical simplicity, high dynamic range, low power requirements, large force capacity and robustness. MR fluids respond to a magnetic field with a significant change in rheological behavior. These

fluids can reversibly and instantaneously change from a free-flowing liquid to a semi-solid with controllable yield strength when exposed to a magnetic field [1]. MR dampers have been applied over a wide range of vibration control applications: from automobiles [2, 3] to railway vehicles [4] and civil structures such as buildings [5, 6]. This paper concerns the identification techniques for modelling the dynamic behaviour of an MR damper and their use in the control of such a damper.

Identification techniques can be broadly classified into two categories: parametric and non-parametric techniques. Parametric models are based on mechanical idealization involving representation by an arrangement of springs and viscous dashpots [14, 50, 67-69]. The most parametric model for the identification of an MR damper is the modified Bouc–Wen model [14]. This is a semi-empirical relationship in which 14 parameters are determined for a given damper through curve fitting of experimental results. Parametric models are useful for direct dynamic modelling of MR dampers i.e. the prediction of the damper force for given inputs (voltage signal and the time history of the relative displacement across the damper's ends).

Unlike parametric models, nonparametric models do not make any assumptions on the underlying input/output relationship of the system being modelled. Consequently, an elevated amount of input/output data has to be used to identify the system, enabling the subsequent reliable prediction of the system's response to arbitrary inputs within the range of the training data. The principal non-parametric identification techniques proposed for MR dampers are interpolating polynomial fitting (Restoring Force Surface (RSF) method) [63], neural networks [23, 38, 40-42] and neuro-fuzzy modelling [43]. Unlike the RSF method, neural-based techniques

can handle hysteretic effects i.e. possible multi-valuedness of the damper force for given instantaneous values of displacement, velocity and applied voltage. Neural-based techniques have the additional advantage that they are useful not just for direct dynamic modelling of MR dampers, but also their inverse dynamic modelling. Inverse modelling involves the prediction of the voltage signal (applied to the damper's electromagnet) that will produce a desired damper force signal when the damper is subjected to a given time history of the relative displacement across its ends.

Neural networks are able to approximate any complicated multi-input/multi-output continuous function. Neural networks used for modelling MR dampers are typically multilayer networks with either perceptron or sigmoid transfer function neurons e.g. [23, 38, 40, 41]. Radial basis function networks have also been used to a lesser extent [42]. Due to hysteretic effects of the MR damper, the output variable of the mapping (i.e. force, in case of the direct problem, or voltage, in case of the inverse problem), suitably delayed, is included with the inputs to the neural network [23]. In the case of a "feed-forward" neural network (FNN), this extra input is the *actual* value of the output variable (i.e. the value that truly corresponds to the other input variables) and so is taken not from the network output but from some other independent source of information (e.g. a force sensor on the damper in the case of the direct problem) [23]. In the case of a "recurrent" neural network (RNN), this extra input is taken from the output of the network itself [23, 41]. For the direct problem, a trained RNN has the advantage of not requiring a force sensor, although it would be slightly less precise than the FNN. For the inverse problem, the RNN is the only practical approach since the FNN would require real-time knowledge of the

correct desired voltage (to include with the other inputs) - this of course would not be possible unless one has previously solved the direct form of the same problem. Direct and inverse dynamic modelling using FNN and/or RNN have been considered in [23, 38, 40, 41]. These works used optimisation algorithms including "optimal brain surgeon strategies" to prune the weights of the network and optimise their values. It is important to note that in all such works the networks have been trained and validated through simulated data generated from the numerical solution of the modified Bouc-Wen model [14] rather than measured data.

Most of the above-mentioned works on MR damper modelling have not explored the effect of temperature on the dynamic behaviour of the MR-damper. The reason for this may be attributed to the observation made by Spencer et al. [14] that MR damper performance is reasonably stable over a broad temperature range (−40 to 150°C). However, recent research [71, 72] has shown that the influence of temperature on the damper force is not insignificant. A temperature-dependent skyhook controller for an MR vehicle suspension was introduced by [71]. Using a quasi-steady damper model, simulation results were presented to show how temperature feedback can improve the suspension performance by adjusting the controller for variations in viscosity. The damper model developed in [72] took into account temperature variation and studied the effect of MR damper cylinder's surface temperature on the damping force through numerical and experimental studies [72].

A vibration control system using an MR damper requires two nested controllers: (i) an overall system controller, and (ii) an MR damper controller. The former controller computes the desired damping force required for given system conditions.

This is typically done through a sliding mode control algorithm which forces the real system to emulate an idealised reference system [2]. The function of the damper controller is to command the damper to produce the desired force. The effectiveness of this controller depends on its ability to deal with the nonlinear nature of the device (i.e. the nonlinear relationship between damper force and relative velocity across it) and its semi-active nature. This latter means that it is the applied voltage, rather than the desired force, that can be commanded directly. The most basic MR damper controller algorithm is "on-off" control, also known as the Heaviside Function method (HSF), where the applied voltage is either 0 or maximum [5]. An improvement on this algorithm is the Signum Function method (SFM), which, under certain conditions, allows the applied damper voltage to switch between discrete voltage levels below the maximum [48]. In both these controllers, the command voltage signal is discontinuous. Allowing the voltage signal to be continuous ensures more effective control, lower power requirement and extended service life of the damper. The Continuous State control (CSC) method allows the command of a continuous voltage signal. CSC was introduced in [48] for an ER damper and was used in [2] for an MR damper, although no comparison was made in either [49] or [2] with alternative control strategies. An alternative method of commanding a continuous voltage signal is through a neural network of the inverse dynamics of the MR damper, as discussed above. This has the advantage over CSC of not requiring a force sensor. Such a strategy was introduced in [23] but it was only compared with simple "on-off" control. It should also be mentioned that the evaluation of these MR damper controllers has so far been done on simulated data obtained from the parametric modelling of the MR damper.

The novel contributions of this paper are as follows:

- The neural network identification of both direct and inverse dynamics of an MR damper through an experimental procedure.
- The experimental evaluation of a neural network MR damper controller relative to the alternative controllers available (Heaviside Function, Signum Function and Continuous State).

Both FNN and RNN are considered and their architectures and learning methods will be described.

The rest of this article is organized as follows: Section 5.2 describes the experimental setup. Section 5.3 describes the identification procedure. The direct and inverse neural network models of the MR damper and their validation are then considered for both FNN architecture (Section 5.4) and RNN architecture (Section 5.5). Section 5.6 shows the effect of damper cylinder's surface temperature on damping force and the performance of the RNN. Section 5.7 considers the semi-active control of MR dampers, focusing on the damper controller, and compares a RNN damper controller against the above-mentioned alternative controllers.

5.2 MR fluid damper and test setup

An MR damper typically consists of a piston rod, electromagnet, accumulator, bearing, seal, and damper cylinder filled with MR fluid as shown in Fig. 5.1. The magnetic field generated by the electromagnet changes the characteristics of the MR fluid, which consists of small magnetic particles in non-conducting (magnetically inert) a fluid base. Consequently, the strength of the electromagnet's input current

determines the physical characteristics of the MR dampers. The damper used in this research is the Lord RD-1005-3. Continuously variable damping is controlled by the increase in yield strength of the MR fluid in response to magnetic field strength. In this damper, MR fluid flows from a high pressure chamber to a low pressure chamber through an orifice in the piston head. The damper is 209 mm long in its extended position, and the main cylinder is 38 mm in diameter. The main cylinder houses the piston, the magnetic circuit, an accumulator, and 50 ml of MR fluid. The damper has a ±52 mm stroke. The magnetic field, which is perpendicular to the fluid flow, is generated by a small electromagnet in the piston head.

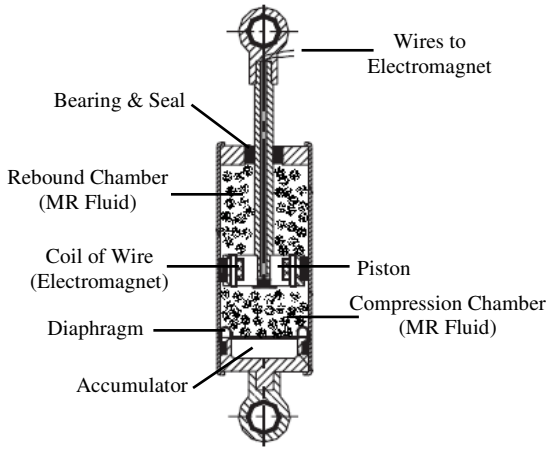

Fig. 5.1 Small scale MR fluid damper

The MR damper was tested by using the Electro-Servo Hydraulic (ESH®) tensile testing machine, as shown in Fig. 5.2. The schematic diagram of the test setup is illustrated in Fig. 5.2(a). The tensile testing machine had an upper and lower head with grippers that grasped the damper at the appropriate locations. The upper head was the moveable end and was operated by a hydraulic actuator that could take a computer-generated prescribed displacement signal. The lower head incorporated a load cell (Fig. 5.2(a)) allowing the operator to measure the force applied to the MR

damper. An LVDT sensor was integrated with the test machine to measure the displacement of the damper. Also, the current excitation to the damper-coil was provided by a computer-generated voltage signal. The required signals were generated on a PC running Matlab® and Simulink®. The Real-Time Workshop® and Real-Time Windows Target® tool-boxes were used for real-time computation and interfacing with the experimental hardware via the data acquisition card.

A thermocouple was fixed on the middle of the damper cylinder to assure that all the tests were accomplished within the range of 20 ^{o}C.

5.3 Overview of neural network identification of an MR damper

The identification scheme for the direct dynamic model of an MR damper is illustrated in Fig. 5.3(a). The inputs of the mapping are the time histories of the relative displacement *x* across the damper and the voltage *v* applied to the coil and the output is the damper force. The output of the actual (physical) system, denoted by *F*, is basically input to the NN for training. The output from the identified neural model is denoted by $\hat{F}$. x_k, v_k,…etc denote the values of the k^{th} data point of the time-histories of $x(t)$, $v(t)$,…etc where $k = 1, 2, 3....$ i.e. $x_k = x((k-1)\Delta)$, $v_k = v((k-1)\Delta)$…etc, Δ being the sampling time resolution. The tapped delay line ("TDL") taken from the channel of *x* is a multi-channel line wherein the respective channels carry delayed signals x_{k-1}, x_{k-2}, ..etc. Due to the influence of the velocity $\dot{x}$, the network requires at least one delayed displacement input (x_{k-1}) in addition to x_k and v_k. In order to adequately capture hysteretic effects of the MR damper, the network is also fed with additional delayed versions of *x* and *v*,

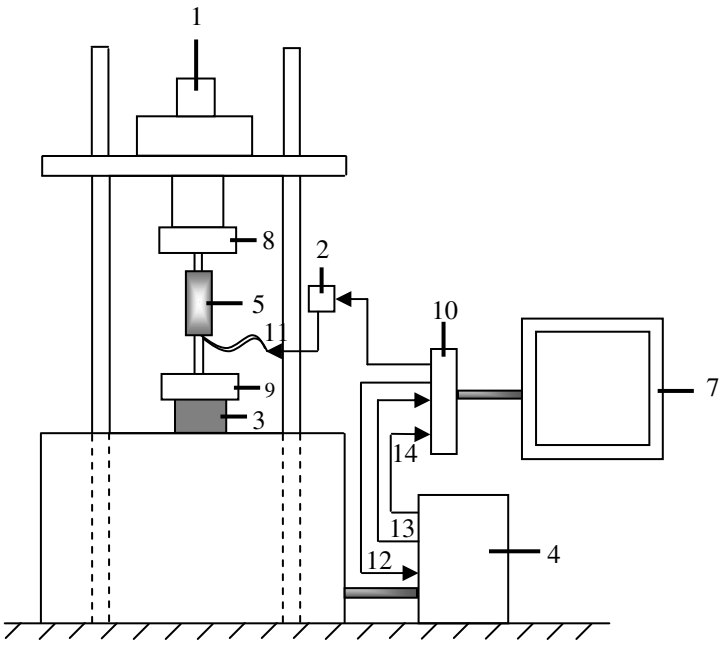

(a)

(b)

1- Hydraulic actuator	**2- Current driver**	**3- Load cell**	**4- ESH Control panel**
5- MR damper	**6- Thermometer**	**7- Computer**	**8- Moving head**
9- Fixed head	**10- Data acquisition card**	**11- Voltage signal**	**12- Displacement signal**
13- Force signal	**14- LVDT signal**		

Fig. 5.2 Test Setup
(a) Schematic Diagram
(b) Photo of Experimental Setup and ESH Machine

and is also fed the output of the mapping and its delayed versions. The symbol u is used here to denote the output of the mapping that is fed into the neural network. As discussed in the introduction, for the direct NN model of the MR damper u will be either F or $\hat{F}$, depending upon whether the network is feed-forward (FNN) or recurrent (RNN):

$$u = \begin{cases} F, & \text{if NN is FNN} \\ \hat{F}, & \text{if NN is RNN} \end{cases} \tag{5.1a,b}$$

As shown in Fig. 5.3(a) during the training phase of the identification, the NN is subjected to known input/true output data sets and the parameters (weights and biases [73]) of the network tweaked such that the error e_k between the true output and the NN output is minimised. It is noted that the output of the neural network proper is actually $\hat{F}_{k+1}$, but this is subsequently delayed by one time-step to produce $\hat{F}_k$ for comparison with F_k. During the validation phase, the trained NN is subjected to input signals different from those used for training and is judged to be validated if its output is in satisfactory agreement with the true output.

A similar identification scheme is used for the inverse dynamic model of the MR damper (Fig. 5.3(b)). In this case, the inputs of the mapping are the time histories of the relative displacement x across the damper and the desired force F. The output is the applied voltage that will produce the desired force. The output of the actual physical mapping is denoted by v whereas the output from the identified neural model is denoted by $\hat{v}$. The symbol u is again used to denote the output of the mapping that is fed into the neural network.

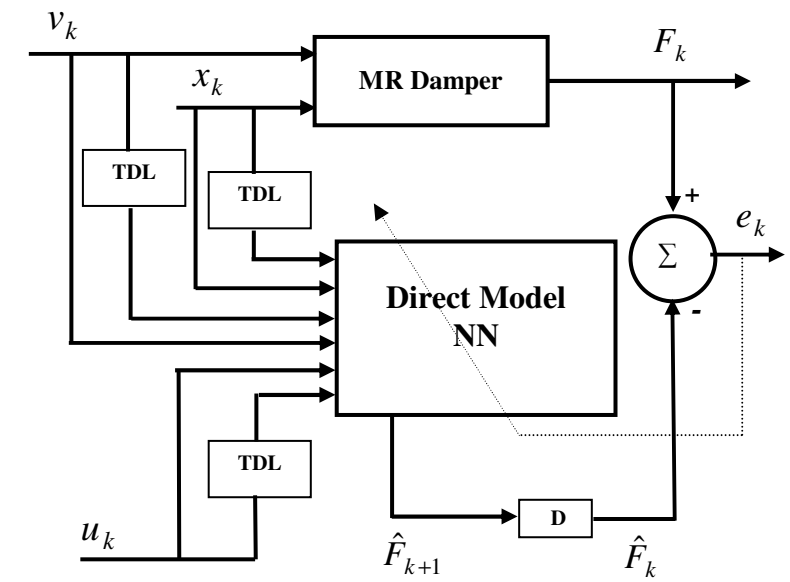

(a)

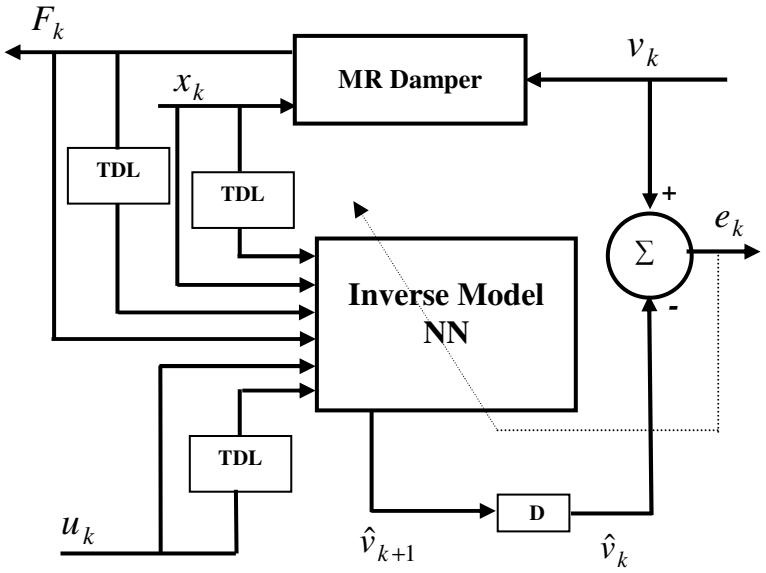

(b)

Fig. 5.3 Scheme of identification of the MR damper:
(a) direct dynamic model; (b) inverse dynamic model
(D: delay by one time step; TDL: tapped delay line)

In the case of the NN of the inverse model:

$$u = \begin{cases} v, & \text{if NN is FNN} \\ \hat{v}, & \text{if NN is RNN} \end{cases} \qquad (5.2a,b)$$

The architectures of the neural networks used in Figs. 5.3(a,b) are discussed in Section 5.4. All neural networks and control systems were implemented on Matlab® and Simulink® using the Neural Network Toolbox® [73].

5.3.1 Data collection for training and validation

In order to obtain a reliable neural network, appropriate training and validation data sets are required. The training data must cover the majority of situations of practical applications in order to ensure that the proposed network models trained using these samples can accurately represent the behaviour of the MR damper well. In this paper, training and validation data sets of the proposed neural networks were obtained by prescribing displacement and voltage signals to an MR damper using the experimental setup shown in Fig. 5.2.

Normally, the limits of these input signals are dependent on the characteristics of the MR damper and ESH® testing machine together. Previous knowledge of the input signals enables the creation of more useful training data. Table 5.1 illustrates the data sets to be used to train the neural network models for MR fluid dampers.

In this table, the displacement input is a band-limited Gaussian white noise signal and the input voltage consists of different signals within different time intervals. The damping force is generated by the MR damper according to the displacement and input voltage inputs. The Gaussian white noise signals were filtered to give appropriate random signals in indicated frequency ranges. These frequency ranges are appropriate for automotive applications. Figure 5.4 shows the time histories of displacement x and input voltage v signals and the corresponding measured damper force F over a 50 s test.

Table 5.1 Training data set

Signals	Time interval (s)				
	0 – 30	30 – 35	35 - 40	40 – 45	45 – 50
Displacement	GWN[a]				
Voltage	GWN[b] + 2.5	5	2.5	0	2.5+2.5sin(4πt)

[a] Gaussian white noise (frequency: 0-3 Hz; amplitude: $\pm$ 0.02 m).

[b] Gaussian white noise (frequency: 0-4 Hz; amplitude: $\pm$ 2.5 V).

Table 5.2 Definition of validation sets

Validation Set	Displacement (m)	Voltage (V)	Force (N)[c]	Time span (s)
1	$A \sin(4 \pi t)$	V	Generated by MR damper	2
2	$A \sin(4 \pi t)$	$2+2\sin(2 \pi f t)$		2
3	$A \sin(4 \pi t)$	GWN[d] + E		2

[c] Only for validation of inverse modelling.

[d] Gaussian white noise (frequency: 0-2 Hz; amplitude: $\pm$ 2.5 V).

A series of tests were performed to validate the effectiveness and the accuracy of the proposed neural networks through experimentation for both direct and inverse models of MR dampers. These validation sets are listed in Table 5.2. The displacement signal was a 2 Hz sinusoidal signal of adjustable amplitude A, applied to the MR damper through the tensile testing machine. Three input voltage signals were used: the first was a constant voltage V, the second one was a 2 Hz sinusoidal signal with mean value of 2 V, the last voltage signal was a part of the training data set produced by Gaussian white noise but it was band-limited between 0-2 Hz. The time duration for the validation sets was 2 s. The sampling interval used for both training and validation sets was $\Delta = 0.001\,\text{s}$.

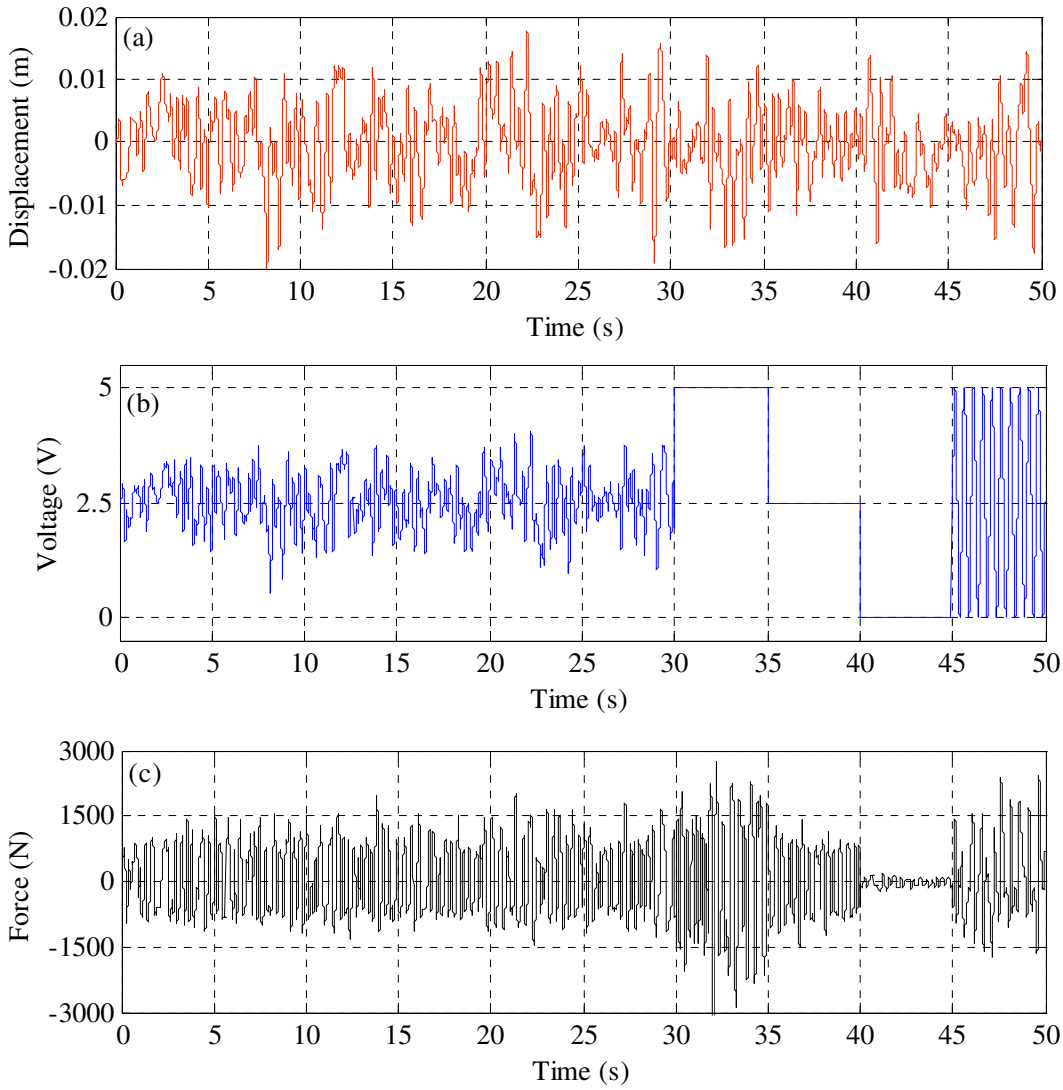

Fig. 5.4 The time history of training data sets for neural network models:

(a) Displacement, (b) Input Voltage, (c) Damping Force.

The results of the validation tests in Sections 5.4 and 5.5 are presented in the form of time histories of the network output since the authors consider these to be more appropriate than force/displacement and force/velocity loops when assessing a network's ability to track a desired output. Moreover, the prediction of such loops by neural networks has been illustrated in [23, 38]. Force/displacement and force/velocity loops are however presented in Section 5.6 where the effect of temperature is studied.

5.4 Modelling of MR fluid dampers using FNN

The identification scheme for the direct model (Fig. 5.3(a)) is specialised as in Fig. 5.5(a) for a FNN, in accordance with Eq. (5.1a). Similarly, the identification scheme for the inverse model (Fig. 5.3(b)) is specialised as in Fig. 5.5(b) for a FNN, in accordance with Eq. (5.2a). It is noted that, for efficient network training, the training data signals in Fig. 5.4 were normalized so that they have means of zero and standard deviations of 1. The normalised version of any quantity $(\bullet)$ is indicated here by $(\bullet)'$. Once the network was trained, subsequent applied inputs were similarly normalised before passage to the network and, if required, the network output was reverse-normalised to yield the physical output. The same pre- and post-processing technique was also used for all other networks in the paper.

As noted in the Introduction, even after training, the FNNs in Figs. 5.5(a,b) require monitoring of the true output of the mapping in order to operate since this is used for some of the networks' inputs. Hence, such networks are only useful for tracking a known quantity. The direct model FNN tracks a measured damper force F (i.e. predicts an estimate $\hat{F}_{k+1}$ for F_{k+1} through knowledge of F_k, v_k, x_k and their delayed versions). Similarly, the inverse model FNN tracks a pre-determined applied voltage v that produces a given damper force F for known x (i.e. predicts an estimate $\hat{v}_{k+1}$ for v_{k+1} through knowledge of v_k, F_k, x_k and their delayed versions). Such networks are clearly limited in their applicability, particularly for the inverse problem. Nonetheless, the FNN is considered in this research since it gives a good preliminary insight into the capability of neural networks and the results obtained

provide a benchmark for comparing with the results of the more practical RNN (Section 5.5).

5.4.1 Direct model FNN

With reference to Fig. 5.5(a), the architecture of the direct model FNN is shown in Fig. 5.6. The FNN has three layers of neurons. If $S^{(j)}$ is the number of neurons in the j^{th} layer, then $S^{(3)} = 1$ since the output layer (layer 3) has a single signal output. Let $\mathbf{p}_k$ be the $R \times 1$ column matrix (vector) comprising the signal inputs to layer 1. If $\mathbf{a}_k^{(j)}$ is the $S^{(j)} \times 1$ vector comprising the signal outputs of the j^{th} layer then:

$$\mathbf{a}_k^{(j)} = \mathbf{g}^{(j)}\left(\mathbf{W}^{(j)}\mathbf{a}_k^{(j-1)} + \mathbf{b}^{(j)}\right), \quad j = 3, 2 \tag{5.3a}$$

$$\mathbf{a}_k^{(1)} = \mathbf{g}^{(1)}\left(\mathbf{W}^{(1)}\mathbf{p}_k + \mathbf{b}^{(1)}\right) \tag{5.3b}$$

where $\mathbf{W}^{(j)}$ and $\mathbf{b}^{(j)}$ are respectively the matrix of weights and vector of biases of the j^{th} layer and $\mathbf{g}^{(j)}(\bullet)$ is a vector operator comprising the transfer functions of the neurons of the j^{th} layer. Each of these transfer functions operates on the respective element of the vector argument $(\bullet)$ of $\mathbf{g}^{(j)}(\bullet)$. The neuron of the output layer was taken as a purely linear transfer function [73]. The transfer functions of all neurons of the "hidden" layers (i.e. layers 1 and 2) were taken as tangent-sigmoid functions [73]. Each hidden layer had 18 neurons.

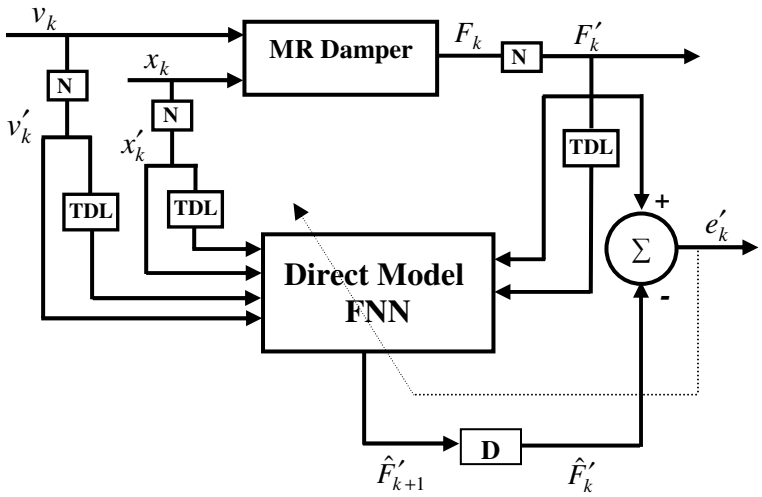

(a)

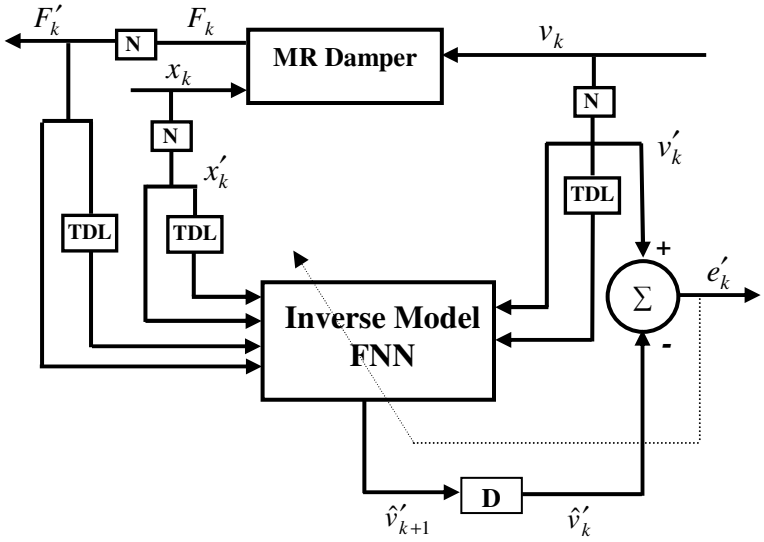

(b)

Fig. 5.5 Scheme of identification of the MR damper by FNN:
(a) direct dynamic model; (b) inverse dynamic model
(D: delay by one time step; TDL: tapped delay line; N: normalisation)

For the present case of the FNN direct model (Fig. 5.6) the network output $\mathbf{a}_k^{(3)} = \hat{F}'_{k+1}$ and:

$$\mathbf{p}_k = \begin{bmatrix} \mathbf{v}'_k \\ \mathbf{x}'_k \\ \mathbf{f}'_k \end{bmatrix}, \quad \mathbf{v}'_k = \begin{bmatrix} v'_k \\ v'_{k-1} \\ v'_{k-2} \end{bmatrix}, \quad \mathbf{x}'_k = \begin{bmatrix} x'_k \\ x'_{k-1} \\ x'_{k-2} \end{bmatrix}, \quad \mathbf{f}'_k = \begin{bmatrix} F'_k \\ F'_{k-1} \\ F'_{k-2} \end{bmatrix} \tag{5.4a-d}$$

Moreover, the inputs are initialised such that v'_k, x'_k, $F'_k = 0$ for $k < 1$. These initialisation conditions apply to all types of networks in this paper.

The network training was performed using the Matlab function *trainlm*©. During the training phase the network was presented with the input-output data sets representing proper network behaviour, obtained from the experimental training signals of Fig. 5.5:

$$\{\mathbf{p}_q, \mathbf{t}_q\}, \quad q = 1, 2 \ldots Q \tag{5.5}$$

where Q is the number of input/output training pairs and $\mathbf{t}_q$ is the proper or target output. For the present case of the FNN direct model (Figs. 5.5(a) and 5.6) $\mathbf{t}_q = F'_q$ and the comparable network output is $\mathbf{a}^{(3)}_{q-1} = \hat{F}'_q$. The function *trainlm*© used the Levenberg-Marquardt algorithm to optimise the weight and bias matrices in Eqs. (5.3a,b) such that the error $e'_q = \left| \mathbf{t}_q - \mathbf{a}^{(3)}_{q-1} \right|$ was minimised.

A comparison between the predicted damping force for the MR fluid damper using the trained FNN model and the experimental behavior of the MR damper for the validation set 1 of Table 5.2 with A = 0.008 m and V = 3 V is shown in Fig. 5.7. It is clearly seen that the trained FNN can perfectly track the direct dynamic behaviour of the MR damper.

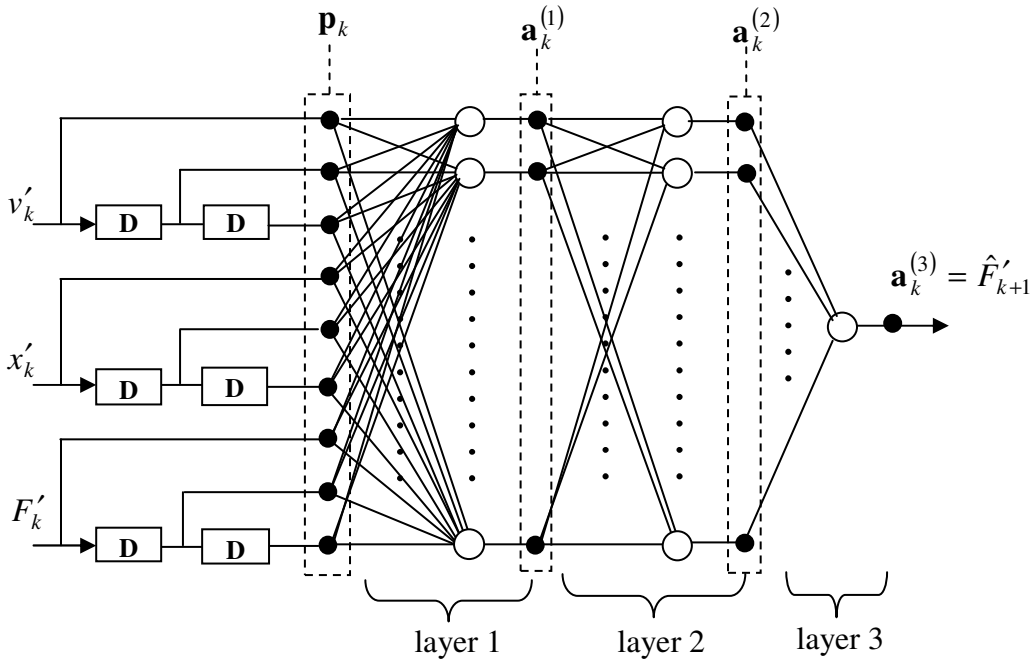

Fig. 5.6 FNN architecture for the direct dynamic model
(D: delay by one time step)

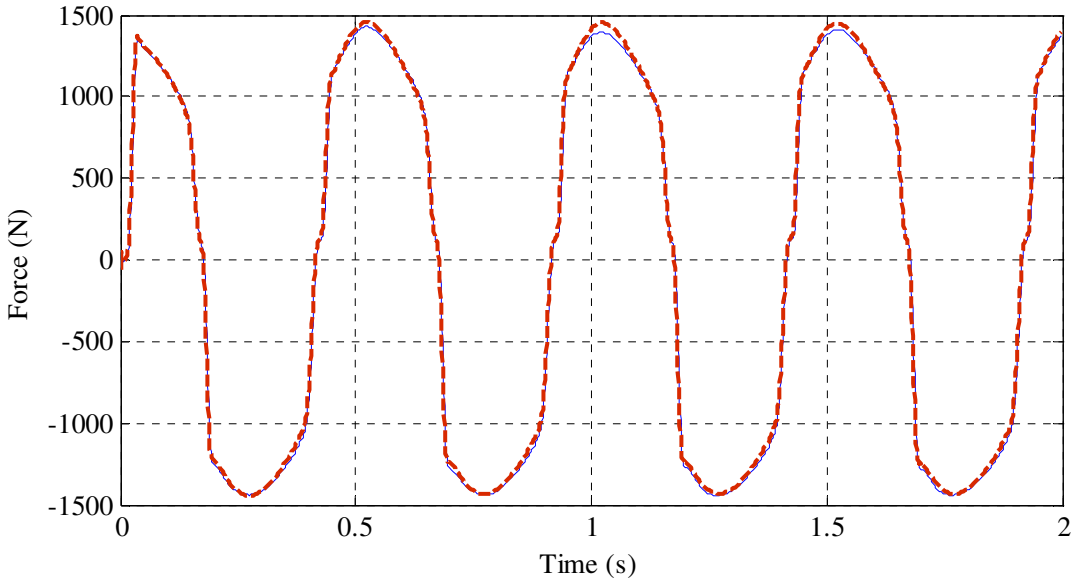

Fig. 5.7 The damping force predicted using the FNN model
according to validation set 1 (A = 0.008 m and V = 3 V)
F ——— ; $\tilde{F}$ - - - - -

5.4.2 Inverse Model FNN

With reference to Fig. 5.5(b), the architecture of the inverse model FNN is as shown in Fig. 5.6 and the input to the first layer $\mathbf{p}_k$ is the same as that in Eqs. (5.4a-d). However, the network output is now $\mathbf{a}_k^{(3)} = \hat{v}'_{k+1}$ and the target vector $\mathbf{t}_q = v'_q$. A similar training procedure to that in Section 5.4.1 was used.

The validation process for the inverse FNN model was done in two steps. Firstly, the test signals for *x*, *F*, and *v* according to Table 5.2 were acquired directly from the test rig and fed into the FNN network to yield the network's estimate $\hat{v}$ for the actual voltage *v* that produced the desired force *F*. In the second step, the signals *x* and $\hat{v}$ were fed into the test rig and the resulting damper force $\tilde{F}$ was measured for comparison with the originally desired force *F*. These two steps were implemented in real-time as per the Simulink® block diagrams in Fig. 5.8.

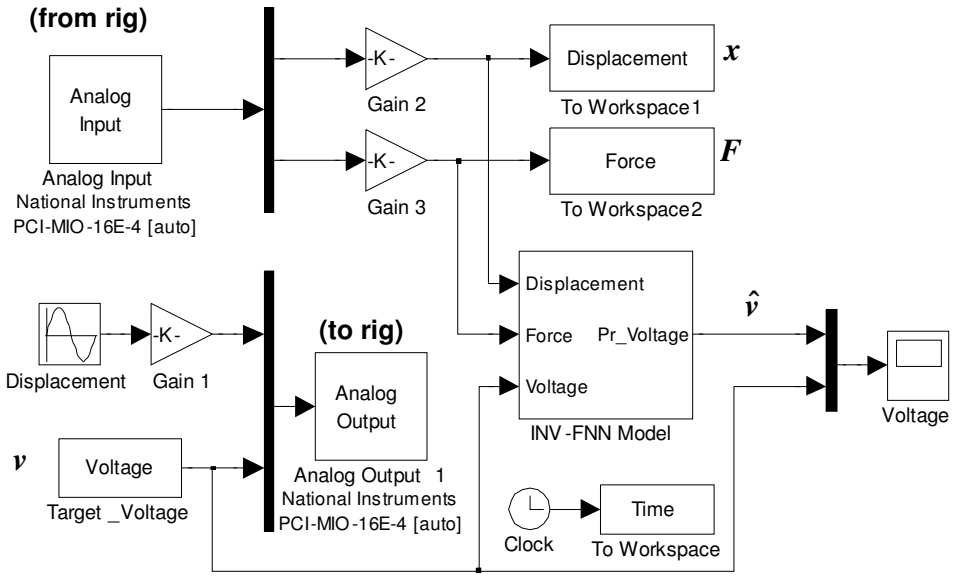

(a)

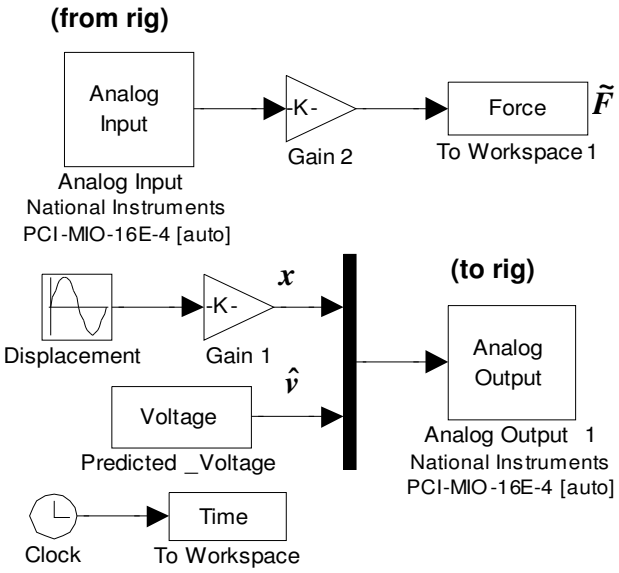

Fig. 5.8 Simulink® implementation of validation scheme for the inverse modelling with the FNN model for the MR damper:
(a) First step; (b) Second step

One validation case is shown here, to present the accuracy of the inverse FNN model as shown in Fig. 5.9. A very good agreement is demonstrated between both $\hat{v}$ and v (Fig. 5.9(a)) and $\tilde{F}$ and F (Fig. 5.9(b)) for validation set 2 of Table 5.2 with A = 0.003 m and f = 2 Hz .

5.5 Modelling of MR fluid dampers using RNN

The identification scheme for the direct model (Fig. 5.3(a)) is specialised as in Fig. 5.10(a) for a RNN, in accordance with Eq. (5.1(b)). Similarly, the identification scheme for the inverse model (Fig. 5.3(b)) is specialised as in Fig. 5.10(b) for a RNN, in accordance with Eq. (5.2b).

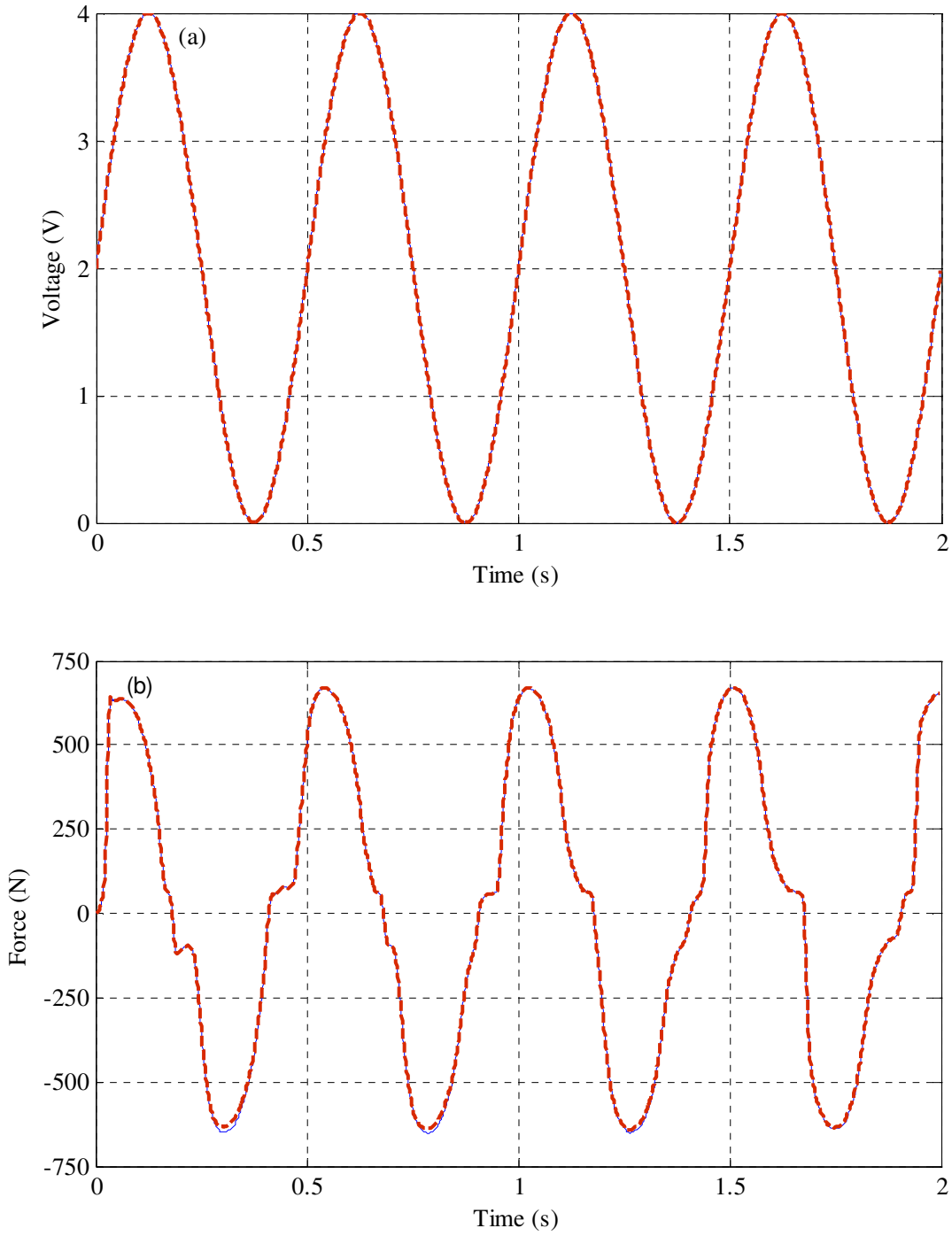

Fig. 5.9 Validation of the inverse modeling for the MR damper using the FNN model (validation set 2, A = 0.003 m, f = 2 Hz): (a) the voltage, (b) the force.

v , F ——— ; $\hat{v}$, $\tilde{F}$ - - - - - -

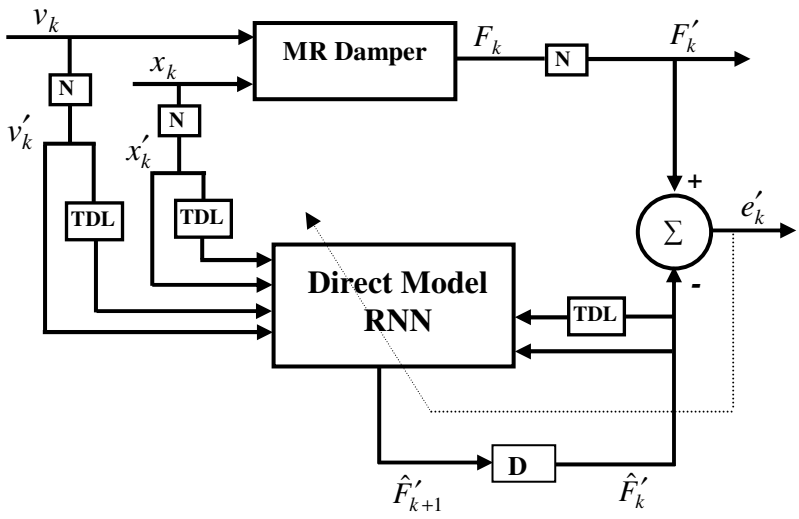

(a)

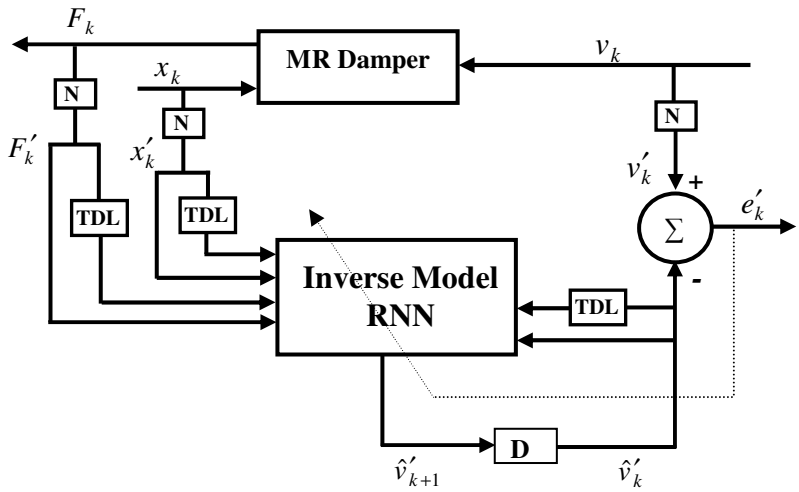

(b)

Fig. 5.10 Scheme of identification of the MR damper by RNN:
(a) direct dynamic model; (b) inverse dynamic model
(D: delay by one time step; TDL: tapped delay line; N: normalisation)

It is clear from Figs. 10(a,b) that, after training is complete, the operation of a RNN does not require monitoring of the true output of the mapping since it is the output of the network itself that is used for some of its inputs rather that the true output of the mapping. This means that a trained RNN is capable of *independently* predicting the output. This makes it more useful than the FNN. As discussed in the Introduction, for the direct problem the trained RNN dispenses with the force sensor hence

improving system reliability and reducing implementation costs. For the inverse problem the RNN provides the only practical solution.

5.5.1 Direct model RNN

With reference to Fig. 5.10(a), the architecture of the direct model RNN is shown in Fig. 5.11. It is a three layer network with one output. The output layer has a single neuron with a linear transfer function and the hidden layers each have 18 neurons, each with a tangent-sigmoid transfer function.

The network output $\mathbf{a}_k^{(3)} = \hat{F}'_{k+1}$ and Eqs. (5.3(a,b)) still apply. However, the vector of inputs to the first layer of the net is now given by:

$$\mathbf{p}_k = \begin{bmatrix} \mathbf{v}'_k \\ \mathbf{x}'_k \\ \hat{\mathbf{f}}'_k \end{bmatrix}, \quad \mathbf{v}'_k = \begin{bmatrix} v'_k \\ v'_{k-1} \\ v'_{k-2} \end{bmatrix}, \quad \mathbf{x}'_k = \begin{bmatrix} x'_k \\ x'_{k-1} \\ x'_{k-2} \end{bmatrix}, \quad \hat{\mathbf{f}}'_k = \begin{bmatrix} \hat{F}'_k & \hat{F}'_{k-1} & \cdots & \hat{F}'_{k-5} \end{bmatrix}^{\mathrm{T}} \qquad (5.6a\text{-}d)$$

The same initialisation conditions of Section 5.4.1 apply. Hence, since true output $F'_k = 0$ for $k < 1$, then, in Eq. (5.6d), $\hat{F}'_k = 0$ for $k < 1$. The network was trained using *trainlm*© in a similar manner to that described in Section 5.4.1 with the target output $\mathbf{t}_q = F'_q$.

A comparison between the predicted damping force for the MR fluid damper using the trained RNN model and the experimental behavior of the MR damper for the validation set 1 of Table 5.2 with A = 0.008 m and V = 3 V is shown in Fig. 5.12. It is evident that the trained RNN model can predict the damping force of the MR damper well and that the results of the FNN model (Fig. 5.7) are only slightly more accurate.

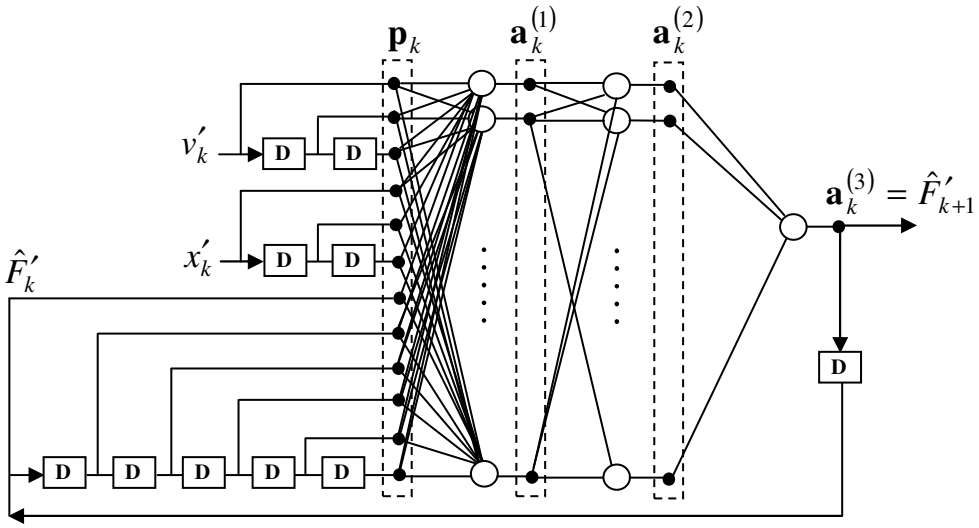

Fig. 5.11 RNN architecture for the direct dynamic model
(D: delay by one time step)

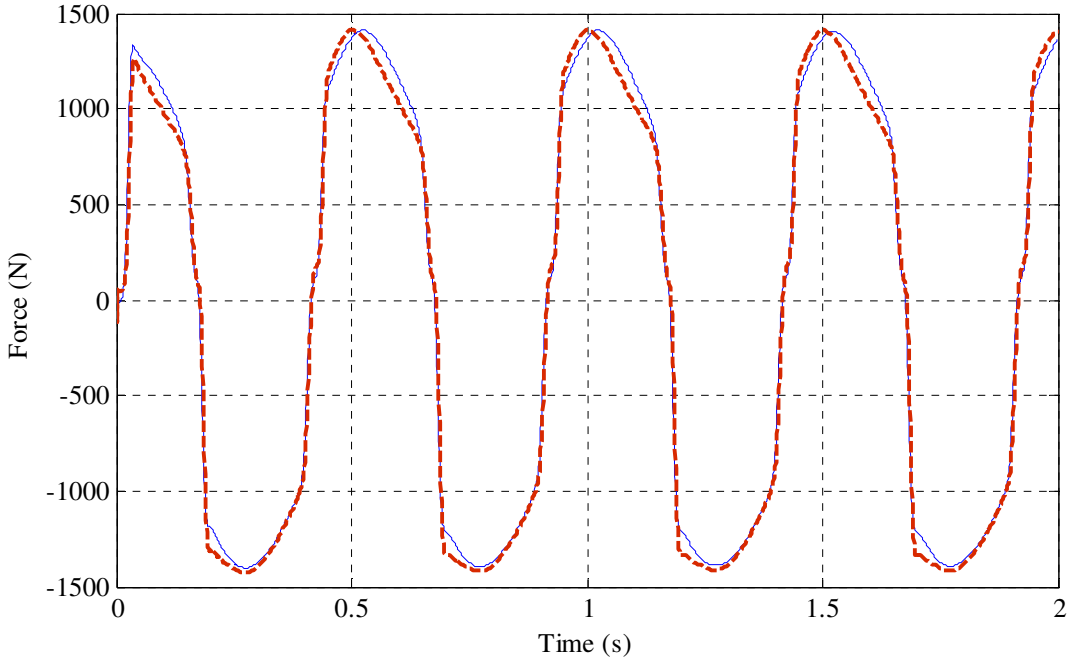

Fig. 5.12 The damping force predicted using the RNN model according to validation set 1 (A = 0.008 m and V = 3 V)

F ——— ; $\tilde{F}$ - - - - - -

5.5.2 Inverse Model RNN

With reference to Fig. 5.10(b), the architecture of the inverse model RNN is shown in Fig. 5.13. It has the same number and type of neurons as all the previous networks. The network output $\mathbf{a}_k^{(3)} = \hat{v}'_{k+1}$. In Eqs. (5.3a,b), the vector of inputs to the first layer of the net is now given by:

$$\mathbf{p}_k = \begin{bmatrix} \mathbf{f}'_k \\ \mathbf{x}'_k \\ \hat{\mathbf{v}}'_k \end{bmatrix}, \quad \mathbf{f}'_k = \begin{bmatrix} F'_k \\ F'_{k-1} \\ F'_{k-2} \end{bmatrix}, \quad \mathbf{x}'_k = \begin{bmatrix} x'_k \\ x'_{k-1} \\ x'_{k-2} \end{bmatrix}, \quad \hat{\mathbf{v}}'_k = \begin{bmatrix} \hat{v}'_k & \hat{v}'_{k-1} & \cdots & \hat{v}'_{k-5} \end{bmatrix}^{\mathrm{T}} \qquad (5.7a\text{-}d)$$

Since true output $v'_k = 0$ for $k < 1$, then, in Eq. (5.7d), $\hat{v}'_k = 0$ for $k < 1$. The network was trained using *trainlm*© in a similar manner to that described in Section 5.4.1 with the target output $\mathbf{t}_q = v'_q$.

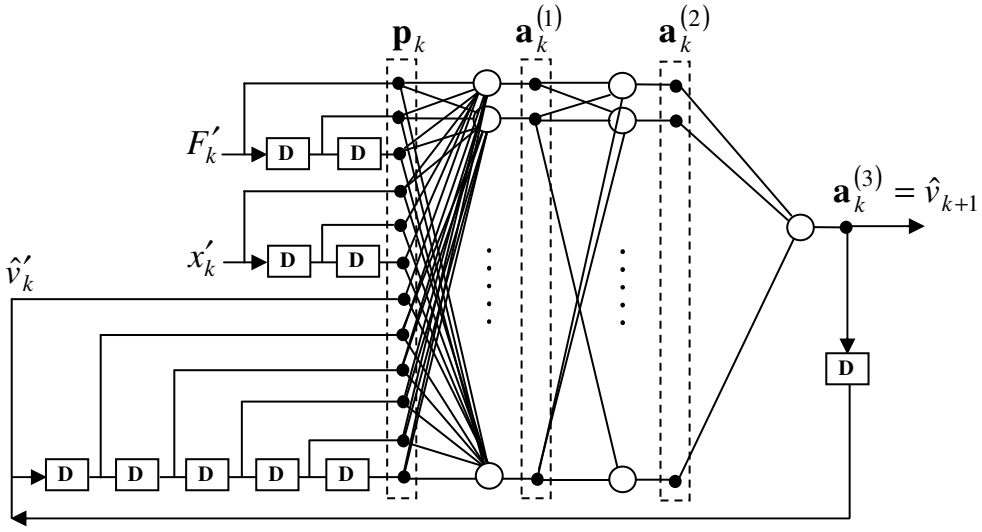

Fig. 5.13 RNN architecture for the inverse dynamic model
(D: delay by one time step)

The validation process for the inverse RNN model was similar to that described in Section 5.4.2 for the direct FNN model. The implementation was identical to that depicted in Fig. 5.8, except that the network block was recurrent and hence it did not receive any input from the actual voltage *v* that produced the desired force *F*.

In order to demonstrate the performance of this model, the results for all validation sets in Table 5.2 are presented in Figs. 5.14 – 5.16. Figs. 5.14(a), 5.15(a), and 5.16(a) show that, unlike the inverse FNN model, the predicted voltage $\hat{v}$ of the inverse RNN model does not satisfactorily reproduce the actual voltage v. However, Figs. 5.14(b), 5.15(b), and 5.16(b) show that the force signal $\tilde{F}$ produced by $\hat{v}$ provides a satisfactory representation of the originally desired force signal F. The same *observation* was made in [23], where the identification and validation were performed using data generated from the Bouc-Wen model. This *observed behaviour* is indeed providential since it allows the use of the inverse RNN model as a damper controller, the prime objective of which is to produce a desired damper force signal.

5.5 Effect of MR damper surface temperature on its damping force

Additional experiments were performed to study the effects of surface temperature on the MR damper force and to examine the robustness of the inverse RNN model against temperature variation. The inverse RNN was considered due to its important use as a damper controller (Section 5.7). A water jacket was placed around the damper cylinder and filled with ice or hot water to adjust the MR damper's cylinder temperature. Once the desired temperature (0 ^{o}C, 20 ^{o}C, 40 ^{o}C, and 60 ^{o}C) was reached, the experimental results from the test rig, Fig. 5.2, were acquired and fed to the PC computer. The surface temperatures were measured using a thermocouple placed at the middle of the damper's cylinder. The thermocouple was insulated from the surrounding water jacket to avoid inaccurate temperature readings.

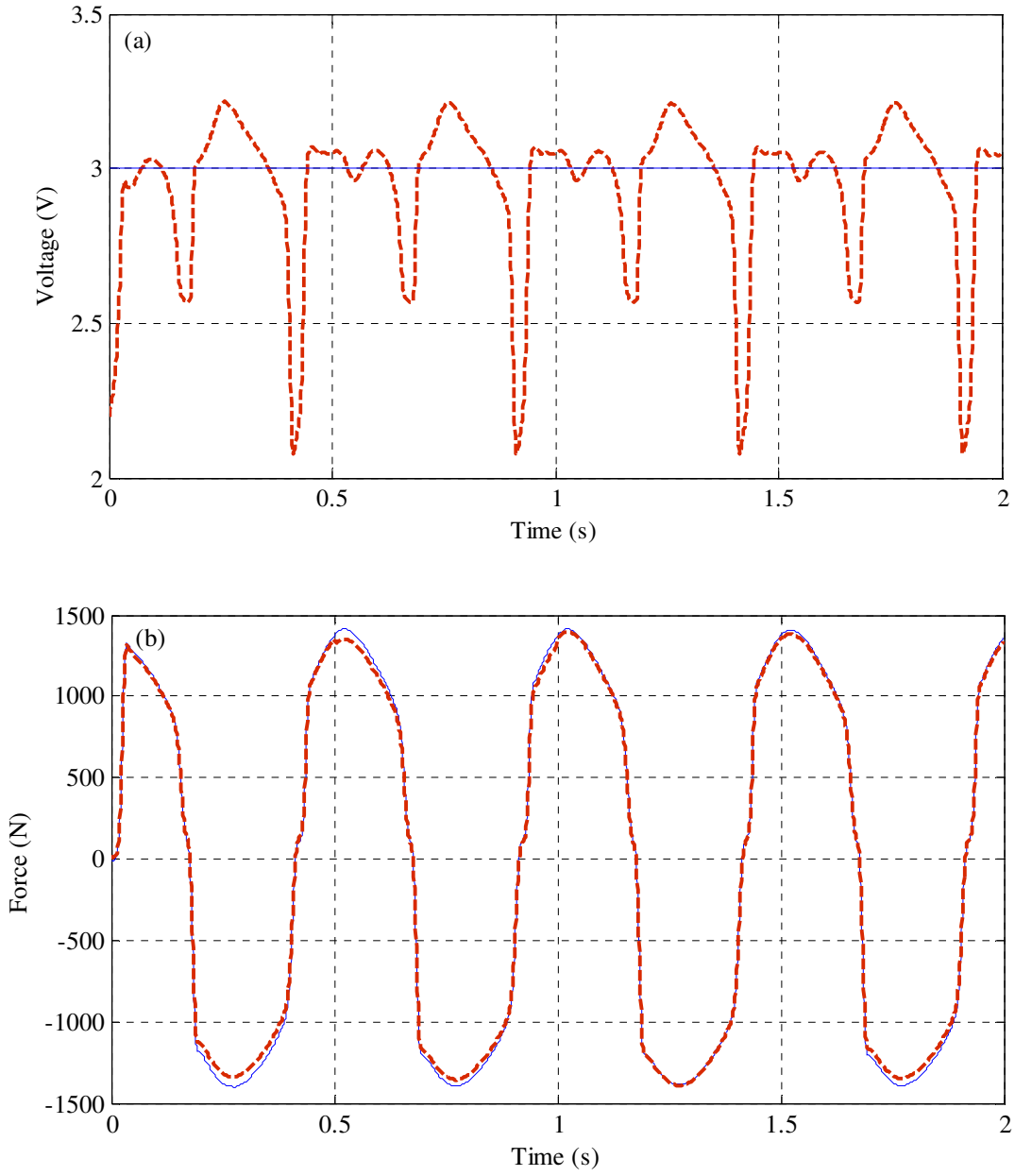

Fig. 5.14 Validation of the inverse modeling for the MR damper using the RNN model (validation set 1, A = 0.008 m and V = 3 V): (a) the voltage, (b) the force.

v , F ——— ; $\hat{v}$, $\tilde{F}$ - - - - - -

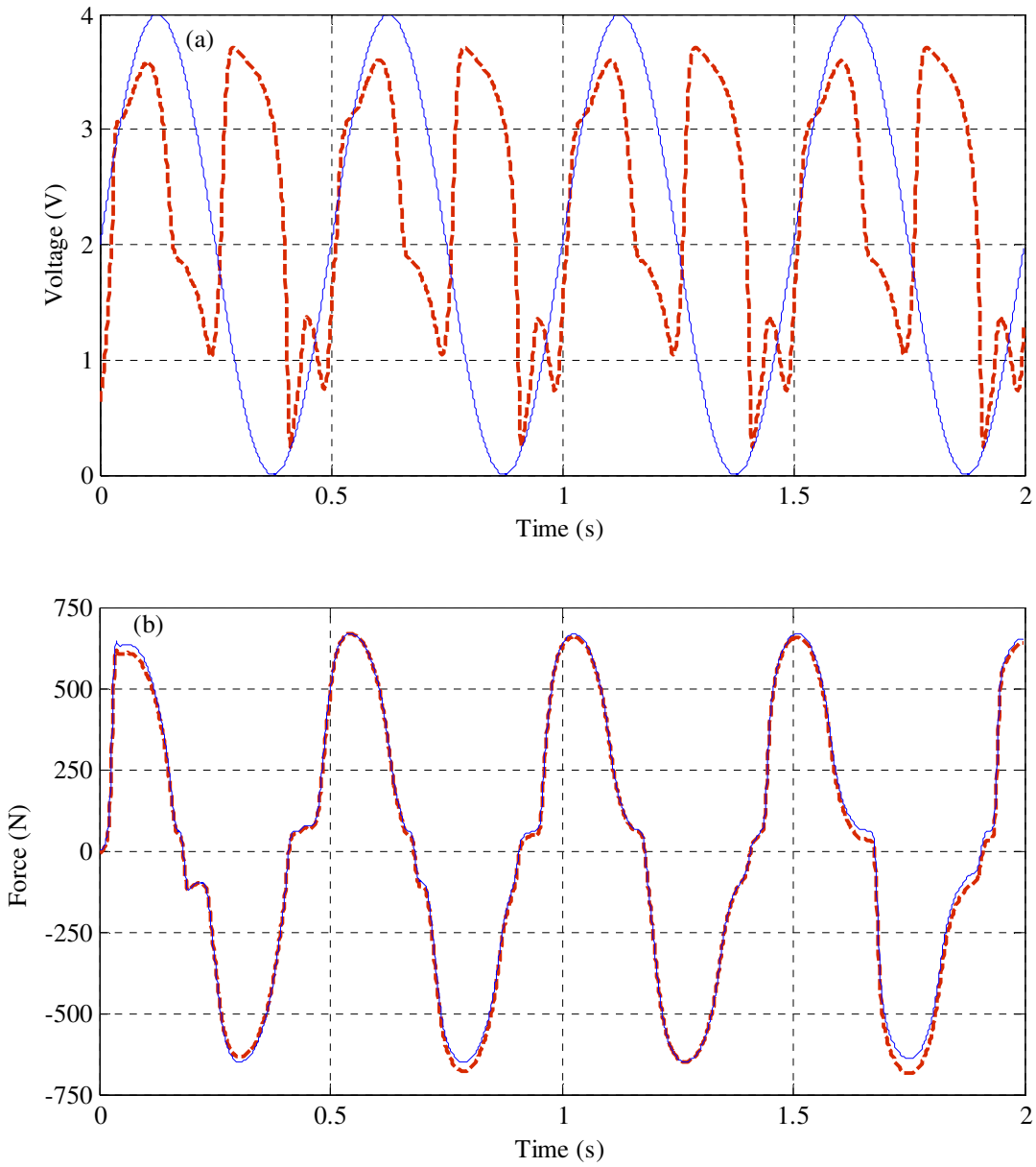

Fig. 5.15 Validation of the inverse modeling for the MR damper using the RNN model (validation set 2, A = 0.003 m and f = 2 Hz): (a) the voltage, (b) the force.

v , F ——— ; $\hat{v}$, $\tilde{F}$ - - - - - -

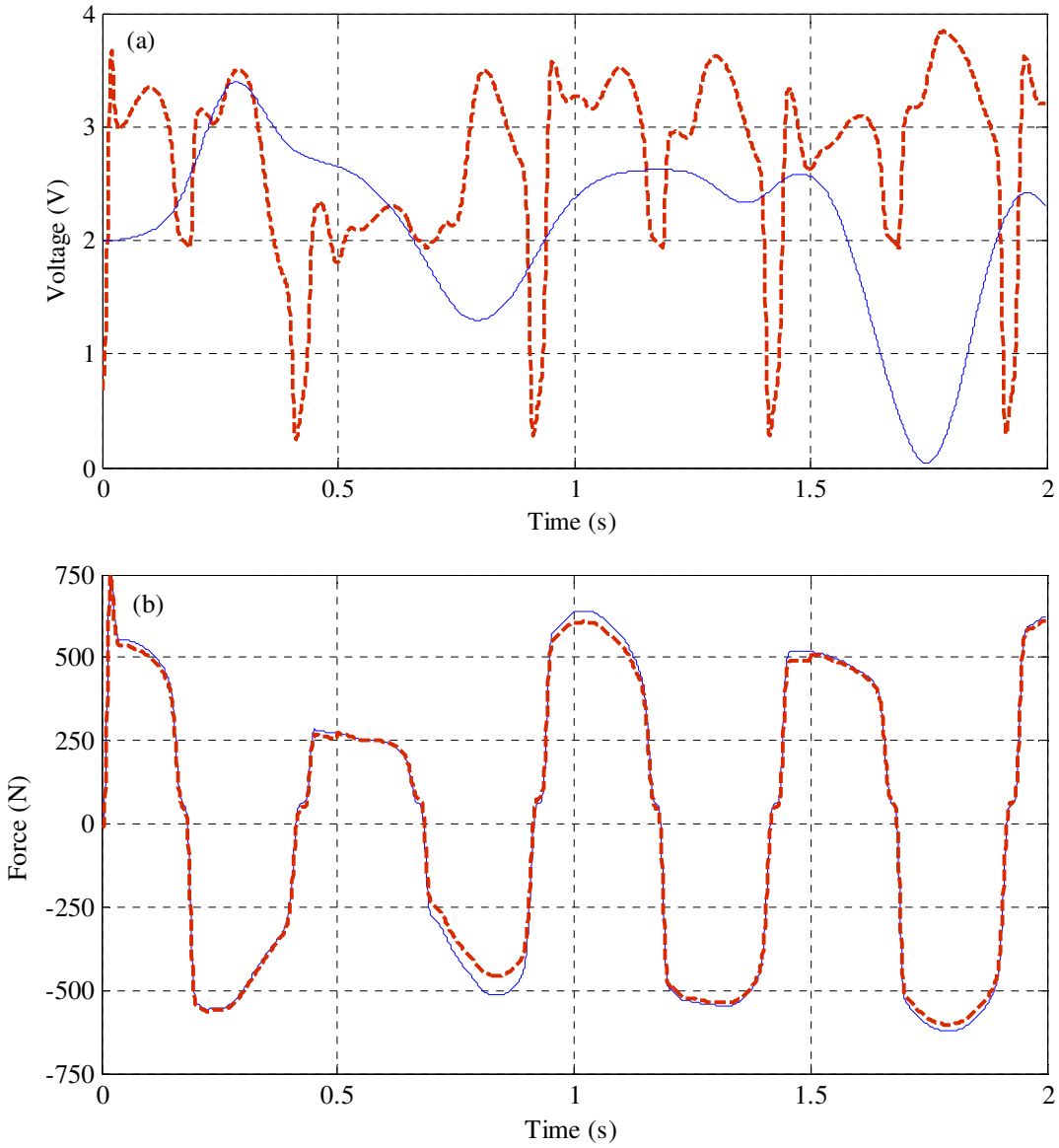

Fig. 5.16 Validation of the inverse modeling for the MR damper using the RNN model (validation set 3, A = 0.0025 m and E = 2 V): (a) the voltage, (b) the force.

v , F ——— ; $\hat{v}$, $\tilde{F}$ - - - - - -

The experimental results, Fig. 5.17, show that the damping force reduces with increasing surface temperature as a result of MR fluid viscosity reduction. As can be seen, the rate of reduction of damping force was observed to be greatest over the range 0 to 40 ^{o}C. Beyond the latter temperature (40 ^{o}C to 60 ^{o}C) there was little

variation in the damping force. Similar behaviour was observed in a previous independent study [72].

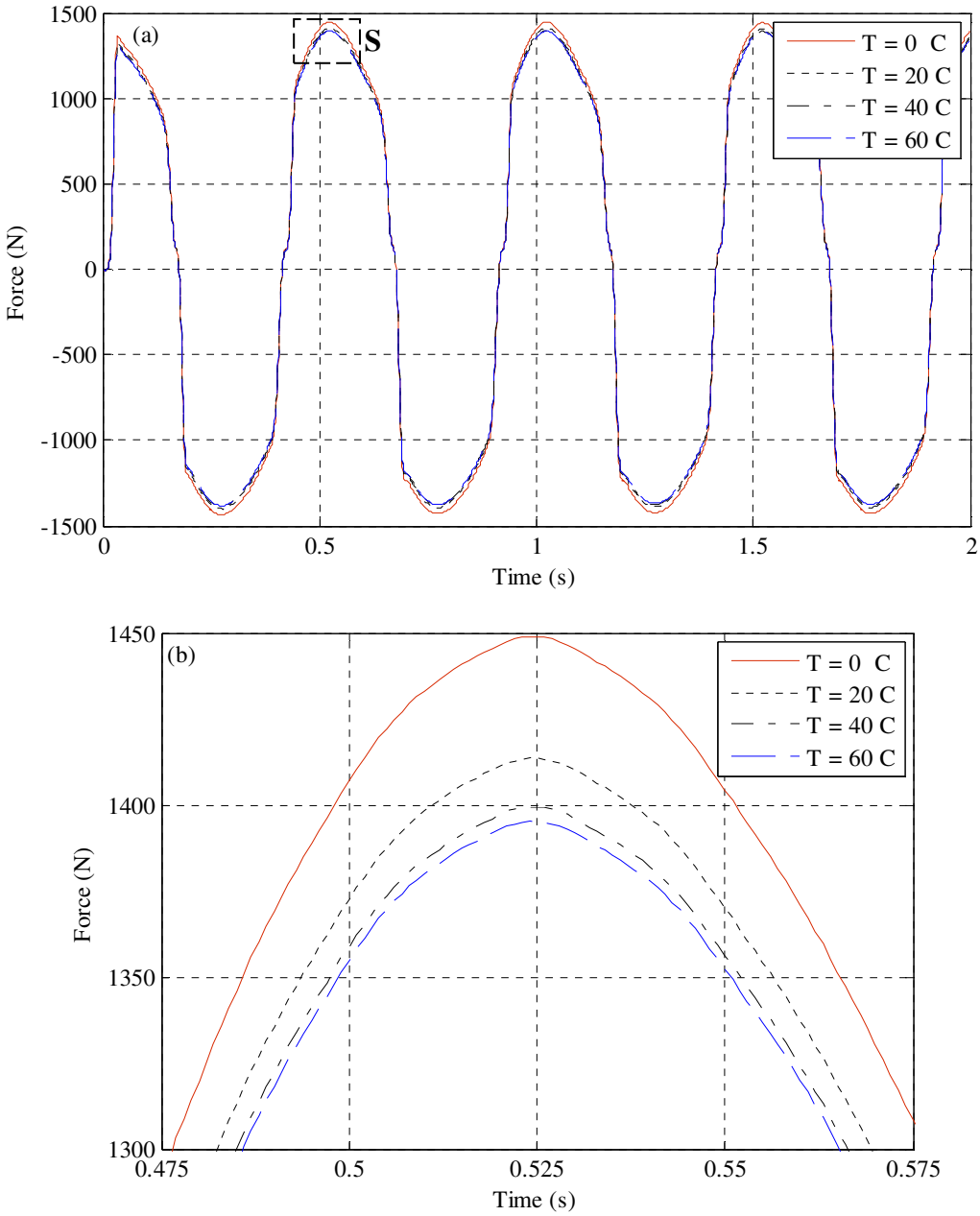

Fig. 5.17 The time history of the damping force at different surface temperature according to validation set 1.
(a) Full graphs (b) Zoomed area S

In order to examine the performance of the inverse RNN model under a different temperature, validation set 3 (Table 5.2) was repeated at a surface temperature of 0

°C. A voltage v was applied to the damper at 0 °C under relative displacement x and the force produced F measured. F and x were then input into the inverse RNN that had been trained at 20 °C. The output $\hat{v}$ was then applied to the damper at 0 °C under x and its force $\tilde{F}$ measured. Fig. 5.18(a) compares $\hat{v}$ with the original voltage v. It is clear that the picture has hardly changed from the corresponding picture in Fig. 5.16.

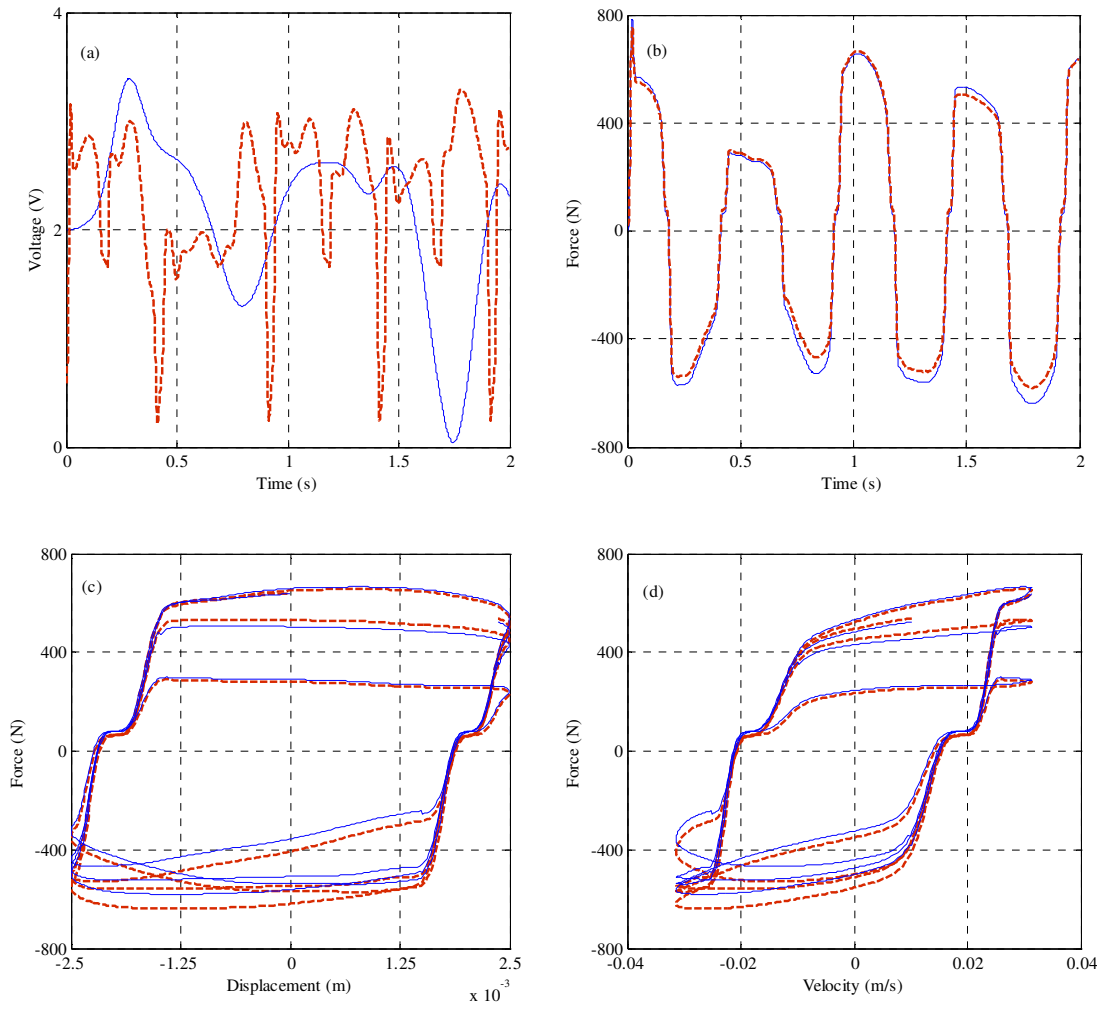

Fig. 5.18 Validation of the inverse modeling for the MR damper using the RNN model at zero temperature (validation set 3, A = 0.0025m, E = 2 V): (a) voltage, (b) force, (c) the force-displacement loop , and (d) the force-velocity loop.

v , F ———— , $\hat{v}$, $\tilde{F}$ - - - - - -

Moreover, the application of $\hat{v}$ to the cold damper resulted in a force $\tilde{F}$ that still closely tracked F, as illustrated in the time history and force-displacement/velocity loops of Figs. 5.18(b-d). These results show that an inverse RNN trained at room temperature is reasonably robust to significant temperature variation. However, if more precision is required, when using the inverse RNN as a damper controller, one can also include networks trained in "cold" and "hot" conditions and use temperature feedback to switch between "cold", "room" and "hot" conditions as appropriate.

5.7 Semi-active control using MR fluid dampers

Figure 5.19 shows the block diagram of a semi-active vibration control system using an MR damper. It consists of two nested controllers; a system controller and a damper controller. The system controller uses the dynamic responses of the plant to compute the desired damping force F_d according to some chosen algorithm such as a sliding mode control [2] and a linear quadratic Gaussian control (LQG) [3]. The damper controller adjusts the voltage v applied to the damper in order to track its actual force F_a to the desired force F_d. This paper deals exclusively with the damper controller. Three conventional types of damper controller (Heaviside function, Signum function and Continuous State control) are considered and evaluated experimentally in comparison with a damper controller based on the RNN. The conventional damper controllers need to be fed with a measurement of F_a from a force sensor, as indicated in Fig. 5.19. This sensor needs to be in series with each MR fluid damper for a multi-damper system, thereby reducing system reliability and increasing its cost. The inverse RNN damper controller does not require an input from F_a, thereby dispensing with the force sensor. This controller uses instead a

measure of the damper relative displacement x which is already available from the sensors used by the system controller.

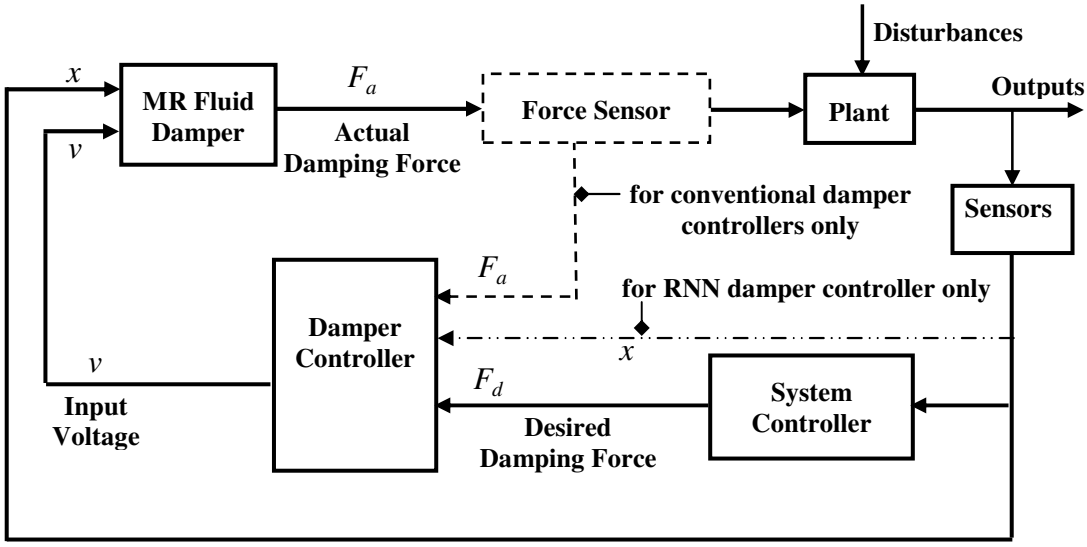

Fig. 5.19 Semi-active control system for a plant integrated with an MR fluid damper.

The following sub-sections provide a description of each type of damper controller in turn, followed by an evaluation of all four controllers.

5.7.1 Heaviside Function Damper Controller

In the Heaviside Function method, the applied voltage has one of two possible values, the minimum value 0 or the maximum value $V_{\max}$, and is determined according to the following algorithm [5]:

$$v = V_{\max} H\{(F_d - F_a)F_a\} \tag{5.8}$$

where $H(\cdot)$ is the Heaviside function: $H(z) = 0$ for $z < 0$ and $H(z) = 1$ for $z > 0$. It is also noted that $\lim_{z \to 0+} H(z) = 1$ and $\lim_{z \to 0-} H(z) = 0$. This means that when the actual force generated by the MR damper is equal to the desired force, the voltage applied to the damper is kept at its current value. If the magnitude of the force generated by

the damper is smaller than the magnitude of the desired force and the two forces have the same sign, the applied voltage is set to its maximum value to increase the force generated by the damper. Otherwise, the voltage is set to zero.

5.7.2 Signum Function Damper Controller

Following the work in [48], in the signum function control method the damper voltage is expressed here as follows:

$$v = v_{Sign1} v_{Sign2} \tag{5.9a}$$

$$v_{Sign1} = \frac{V_{\max}}{N} \sum_{j=0}^{N-1} w_j \,, \qquad w_j = \frac{1 + \mathrm{sgn}\left[\{F_d - (1 + jK) F_a\} F_a \right]}{2} \tag{5.9b,c}$$

$$v_{Sign2} = 1 - \left\{ \left[\frac{1 + \mathrm{sgn}\left(v_{Sign1} - V_{\max}\right)}{2} \right] \cap \left[\frac{1 - \mathrm{sgn}\left(F_a \dot{F}_a\right)}{2} \right] \right\} \tag{5.9d}$$

where $\mathrm{sgn}(\cdot)$ is the signum function, taking values of either 1 or -1; $\cap$ is the logical AND operator; N is a positive integer, K is a small negative constant; $\dot{F}_a$ is the time derivative of F_a. From Eq. (5.9d) it is evident that v_{Sign2} is dimensionless with two possible values of 0 or 1. It is noted that the controller can function without the factor v_{Sign2} and that the purpose of this factor is to improve tracking ability and reduce power requirements [48]. From Eqs. (5.9b,c) it is evident that v_{Sign1} is the sum of N weighted voltages $w_j (V_{\max}/N)$, $j = 1,2,\ldots N$, where the weighting factor w_j is either 1 $(=(1+1)/2)$ or 0 $(=(1-1)/2)$. Hence, the voltage v given by Eq. (5.9a) is allowed to switch between discrete values within the range $[0, V_{\max}]$. For

example, for given *N* and *K* and F_a, $F_d > 0$: (i) if $F_d >> F_a$, v_{Sign1} is typically $V_{\max}$ i.e. all w_j's are 1; (ii) if $F_d << F_a$, v_{Sign1} is typically 0 i.e. all w_j's are 0; (iii) if $F_d \approx F_a$, v_{Sign1} is some fraction of $V_{\max}$, depending on relative values of F_a, F_d i.e. some w_j's are 1 while others are 0. This illustrates the logic improvement on the Heaviside algorithm. Following the research in [48], the values for *N* and *K* used in the present work are 6 and -0.001 respectively.

5.7.3 Continuous-State (CS) Damper Controller

In this method, the applied voltage *v* can vary continuously between minimum and maximum values of 0, $V_{\max}$ respectively according to the following algorithm [2, 49]:

$$v = \begin{cases} 0 & , \quad G(F_d - BF_a)\mathrm{sgn}(F_a) < 0 \\ G(F_d - BF_a)\mathrm{sgn}(F_a) & , \quad 0 \le G(F_d - BF_a)\mathrm{sgn}(F_a) \le V_{\max} \\ V_{\max} & , \quad G(F_d - BF_a)\mathrm{sgn}(F_a) > V_{\max} \end{cases} \tag{5.10}$$

The error signal is $F_d - BF_a$ where *B* is the feedback gain. Just like the Heaviside method (where the error is $F_d - F_a$), the CS controller is only activated when the error and the actual damper force have the same sign. When activated, the CS controller sends a proportional command voltage $v = G|F_d - BF_a| \equiv G(F_d - BF_a)\mathrm{sgn}(F_a)$, where G is the gain, and v is saturated at $V_{\max}$.

5.7.4 RNN Damper Controller

The operation of the RNN damper controller is depicted in Fig. 5.20. It employs the inverse model RNN network of the MR damper that was trained and validated in

Section 5.2. In this diagram, $F_{d_k} = F_d\big((k-1)\Delta\big)$, …etc, Δ being the sampling time resolution.

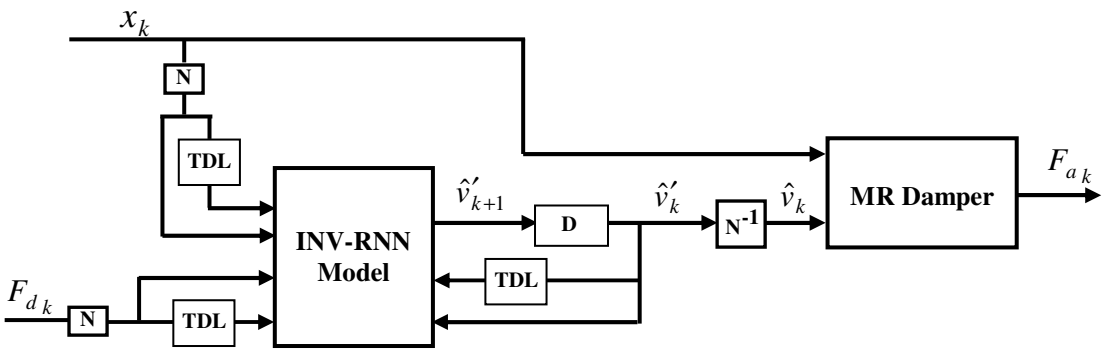

Fig. 5.20 The scheme of the controller for tracking the desired damping force via the inverse RNN model.
(D: delay by one time step; TDL: tapped delay line; N: normalisation; N^{-1}: de-normalisation)

5.7.5 Validation and Evaluation of MR Damper Controllers

The experimental set-up in Fig. 5.2 was used to test the damper controllers. All four controllers were provided with a computer-generated desired damper force signal F_d and their ability to command the experimental damper to track this signal in real-time, under a prescribed random relative displacement signal *x*, was assessed. The signal F_d was the output of the system controller of a vehicle MR-suspension subjected to random road excitation that will be considered in a forthcoming paper. Figure 5.21 shows the Simulink® implementation for the validation of the inverse RNN damper controller. The implementation for the conventional controllers is similar to Fig. 5.21 except that the displacement input into the controller is replaced by the measured force. For the case of CSC, the values of G and B in eqs. (5.10) were 0.0038 V/N and 1 respectively. These values were selected from reference [2] which considered a CS damper controller in a similar vehicle suspension application.

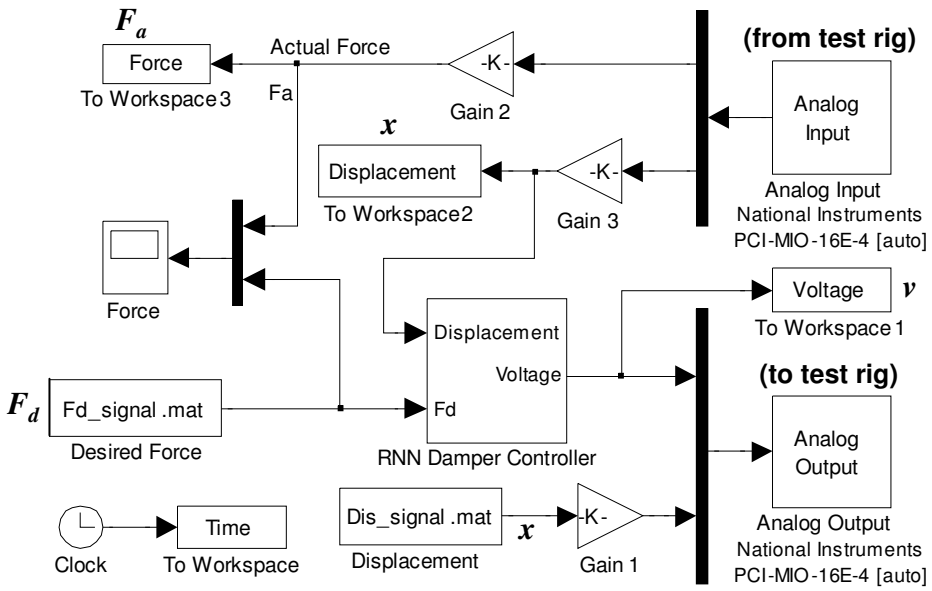

Fig. 5.21 Simulink® implementation for the experimental validation of the inverse RNN damper controller.

Figure 5.22 shows the results obtained for voltage v and the actual damper force F_a, for the random prescribed displacement x in Fig. 5.22(a), and its corresponding desired force signal F_d. Figure 5.22(b) shows that the input voltage produced by both the Heaviside step function (HSF) and Signum function method (SFM) controllers was a discrete pulse with changing time width, which therefore needed a fast dynamic response of the current driver of MR damper. The input voltage $\hat{v}$ generated by the inverse RNN model was a continuously varying low level voltage. This should extend the working life of MR dampers for three reasons: (a) reduced dynamic response requirements on the current coil; (b) reduced current loading; (c) reduced evaporation of the MR fluid (due to lower temperatures). The input voltage produced by the Continuous State controller (CSC) has a different behaviour which at $V_{\max}$ or 0, at other times it is a continuously varying voltage. Figure 5.22(c) can be considered as in-between the previous types: sometimes it is a discrete pulse

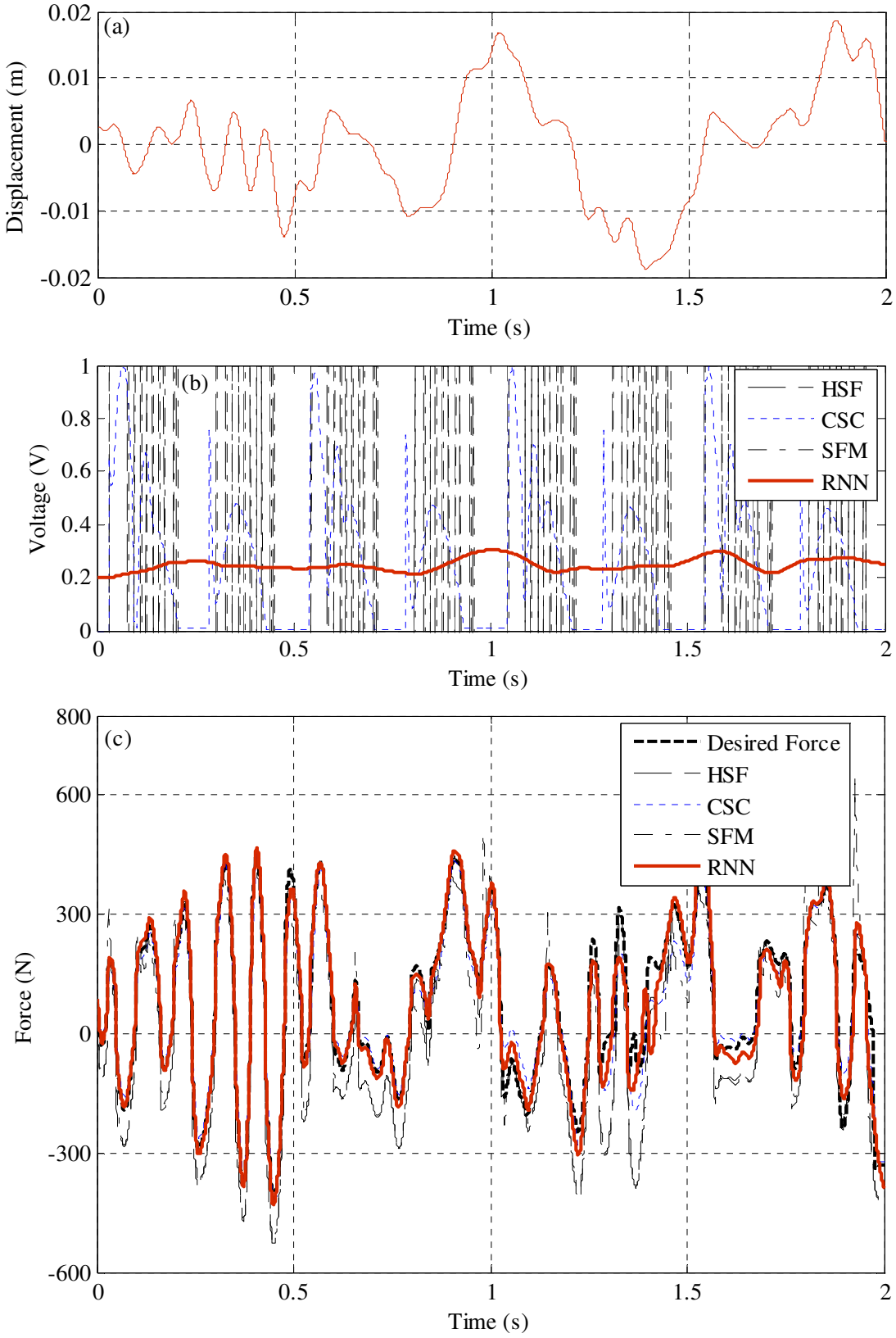

Fig. 5.22 Comparison between experimental validation results of damper controllers investigated for random displacement input
(a) Relative displacement. (b) Input voltage
(c) Force generated by the MR damper

compares the desired damping force with the force signals F_a resulting from the various damper controllers considered. It can be clearly seen that the damping force produced by the inverse RNN model can successfully track the desired damping force and it offers a superior tracking among the controllers investigated.

5.8 Conclusions

In this paper the neural network identification of both direct and inverse dynamics of an MR fluid damper has been performed for the first time using an experimental procedure. Both feed-forward (FNN) and recurrent neural (RNN) networks were considered and their architectures and the learning methods were described. The RNN is more practical since it does not require monitoring of the mapping's true output. Experimental validation tests showed that the RNN is almost as accurate as the FNN for direct modelling purposes. These tests also showed that the voltage output from the inverse model RNN was capable of commanding a damper to closely track a desired damping force signal. Some additional experiments were done to show the effect of the surface temperature on the damping force and the voltage predicted by an inverse RNN model. The inverse RNN model was shown to be reasonably robust against significant temperature variation. For the first time, an experimental evaluation has been performed on all principal alternative MR damper controllers (RNN, Heaviside Function, Signum Function and Continuous State control). The results showed that the RNN damper controller gave the best tracking of the desired damper force signal. Moreover, this controller produced the smoothest input voltage to the MR damper coil, thereby ensuring low-power requirement and extended damper life. These observations, together with the RNN controller's

independence of a force sensor, indicate that among the controllers investigated a neural-based damper controller potentially offers the most cost-effective semi-active vibration control solution.

CHAPTER 6

An investigation into the use of neural networks for the semi-active control of a Magneto-rheologically damped vehicle suspension

Authors:

Hassan Metered, Philip Bonello and S Olutunde Oyadiji

Reformatted version of paper Published in:

Proceedings of the Institution of Mechanical Engineers, Part D: Journal of Automobile Engineering, 2010, Volume: 224 (7), pp 829–848

Abstract

Neural networks are highly useful for the modelling and control of magneto-rheological (MR) dampers. A damper controller based on a recurrent neural network (RNN) of the inverse dynamics of an MR damper potentially offers significant advantages over conventional controllers in terms of reliability and cost through the minimal use of sensors. This paper introduces a neural-based MR damper controller

for use in conjunction with the system controller of a semi-active vehicle suspension. A mathematical model of a semi-active quarter-vehicle suspension using an MR damper is derived. Control performance criteria are evaluated in the time and frequency domains in order to quantify the suspension effectiveness under bump and random road disturbance. Studies using the modified Bouc-Wen model for the MR damper as well as an actual damper fitted in a hardware-in-the-loop simulation (HILS) both showed that the inverse RNN damper controller potentially offers significantly superior ride comfort and vehicle stability over a conventional MR damper controller based on continuous state (CS) control. The neural controller produces a smoother and lower input voltage to the MR damper coil, respectively ensuring extended damper life and lower power requirement. Further studies performed using an RNN model of the forward dynamics of the MR damper showed that it is a reliable substitute for HILS for validating multi-damper control applications.

Key Words: Semi-active, Vehicle suspension, Magnetorheological damper, Sliding mode, Neural network

6.1 Introduction

The design of a better quality suspension system remains an important development objective for the automotive industry. An ideal vehicle suspension system should have the capability to reduce the displacement and acceleration of the vehicle body, maximising ride comfort. It should also aim to minimise the dynamic deflection of the tyre to maintain tyre-terrain contact. Ride comfort and vehicle stability are two

conflicting requirements which the suspension's vibration control strategy has to satisfy [7].

There are three main categorizations of suspension systems: passive, active, and semi-active. Passive suspension systems using oil dampers (conventional passive) are simple, reliable and cheap. However, performance limitations are unavoidable. Active and semi-active suspensions have control systems which force the system to follow the behaviour of some reference system. Active suspensions use active devices (electro-hydraulic actuators) which can be commanded directly to give a desired control force. Compared with the conventional passive system, an active suspension can offer high control performance over a wide frequency range. However, it is not cost-effective for commercial application since it requires a high power supply, many sensors, and servo-valves. A semi-active suspension uses semi-active dampers whose force is commanded indirectly through a controlled change in the dampers' properties. A semi-active suspension combines the advantages of both active and passive suspensions. It can be nearly as efficient as a fully active suspension in improving ride comfort and is much more economical [9, 10]. It is also safer since if the control system fails, the semi-active suspension can still work as a passive suspension system.

Magnetorheological (MR) fluid dampers are becoming popular in semi-active vehicle suspension applications due to their mechanical simplicity, high dynamic range, low power requirements, large force capacity and robustness. Moreover, most vehicles have the facility to provide the voltage (or current) that is required to generate a controllable variable damping force. Semi-active suspension systems

using MR dampers have been shown to offer a compromise solution for ride comfort and vehicle stability requirements [11-13]. With passive damping these requirements are conflicting, since a "hard" damper results in better stability but reduced ride comfort, whereas a "soft" damper results in the converse effect [7].

An MR damper is a semi-active control device since it is only the voltage applied to its electromagnet that can be commanded directly. Hence, in addition to a system controller that calculates the damper force required for the system to follow a reference model, a damper controller is also required. This latter controller determines the voltage v to be applied to the damper such that its actual force f_a tracks the desired force f_d. Different control strategies have been proposed and evaluated for the system controller: e.g. skyhook control [11, 47 and 55], H∞ control [51, 52, 74], adaptive control based on neural network [53], Linear Quadratic Gaussian control (LQG) [3, 4], Robust control [54], Fuzzy Logic control [56], and sliding mode control [2, 50]. The latter approach is used in this paper for the system controller since it has been shown to be robust in the presence of vehicle loading uncertainty [2].

With regard to the damper controller, its effectiveness depends on its ability to deal with the nonlinear and hysteretic nature of the device. The most basic MR damper controller algorithm is "on-off" control, also known as the Heaviside Step Function method (HSF), where the applied voltage is either 0 or maximum [5]. It was first introduced in [5] to research the MR damper control of structural responses due to seismic loads. It was subsequently used in [3, 54] to research the MR damper control of an automobile suspension system. An improvement on this algorithm is

the Signum Function method (SF), which, under certain conditions, allows the applied damper voltage to switch between discrete voltage levels below the maximum [48]. This method was introduced by Wang and Liao in [48] and was used by the same researchers in [4] in their investigation into the control of train suspensions by MR dampers. In both the HSF and SF damper controllers, the command voltage signal is discontinuous. Allowing the voltage signal to be continuous ensures more effective control, lower power requirement and extended service life of the damper [23]. The Continuous State (CS) control method allows for intervals of continuous voltage between periods of discontinuous pulses [49]. CS control was used in [2, 50] for an MR damper controller in vehicle suspension systems.

The main disadvantage of the HSF, SF and CS damper controllers is that they need to be fed with a measurement of the actual damper force f_a. Hence, a force sensor needs to be in series with each MR damper for a multi-damper system, thereby reducing system reliability and increasing its cost.

An alternative method of commanding a voltage signal is through a damper controller that is a neural network model of the inverse dynamics of the MR damper. By "inverse dynamics" is meant the functional relationship between the time histories of the applied voltage v (function output) and the relative displacement x across the damper and desired force f_d (function inputs). A recurrent neural network (RNN) of the inverse MR dynamics only requires a measure of x, thereby improving reliability and reducing cost [23]. Such a network was shown in [23] to produce a completely continuous voltage.

An inverse RNN damper model was identified and validated in [64] using experimental training data. It was shown to be more capable of accurately tracking an arbitrary desired force signal than the CS control algorithm. The main contribution of the present paper is to introduce this model as an MR damper controller within a quarter-vehicle suspension. Except for the damper controller, this suspension is similar to that considered by Lam and Liao [2] who used a sliding mode control algorithm for the system controller and CS control for the damper controller. Control performance criteria are evaluated in the time and frequency domains in order to quantify the suspension effectiveness for the two alternative types of damper controller (inverse RNN and CS), as well as MR passive damping (zero applied voltage) and conventional passive damping.

For a comprehensive study of the suspension performance, the results are obtained using three alternative ways to obtain the MR damper force f_a for given signals v and x:

(a) Computationally, through the modified Bouc-Wen model [14];
(b) Experimentally in real-time, from a real MR damper mounted in a tensile testing machine subjected to v and x in a hardware-in-the-loop simulation (HILS);
(c) Computationally, from a neural network of the forward dynamic model of an MR damper trained using experimental data (i.e. x, v being the inputs and f_a the output).

The modified Bouc-Wen model is used here for obtaining the suspension response when subjected to road disturbances x_r of sizeable amplitude and/or wide frequency

range, since such conditions would be difficult to reproduce in the HILS approach due to restrictions on the signal x that can be prescribed to the tensile test machine. HILS is used to experimentally validate the proposed semi-active system by demonstrating its practical implementation. The forward neural network model of the MR damper is used to obtain the response to the same disturbance x_r used in HILS, in order to ascertain that it is a reliable substitute for the real damper. Such validation would allow it to be used for those applications where HILS is not practicable, particularly in multi-degree-of-freedom suspension models that have up to four independent dampers. It is noted that wherever HILS has been applied to half/full vehicle suspension systems, the simulation was simplified in one of two ways to avoid using more than one tensile test machine:

(a) Mounting one real damper on the machine and modelling the remaining dampers by solving an MR analytical model as in [52].

(b) Assuming the force from all dampers is identical at all times and equal to that of a real damper mounted on the tensile test machine [75].

It is noted that method (a) is not entirely a HILS approach while method (b) means that the dampers are not independent.

The rest of this article is organized as follows. Section 6.2 gives an overview of the quarter vehicle model. Section 6.3 describes the semi-active control system. Section 6.4 describes the three alternative ways of determining the system response. The results obtained for different road disturbance inputs are presented and discussed in section 6.5.

6.2 Quarter vehicle model overview

Figure 6.1 illustrates the two-degree-of-freedom (2DOF) system that represents the quarter vehicle suspension model. It consists of an upper mass, m_b, representing the body mass, as well as a lower mass, m_w, representing the wheel mass and its associated parts. The vertical motion of the system is described by the displacements x_b and x_w while the excitation due to road disturbance is x_r. The suspension spring constant is k_s and the tyre spring constant is k_t (tyre damping neglected). The data employed here for the quarter vehicle system is the same as that in [76], see Table 6.1. By applying Newton's second law to the quarter vehicle model, the Eqs. of motion of m_b and m_w are:

$$\begin{aligned} m_b\ddot{x}_b + k_s(x_b - x_w) + f &= 0 \\ m_w\ddot{x}_w - k_s(x_b - x_w) + k_t(x_w - x_r) - f &= 0 \end{aligned} \tag{6.1a,b}$$

where, the force from the damping device is given by

$$f = \begin{cases} c_s(\dot{x}_b - \dot{x}_w), & \text{for conventional passive suspension} \\ f_a, & \text{for semi - active suspension} \end{cases} \tag{6.2a,b}$$

where, c_s being the coefficient for the passive suspension's damper.

For the semi-active suspension, the MR damper force f_a depends on the time histories of the applied voltage to the magnetic coil v and the relative displacement x across it:

$$x = x_b - x_w \tag{6.3}$$

x is also referred to as the suspension working space (SWS). The voltage signal v is calculated by the control system, which is described in section 6.3. For given signals

v and x, the force f_a is then determined by three alternative methods in this research, as discussed in the Introduction. These methods are presented in section 6.4.

Table 6.1 Quarter vehicle suspension parameters [76]

Parameter	Symbol	Value (Unit)
Mass of vehicle body	m_b	240 (kg)
Mass of vehicle wheel	m_w	36 (kg)
Suspension stiffness	k_s	16 (kN/m)
Damping coefficient	c_s	980 (Ns/m)
Tyre stiffness	k_t	160 (kN/m)

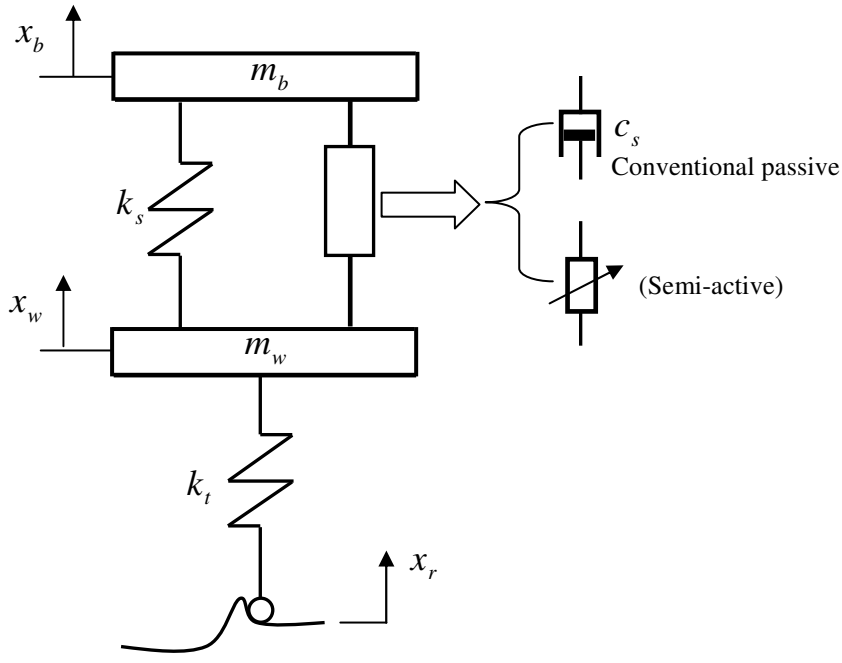

Fig. 6.1 Quarter-vehicle suspension model

6.3 The semi-active control system using MR dampers

The complete semi-active control system is illustrated in Fig. 6.2. As stated in the Introduction, the control system regulates *v* such that the actual body response x_b follows the response $x_{b,ref}$ of some chosen reference system. The system controller calculates the damper force f_d necessary to do so, based on the real-time system response. A damper controller then estimates the voltage *v* that would enable the damper force to closely track f_d. As can be seen from Fig. 6.2, a conventional MR damper controller like the CS controller requires a measure of the actual damper force f_a. The following sub-sections provide a brief description of the system controller and the two alternative types of damper controller considered.

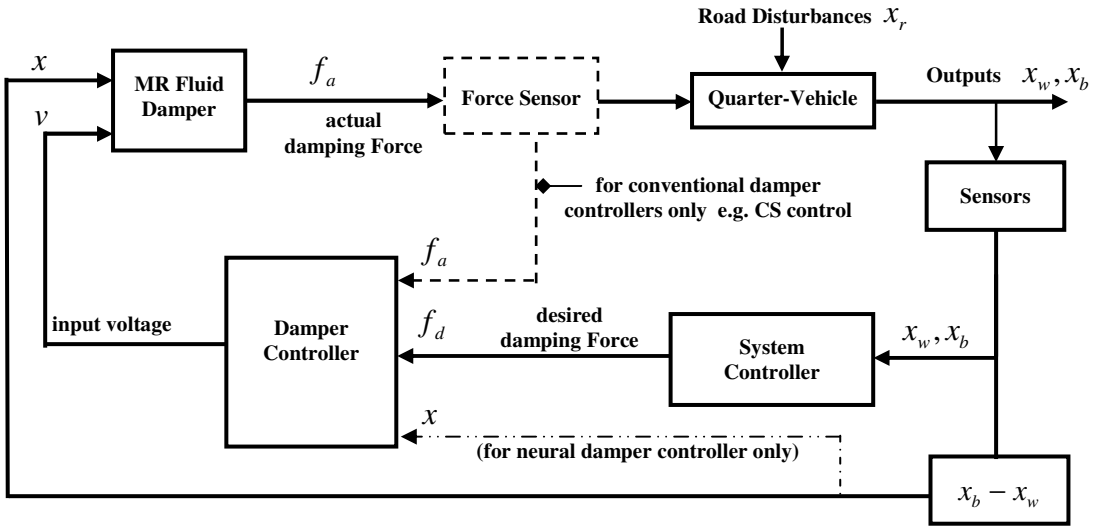

Fig. 6.2 Semi-active control system for a vehicle suspension integrated with MR dampers

6.3.1 System Controller

This section gives an overview of the system controller, which was derived in reference [2]. The reference system used by the system controller is the ideal

skyhook system shown in Fig. 6.3(a). As can be seen from this figure, the tyre flexibility has been omitted for simplicity, since the tyre is much stiffer than the suspension spring. The displacement of the lower mass of the reference system is then taken to be identical to x_w, the displacement of the unsprung mass of the actual system. Hence, the equation of motion of the reference system is given by:

$$m_{b,ref}\ddot{x}_{b,ref} = -c_{s,ref}\dot{x}_{b,ref} - k_{s,ref}\left(x_{b,ref} - x_w\right) \tag{6.4}$$

The sliding mode control algorithm is used to formulate the system controller. The sliding surface is defined as:

$$S = \dot{e} + \lambda e \tag{6.5}$$

where

$$e = x_b - x_{b,ref} \tag{6.6}$$

and λ is a constant. In order to ensure that all states converge towards the state $S, \dot{S} = 0$ a sliding condition $\dot{S} \le -\varphi|S|/S$ is used, where φ is a positive constant. Based on this condition, and allowing for uncertainties in the sprung mass m_b due to variations in the loading conditions, the desired damper force is given by [2]

$$f_d = \begin{cases} f_{d0} + K \times \text{val}(S) & |S| \le \Phi \\ f_{d0} + K\,\text{sgn}(S) & |S| > \Phi \end{cases} \tag{6.7}$$

where Φ is an appropriately chosen constant and:

$$f_{d0} = -k_s\left(x_b - x_w\right) - m_{b0}\ddot{x}_{b,ref} + m_{b0}\lambda\dot{e} \tag{6.8}$$

$$K = (\mu - 1)\left(|f_{d0}| + k_s|x_b| + k_s|x_w|\right) + m_{b0}\mu\varphi \tag{6.9}$$

In eq. (6.7) $\text{val}(S)$ is defined as the numerical value of *S*, including its sign. This notation is introduced here to preserve dimensional consistency since K has the same dimensions as force and *S* has dimensions of velocity (eq. (6.7)). In eq. (6.9)

μ is a parameter that is used to form boundaries for the ratio of the actual value m_b of the sprung mass to its nominal value m_{b0}:

$$\frac{1}{\mu} \leq \frac{m_b}{m_{b0}} \leq \mu, \quad m_b = m_{b0} + \Delta m_b \tag{6.10, 6.11}$$

where Δm_b is the uncertain part due to variations in passengers and payload. The mass $m_{b,ref}$ of the reference system is set to the nominal sprung mass m_{b0}. The control algorithm is designed to function for fluctuations Δm_b that satisfy eq. (6.10).

The system controller described above is summarised in Fig. 6.3(b). The control system parameters used in this research are the same as those used in [2] and are summarised in Table 6.2. It is to be noted that, in eq. (6.7), e, $\dot{e}$ are dimensional (as in other implementations of this algorithm e.g. [2, 77]). Hence, the values of λ, Φ, φ given in Table 6.2 are appropriate only for units of m and m/s for e, $\dot{e}$ respectively. It is noted that $m_{b,ref} = m_{b0} = 200\,\text{kg}$. From Table 6.1 it is seen that $m_b = 240\,\text{kg}$. Hence, the uncertain part $\Delta m_b = 40\,\text{kg} = 0.2 m_0$. Since $\mu = 1.25$, it can be seen from eq. (6.10) that this uncertainty can be handled by the control algorithm.

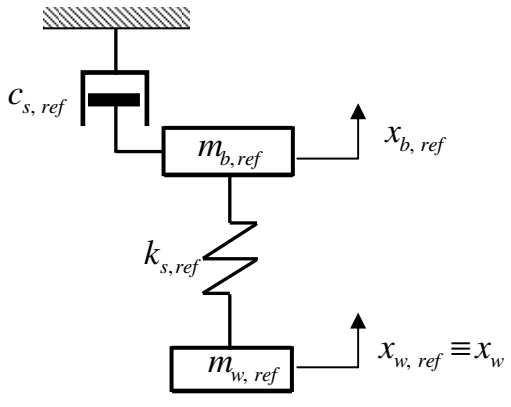

(a)

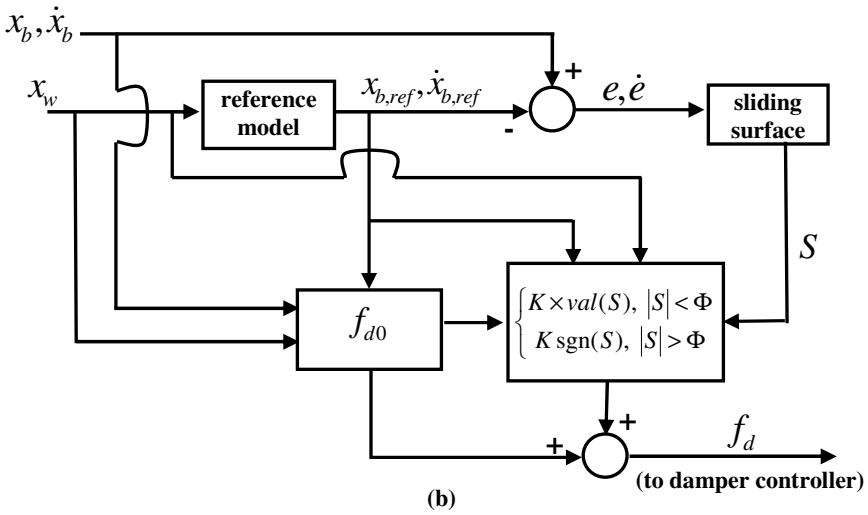

Fig. 6.3 System controller:
(a) reference model (skyhook damped);
(b) schematic diagram of sliding mode control algorithm

Table 6.2 System controller parameters

Parameter	Symbol	Value (Unit)
Reference body mass	$m_{b,ref}$	200 (kg)*
Reference damping coefficient [2]	$c_{s,ref}$	128625 (Ns/m)
Reference suspension stiffness [2]	$k_{s,ref}$	50 (kN/m)
The uncertainty ratio boundary [2]	μ	1.25
Sliding mode control gain [2]	λ	120
Sliding mode control gain [2]	φ	1
Sliding mode control gain [2]	Φ	1

* *Set equal to nominal sprung mass* m_{b0}

6.3.2 Damper Controller

Two alternative types of damper controllers are considered for adjusting the real-time voltage *v* applied to the MR damper so that its force f_a closely tracks f_d: (a) the continuous state (CS) damper controller; (b) the inverse recurrent neural network (RNN) controller.

6.3.2.1 Continuous-State (CS) Damper Controller

In this controller, the command voltage v can vary continuously between minimum and maximum values of 0, $V_{\max}$ respectively according to the following algorithm [2, 23]:

$$v = \begin{cases} 0 & , \quad G(F_d - HF_a)\mathrm{sgn}(F_a) < 0 \\ G(F_d - HF_a)\mathrm{sgn}(F_a) & , \quad 0 \le G(F_d - HF_a)\mathrm{sgn}(F_a) \le V_{\max} \\ V_{\max} & , \quad G(F_d - HF_a)\mathrm{sgn}(F_a) > V_{\max} \end{cases} \tag{6.12}$$

The error signal is $F_d - HF_a$ where H is the feedback gain. The CS is only activated when the error and the actual damper force have the same sign. When activated, the CS sends a proportional command voltage $v = G|F_d - HF_a| \equiv G(F_d - HF_a)\mathrm{sgn}(F_a)$, where G is the gain, and v is saturated at $V_{\max}$. The values of G and H are decided by the trial and error method. In this paper, the values of G, H and $V_{\max}$ were set to be 0.0038 V/N , 1, and 2 V respectively, as in [2].

6.3.2.2 Inverse Recurrent Neural Network (RNN) Controller

This controller is based on a recurrent neural network simulating the inverse dynamics of the MR damper (Fig. 6.4). Its inputs are the time histories of the relative displacement x across the damper and the desired force f_d. Let $x_k = x((k-1)\Delta)$, $f_{dk} = f_d((k-1)\Delta)$, $v_k = v((k-1)\Delta)$ where $k = 1, 2, 3....$ and Δ is the sampling time resolution. The network works with versions of these quantities that are normalised according to the data signals used to train the network [64]. The normalised version of any quantity $(\bullet)$ is indicated here by $(\bullet)'$.

If $S^{(j)}$ is the number of neurons in the j^{th} layer, then $S^{(3)}=1$ since the output layer (layer 3) has a single signal output. Let $\mathbf{p}_k$ be the $R\times 1$ column matrix (vector) comprising the signal inputs to layer 1:

$$\mathbf{p}_k=\begin{bmatrix}\mathbf{f}'_{dk}\\ \mathbf{x}'_k\\ \mathbf{v}'_k\end{bmatrix},\quad \mathbf{f}'_{dk}=\begin{bmatrix}f'_{dk}\\ f'_{dk-1}\\ f'_{dk-2}\end{bmatrix},\quad \mathbf{x}'_k=\begin{bmatrix}x'_k\\ x'_{k-1}\\ x'_{k-2}\end{bmatrix},$$

$$\mathbf{v}'_k=\begin{bmatrix}v'_k & v'_{k-1} & \cdots & v'_{k-5}\end{bmatrix}^{\mathrm{T}},\qquad v'_k=0 \text{ for } k<1 \tag{6.13a-d}$$

If $\mathbf{a}_k^{(j)}$ is the $S^{(j)}\times 1$ vector comprising the signal outputs of the j^{th} layer then:

$$v'_{k+1}=\mathbf{a}_k^{(3)}=\mathbf{g}^{(3)}\left(\mathbf{W}^{(3)}\mathbf{a}_k^{(2)}+\mathbf{b}^{(3)}\right) \tag{6.14a}$$

$$\mathbf{a}_k^{(2)}=\mathbf{g}^{(2)}\left(\mathbf{W}^{(2)}\mathbf{a}_k^{(1)}+\mathbf{b}^{(2)}\right) \tag{6.14b}$$

$$\mathbf{a}_k^{(1)}=\mathbf{g}^{(1)}\left(\mathbf{W}^{(1)}\mathbf{p}_k+\mathbf{b}^{(1)}\right) \tag{6.14c}$$

…where $\mathbf{W}^{(j)}$ and $\mathbf{b}^{(j)}$ are respectively the matrix of weights and vector of biases of the j^{th} layer and $\mathbf{g}^{(j)}(\bullet)$ is a vector operator comprising the transfer functions of the neurons of the j^{th} layer. Each of these transfer functions operates on the respective element of the vector argument $(\bullet)$ of $\mathbf{g}^{(j)}(\bullet)$. The neuron of the output layer was taken as a purely linear transfer function [73]. The transfer functions of all neurons of the "hidden" layers (i.e. layers 1 and 2) were taken as tangent-sigmoid functions [73]. Each hidden layer had 18 neurons. The network parameters (weights and biases in equation (6.14)) were determined by training the network on empirical input-output data from dynamic tests on the damper mounted on a tensile test machine and the complete details of the this controller can be found in the text of Ref. [64]. The MR damper used throughout this research was a Lord RD-1005-3.

It is noted that the network parameters used in this paper were obtained for the damper at room temperature. It is shown in [64] that such a neural controller trained at room temperature still works well when controlling a damper subjected to a significant temperature variation. However, if more precision is required, one can also include similar networks trained in "cold" and "hot" conditions and use temperature feedback to switch between "cold", "room" and "hot" networks as appropriate.

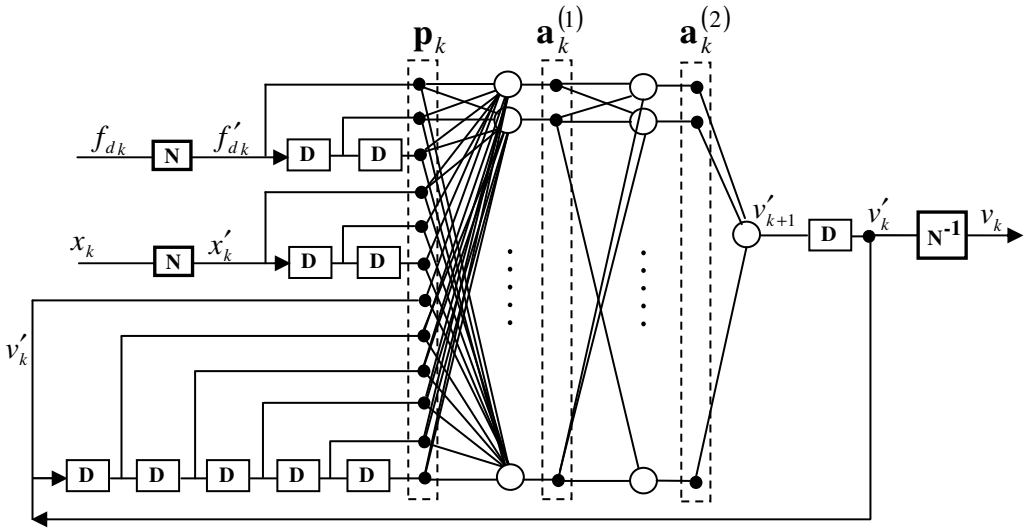

Fig. 6.4 Damper controller based on the RNN architecture of the inverse dynamics of the MR damper
(D: delay by one time step; N: normalisation; N^{-1}: de-normalisation)

6.4 Determining the System Response

For the semi-active system, the response for a given input signal x_r is obtained by integrating equations (6.1) and (6.4). f_d is determined from equation (6.7) and v from either equation (6.12) (CS control) or equation (6.14) (inverse RNN control).

For given x and v the actual damper force f_a at each time step is obtained by one of three alternative methods which are described in the following sub-sections.

6.4.1 Determination of f_a: Modified Bouc-Wen Model

As stated in the Introduction, this model is used in this research for studies involving sizeable SWS and/or frequency range that cannot be reproduced by the tensile test machine used in HILS. f_a is given by the following equations, which have been adapted from [14] for use in a suspension as shown in Fig. 6.5:

$$f_a = c_1\dot{y} + k_1(x - x_0) \tag{6.15}$$

$$\dot{y} = \frac{1}{c_0 + c_1}\{\alpha z + c_0\dot{x} + k_0(x - y)\} \tag{6.16}$$

$$\alpha = \alpha(u) = \alpha_a + \alpha_b u\ ,\ c_1 = c_1(u) = c_{1a} + c_{1b}u\ ,\ c_0 = c_0(u) = c_{0a} + c_{0b}u \tag{6.17a-c}$$

$$\dot{z} = -\gamma|\dot{x} - \dot{y}||z|^{n-1}z - \beta(\dot{x} - \dot{y})|z|^n + \delta(\dot{x} - \dot{y}) \tag{6.18}$$

$$\dot{u} = -\eta(u - v) \tag{6.19}$$

where y is the internal displacement of the MR fluid damper, u is the output of a first-order filter and z is an evolution variable to cater for the hysteretic effect. The accumulator stiffness is represented by k_1; the viscous damping observed at high and low velocities are represented by c_0 and c_1, respectively. k_0 is present to control the stiffness at high velocities; x_0 is used to account for the effect of the accumulator. The scale and shape of the hysteresis loop can be adjusted by γ, β, δ and η. A total of 14 model parameters [50], which are given in Table 6.3, are used to characterize the MR fluid damper. In order to calculate f_a by Eq. (6.13), Eqs. (6.14-6.16) have to be solved along with Eqs. (6.1), and (6.4) i.e. three extra state variables (y, z, u) are introduced.

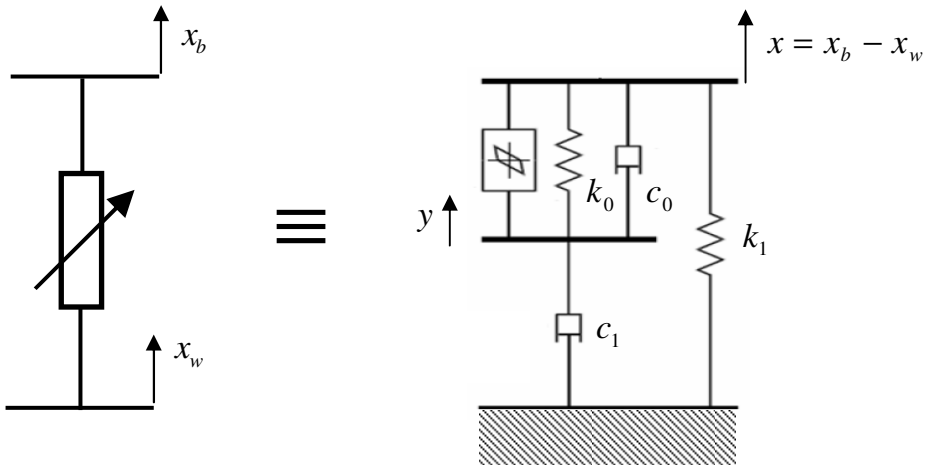

Fig. 6.5 Modified Bouc-Wen model adapted for use in the quarter-vehicle suspension model

Table 6.3 Parameters for the model of MR fluid damper [50]

PARAMETER	VALUE	PARAMETER	VALUE
c_{0a}	784 Nsm^{-1}	α_a	12441 Nm^{-1}
c_{0b}	1803 $NsV^{-1}m^{-1}$	α_b	38430 $NV^{-1}m^{-1}$
k_0	3610 Nm^{-1}	γ	136320 m^{-2}
c_{1a}	14649 Nsm^{-1}	β	2059020 m^{-2}
c_{1b}	34622 $NsV^{-1}m^{-1}$	A	58
k_1	840 Nm^{-1}	n	2
x_0	0.0245 m	η	190 s^{-1}

6.4.2 Determination of f_a: Hardware-in-the-Loop Simulation (HILS)

Hardware-in-the-loop simulation (HILS) is distinguished by the operation of real parts in connection with real-time simulated components. The setup is illustrated in Fig. 6.6(a). The hardware part consists of the MR damper mounted on an Electro-Servo Hydraulic (ESH®) tensile testing machine. The schematic diagram of the test

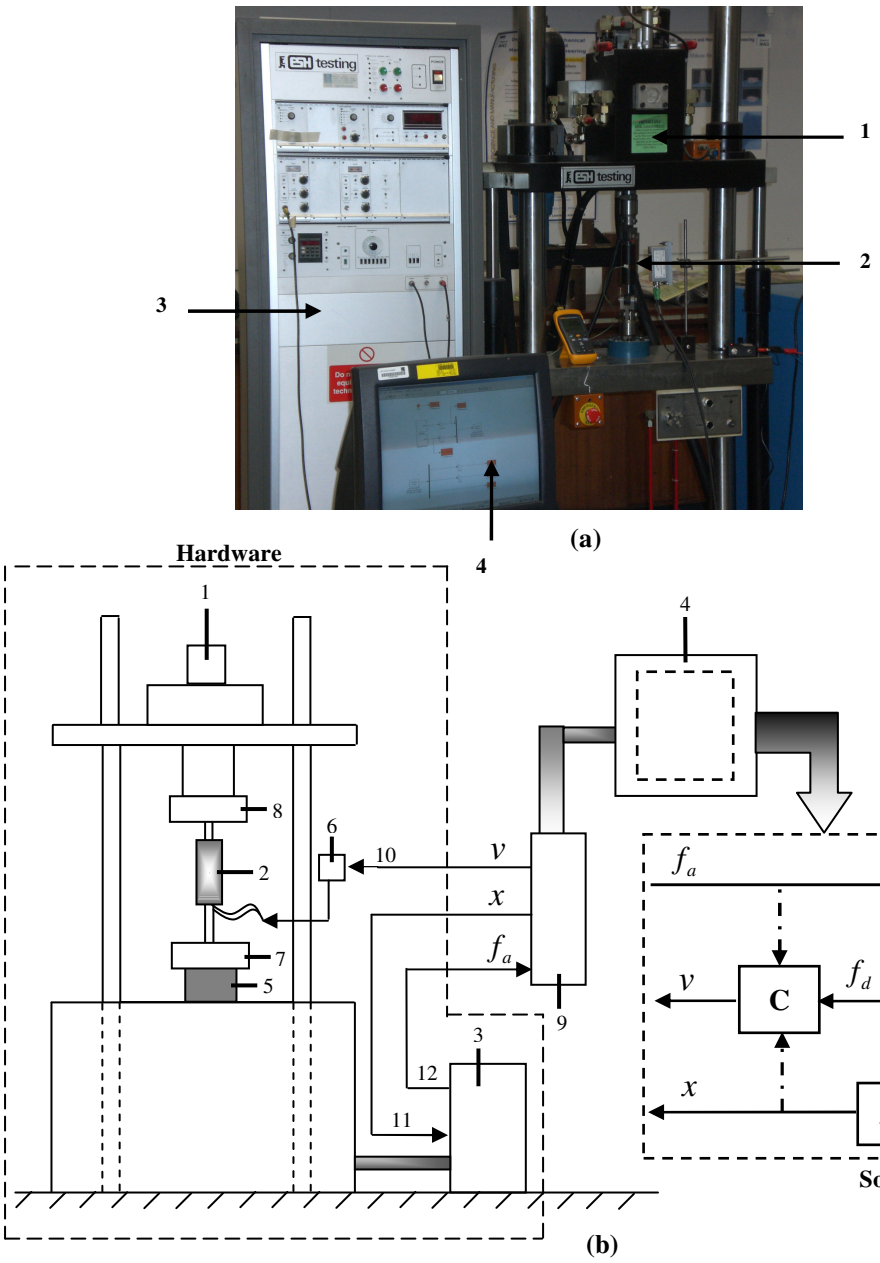

1- Hydraulic actuator **2- MR damper** **3- ESH Control panel**

4- Computer **5- Load cell** **6- Current driver**

7- Fixed head **8- Moving head** **9- Data acquisition card**

10- Voltage signal **11- SWS signal** **12- Actual Force signal**

A- Quarter vehicle model (Fig. 6.1) **B- System controller (Fig. 6.3)**

C-Damper controller (Fig. 6.4 or Eq. (6.10))

Fig. 6.6 Hardware-in-the-loop simulation (HILS) setup
a- HILS photo b- Schematic diagram

setup is illustrated in Fig. 6.6(b). The tensile testing machine had upper and lower jaws that grasped the damper at the appropriate locations. The upper head was the moveable end and was operated by a hydraulic actuator that could be driven by a computer-generated displacement signal (SWS, x). The lower head incorporated a load cell to measure f_a. Also, the current driver of the damper coil could take an applied voltage signal (v).

The software part consists of the mathematical model of the quarter vehicle suspension system, the system controller and the damper controller. The software receives the measured damper force f_a and sends signals x and v to the tensile test machine and the damper current driver respectively. The software was written in Matlab and Simulink and the Real-Time Workshop® and Real-Time Windows Target® tool-boxes were used for real-time computation and interfacing with the experimental hardware via the data acquisition card.

6.4.3 Determination of f_a: Forward Recurrent Neural Network (RNN) model

This damper model is based on a recurrent neural network simulating the forward dynamics of the MR damper (Fig. 6.7). Its inputs are the time histories of the relative displacement x across the damper and the voltage v. Its output is the damper force f_a. Using the same notation as in section 6.3.2.2, the output is computed in a similar manner to Eqs. (6.14a-c), with the following modifications:

$$f'_{ak+1} = \mathbf{a}_k^{(3)} \tag{6.20}$$

$$\mathbf{p}_k = \begin{bmatrix} \mathbf{v}'_k \\ \mathbf{x}'_k \\ \mathbf{f}'_{ak} \end{bmatrix}, \quad \mathbf{v}'_k = \begin{bmatrix} v'_k \\ v'_{k-1} \\ v'_{k-2} \end{bmatrix}, \quad \mathbf{x}'_k = \begin{bmatrix} x'_k \\ x'_{k-1} \\ x'_{k-2} \end{bmatrix},$$

$$\mathbf{f}'_{ak} = \begin{bmatrix} f'_{ak} & f'_{ak-1} & \cdots & f'_{ak-5} \end{bmatrix}^{\mathrm{T}},\ f'_{ak} = 0 \text{ for } k < 1 \qquad \text{(6.21a-d)}$$

The weights and biases are of course different from the inverse RNN model of section 6.3.2.2 but are obtained using the same experimental training data.

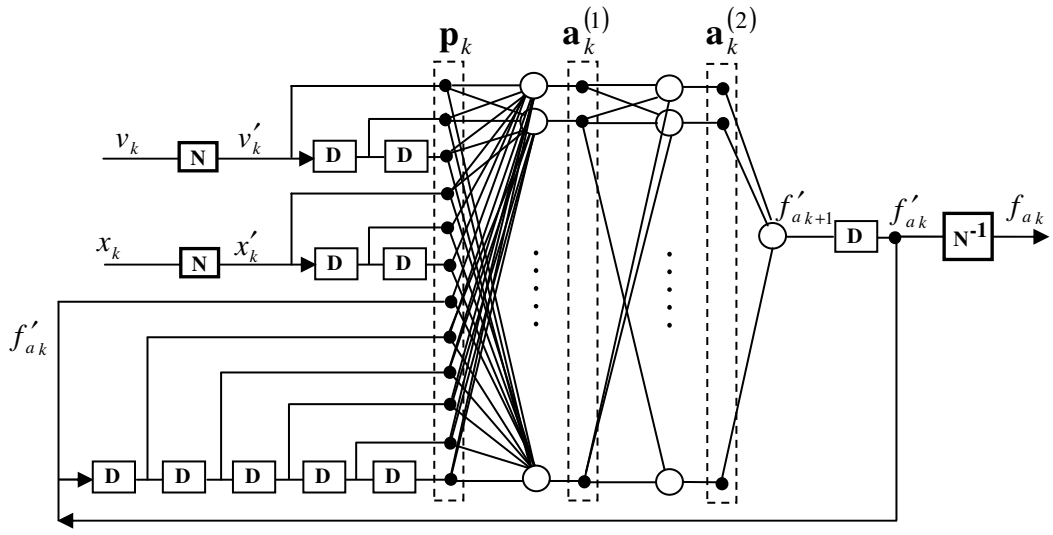

Fig. 6.7 Neural network model of the forward dynamics of the MR damper based on RNN architecture
(D: delay by one time step; N: normalisation; N^{-1}: de-normalisation)

6.5 Results and Discussion

Suspension working space (SWS), vertical body acceleration (BA), and dynamic tyre load (DTL) are the three main performance criteria in vehicle suspension design that govern ride comfort and vehicle stability. Ride comfort is closely related to the BA. To certify good vehicle stability, it is required that the tyre's dynamic deformation $(x_w - x_r)$ should be low [8]. The structural characteristics of the vehicle also constrain the amount of SWS within certain limits. In the present study, the control system forces the suspension to emulate the response of the ideal skyhook system in

Figure 6.3(a). In so doing, it is expected to result in reduced values of BA, SWS and DTL, and hence, improved suspension performance.

This section studies suspension performance for four cases of vibration control: (a) conventional passive damping i.e. Eq. (6.2a) for f, with $c_s = 980\,\text{Ns/m}$ as in [76]; (b) semi-active control with CS-controlled MR damper (Eq. (6.12)); (c) semi-active control with inverse RNN controlled MR damper (Eq. (6.14)); (d) MR passive damping i.e. MR damper used but its current driver is turned OFF. The above-mentioned performance criteria are used to quantify the relative performance of these control methods. This comparative study is performed for each of the three methods for obtaining the damper force f_a for given time histories v and x, as described in section 6.4. Since the conventional damping case is used as a base-line for comparisons it is worth mentioning that the value quoted for c_s is typical for automotive applications [76]. Moreover, preliminary simulations performed with harder and softer conventional dampers ascertained the well-known conflicting requirements of vehicle comfort and stability mentioned in the Introduction.

6.5.1 Studies using Bouc-Wen model for f_a

Two types of road excitation, chosen to be very similar to the real-world road profiles, were considered for this study. The first excitation, normally used to reveal the transient response characteristic, is a road bump and described by [78] as:

$$x_r = \begin{cases} a\ \{1-\cos(\omega_r(t-0.5))\}, & \text{for} \quad 0.5 \le t \le 0.5 + \dfrac{d}{V} \\ 0, & \text{otherwise} \end{cases} \tag{6.22}$$

where a is the half of the bump amplitude, $\omega_r = 2\pi V / d$, d is the width of the bump

and V is the vehicle velocity. In this study a = 0.035 m, d = 0.8 m, V = 0.856 m/s, as in [78].

The time history of the suspension system response under this road disturbance excitation is shown in Fig. 6.8. The displacement of the road input signal is shown in Fig. 6.8(a) and the SWS, BA, and DTL responses are shown in Figs. 6.8(b, c, and d) respectively. The latter figures show the comparison between the controlled semi-active using inverse RNN control, CS control, the MR passive and conventional passive. From these results it is seen that the inverse RNN controlled suspension can dissipate the energy due to bump excitation very well, cut down the settling time, and improve both the ride comfort and vehicle stability. The input voltage for the two controlled systems is compared in Fig. 6.8(e) the results show that in the case of inverse RNN control the signal is more continuous and the maximum value is lower than the case of CS control.

The peak-to-peak (PTP) values of the system response are summarised in Table 6.4, which shows that the two controlled systems have the lowest peaks for the SWS, BA, and DTL, demonstrating their effectiveness at improving the ride comfort and vehicle stability. The controlled system with inverse RNN control can reduce maximum peak-to-peak of SWS, BA and DTL by 24 %, 8.2 and 7.6 %, respectively, compared with the controlled system with CS control. Also, the three MR systems were compared with the conventional passive system and the improvement percentages are listed in Table 6.4. The results show that the semi-active vehicle suspension system controlled with inverse RNN offers a superior performance.

It is noted that the resonance of the body over the suspension spring, assuming a rigid tyre, is 1.3 Hz. The frequency spectrum of the excitation x_r for the speed considered (0.856 m/s, for which ω_r in Eq. 6.22 is 6.72 rad/s or 1 Hz) reveals a main lobe that is maximum at 0 Hz and decreases monotonically to zero at 2.2 Hz. There is also a minor lobe that extends from 2.2 Hz to 3.2 Hz. For higher speeds *V*, the frequency spectrum of x_r is more spread out (the lobe becomes shorter and fatter). Hence, this choice of speed (0.856m/s) can be regarded as a challenging scenario for the suspension system, particularly with regard to ride comfort. It is noted however that as the speed is increased, the higher frequencies appearing in the excitation spectrum contribute to an increase in the damper force. However, by repeating the calculations at higher speeds (twice and four times the above speed) it was verified that RNN control still gives superior performance, as shown in Table 6.5.

The second type of road excitation was a random road profile described by [78] as:

$$\dot{x}_r + \rho V x_r = V W_n \tag{6.23}$$

where W_n is white noise with intensity $2\sigma^2 \rho V$, ρ is the road irregularity parameter, and σ^2 is the covariance of road irregularity. In random road excitation, the values of road surface irregularity (ρ =0.45 m^{-1} and σ^2 =300 mm^2) were selected assuming that the vehicle moves on the paved road with the constant speed *V* = 20 m/s, as in [78].

In order to improve the ride comfort, it is important to isolate the vehicle body from the road disturbances and to decrease the resonance peak of the body mass near 1 Hz which is known to be a sensitive frequency to the human body [8, 79]. Moreover, in

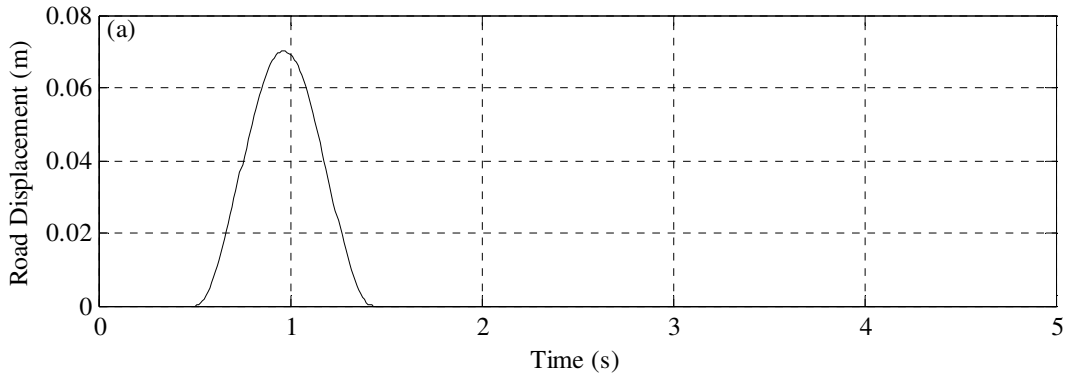
(a)
Road Displacement (m)
0.08
0.06
0.04
0.02
0
0
1
2
3
4
5
Time (s)

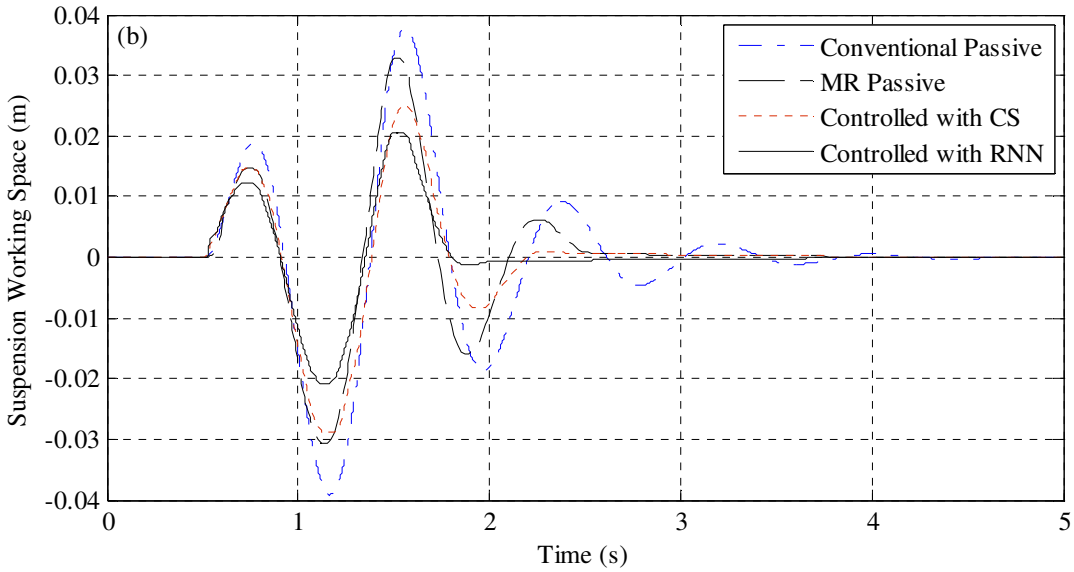
(b)
Suspension Working Space (m)
0.04
0.03
0.02
0.01
0
-0.01
-0.02
-0.03
-0.04
0
1
2
3
4
5
Time (s)
Conventional Passive
MR Passive
Controlled with CS
Controlled with RNN

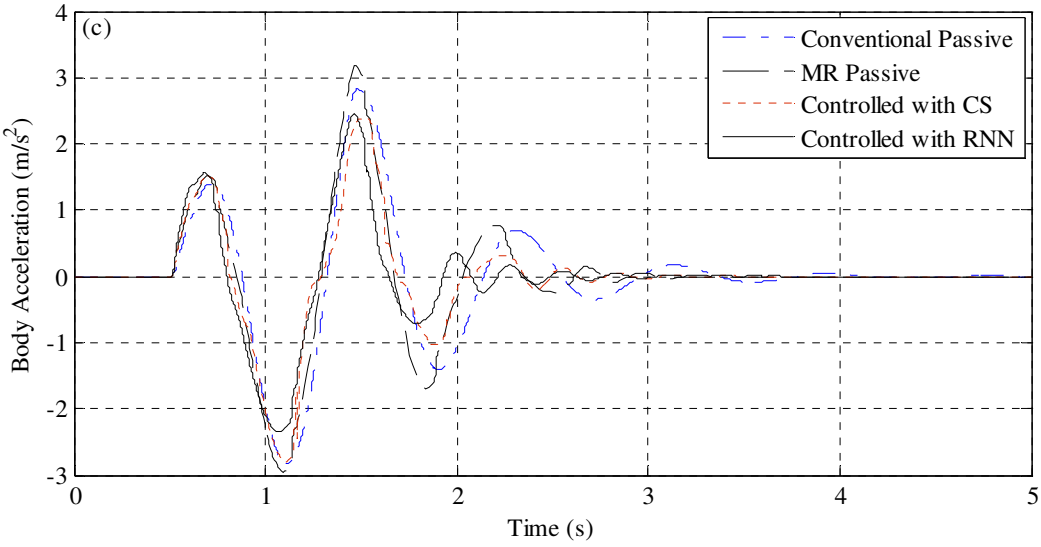
(c)
Body Acceleration (m/s2)
4
3
2
1
0
-1
-2
-3
0
1
2
3
4
5
Time (s)
Conventional Passive
MR Passive
Controlled with CS
Controlled with RNN

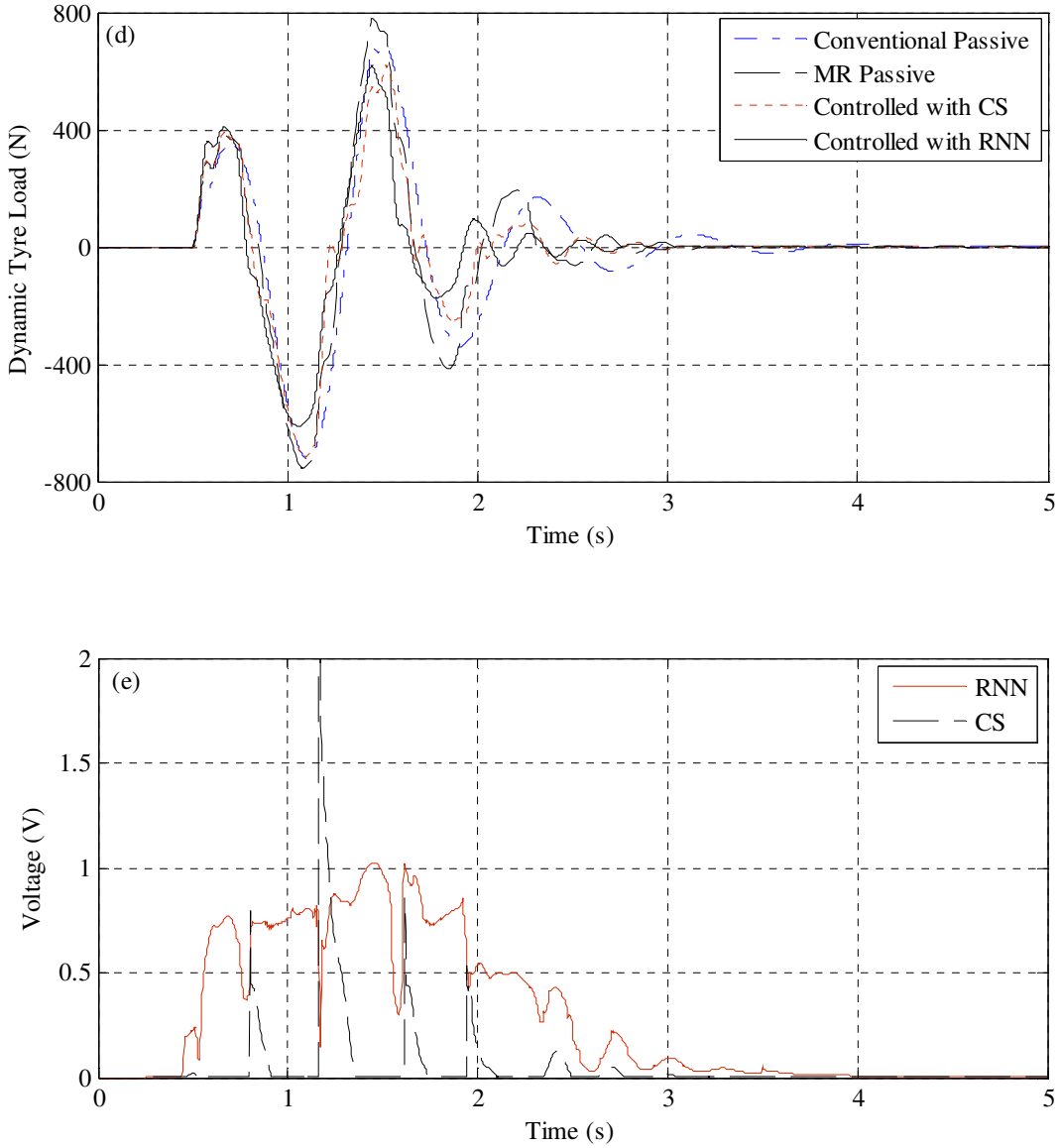

Fig. 6.8 The time history of system response under road bump excitation.
a- Road Displacement b- SWS c- BA
d- DTL e-Input Voltage

order to improve the vehicle stability, it is important to keep the tyre in contact with the road surface and therefore to decrease the resonance peak near 10 Hz, which is known to be a sensitive frequency to the human body [8, 79]. In view of these considerations, the results obtained for the excitation described by Eq. (6.22) are presented in the frequency domain.

Table 6.4 PTP values and improvement ratios of road disturbance excitation

System Type	SWS **(m)**	% Imp. Respect to Con. Passive	% Imp. Respect to MR Passive	% Imp. Respect to CS	BA **(m/s^2)**	% Imp. Respect to Con. Passive	% Imp. Respect to MR Passive	% Imp. Respect to CS	DTL **(N)**	% Imp. Respect to Con. Passive	% Imp. Respect to MR Passive	% Imp. Respect to CS
Conventional Passive	0.076	-	-	-	5.7	-	-	-	1406.7	-	-	-
MR Passive	0.063	17.1	-	-	6.1	-8.1	-	-	1537.7	-9.31	-	-
CS	0.054	28.9	14.3	-	5.2	7.9	14.9	-	1331.2	5.37	13.43	-
RNN	0.041	46	34.9	24	4.8	15.5	21.9	8.24	1230	12.56	20.01	7.6

Table 6.5 PTP values of all control systems for road bump excitation at different vehicle speeds V (V_0=*0.856 m/s*)

System Type	SWS (m)			BA (m/s^2)			DTL (N)		
	$V=V_0$	$V=2V_0$	$V=4V_0$	$V=V_0$	$V=2V_0$	$V=4V_0$	$V=V_0$	$V=2V_0$	$V=4V_0$
Conventional Passive	0.076	0.105	0.128	5.67	8.35	12.63	1406.7	1982	3393
MR Passive	0.063	0.097	0.112	6.13	8.84	13.05	1537.7	2343	3420
CS	0.054	0.084	0.108	5.22	7.95	12.36	1331.2	2190	3250
RNN	0.041	0.073	0.103	4.79	7.21	11.95	1230	1795	3157

Figure 6.9 shows the modulus of the Fast Fourier Transform (FFT) of the SWS, BA, and DTL responses over the range 0.5-20 Hz. The FFT was appropriately scaled and smoothed by curve fitting as done in [80]. It is evident that the lowest resonance peaks for body and wheel can be achieved using the proposed inverse RNN control strategy. According to these figures, just like for the bump excitation, the controlled system with inverse RNN control can dissipate the energy due to road excitation very well and improve both the ride comfort and vehicle stability. The input voltage for the two controlled systems is compared in Fig. 6.9(d) and Fig. 6.9(e) shows a zoomed image for the voltage signals between 6 and 8 seconds. The results again prove that in the case of RNN the signal is more continuous, smoother and the maximum value is lower than the case of CS.

In the case of random excitation, it is the root mean square (RMS) values of the SWS, BA and DTL, rather than their peak-to-peak values, that are relevant. These are presented in Table 6.6, which shows that the controlled system using inverse RNN control has the lowest levels of RMS values for the SWS, BA, and DTL. Inverse RNN control can reduce maximum RMS values of SWS, BA and DTL by 18.7 %, 19.6 and 9.9 %, respectively, compared with CS. Table 6.5 also compares the three MR systems with the conventional passive system. The results again confirm that the semi-active vehicle suspension system controlled with inverse RNN can give a superior response in terms of ride comfort and vehicle stability.

It should be noted that, although the Bouc-Wen model was used to determine f_a in this section, the inverse RNN controller was based on experimentally trained data obtained using a tensile testing machine which was restricted to a lower relative

displacement x and a narrower frequency range than those used in these simulations. Despite this, the inverse RNN controller still gave the best performance results.

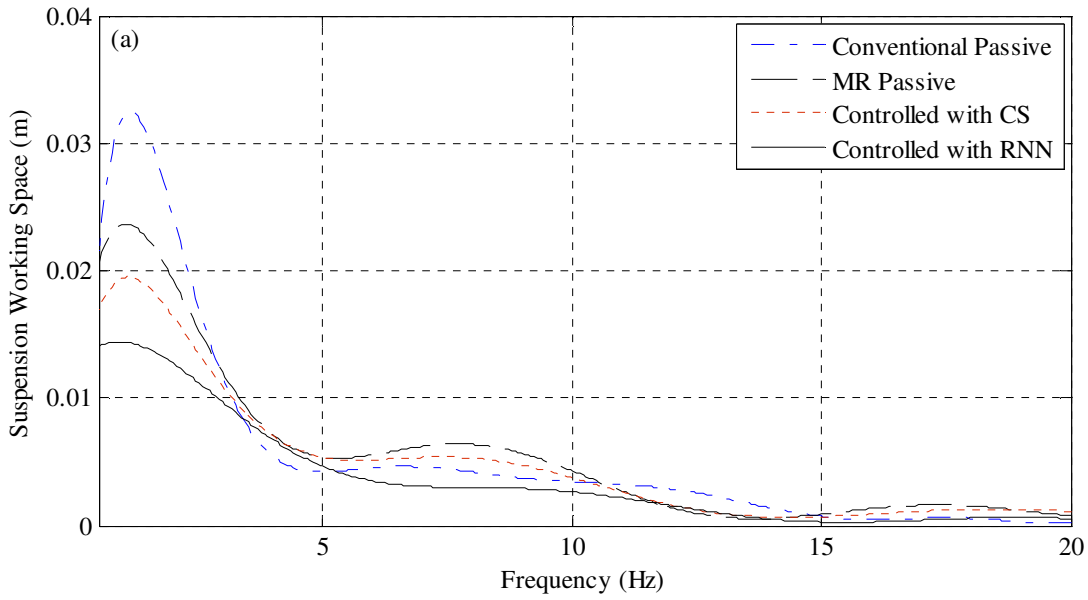

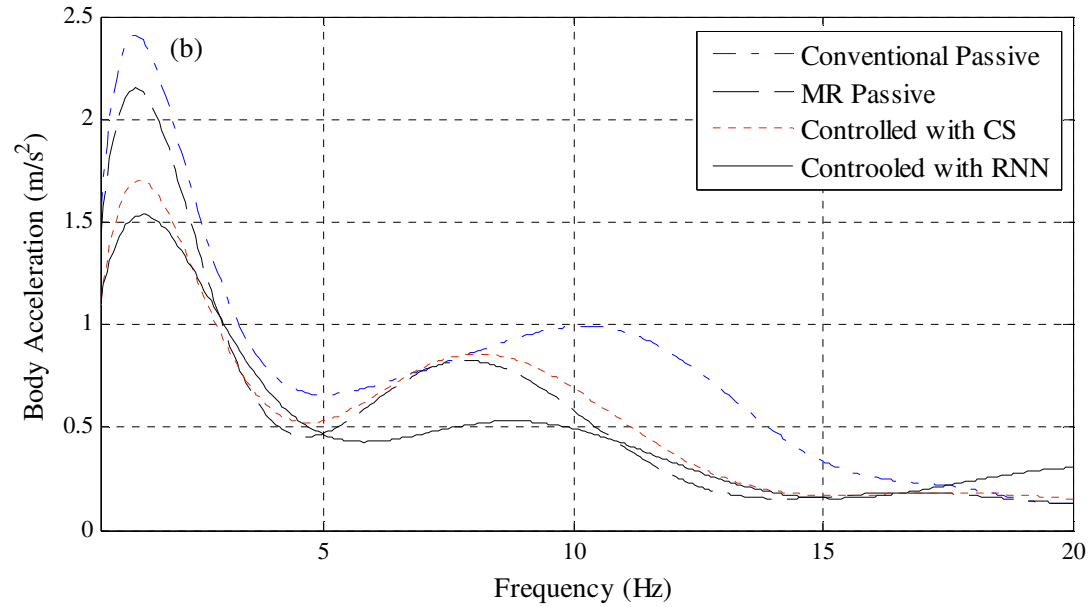

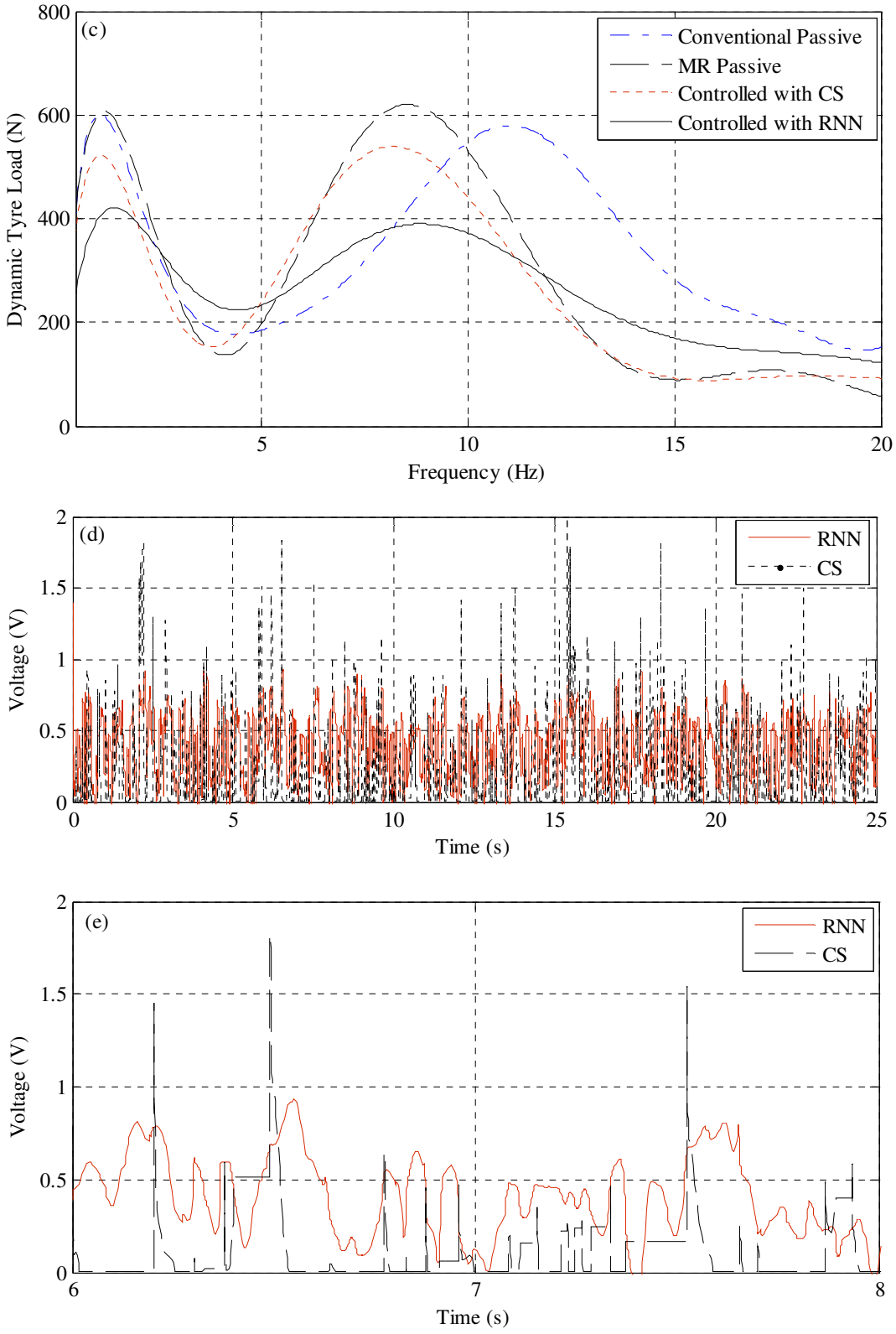

Fig. 6.9 The system response under random road excitation.
a- SWS b- BA c- DTL
d- Input Voltage e- Input Voltage (zoomed)

Table 6.6 RMS values and improvement ratios of random road excitation

System Type	SWS **(m)**	% Imp. Respect to Con. Passive	% Imp. Respect to MR Passive	% Imp. Respect to CS	BA **(m/s^2)**	% Imp. Respect to Con. Passive	% Imp. Respect to MR Passive	% Imp. Respect to CS	DTL **(N)**	% Imp. Respect to Con. Passive	% Imp. Respect to MR Passive	% Imp. Respect to CS
Conventional Passive	0.0139	-	-	-	1.17	-	-	-	455.9	-	-	-
MR Passive	0.0130	6.5	-	-	1.16	0.9	-	-	447.1	1.9	-	-
CS	0.0107	23.0	17.7	-	0.97	17.1	16.4	-	390.0	14.5	12.8	-
RNN	0.0087	37.4	33.0	18.7	0.78	33.3	32.7	19.6	351.5	22.9	21.4	9.9

6.5.2 Study using HILS for f_a

In this test, the road displacement was a band-limited Gaussian white noise signal which was band-limited to the range 0-3 Hz, this frequency range is appropriate for automotive applications and a previous published work used a similar range (0.4-3 Hz such as [81]), with ± 0.02 m amplitude, as in [64].

The time domain SWS, BA, and DTL responses are shown in Figs. 6.10 (a, b, and c) respectively. It is noted that for the case of the conventional passive damping a conventional automotive shock absorber of coefficient 1170 Ns/m was used instead of the MR damper in Fig. 6.6 and its measurement was scaled in Simulink by $980/1170$. This scaling was necessary as the damping coefficient of 1170 Ns/m obtained from the damper is higher than the damping coefficient of 980 Ns/m specified by [76] and listed in Table 6.1. The other parameters in Table 6.1 were used as they are in the HILS procedure or the conventional passive system. From Fig. 6.10, it is again evident that the controlled system with inverse RNN control gave a significant reduction in all the performance criteria over the test time. Also, Fig. 6.10(d) again shows that the voltage signal produced by the inverse RNN controller is more continuous, smoother and the maximum value is lower than the case of CS.

The RMS values of the system response results by HILS are summarised in Table 6.7, which shows that the controlled system using RNN has the lowest levels of RMS values for the SWS, BA, and DTL. The controlled system with RNN can reduce maximum RMS values of SWS, BA and DTL by 31.1 %, 14.1% and 13.5 %, respectively, compared with the controlled system with CS. Table 6.6 also compares

Table 6.7 RMS values and improvement ratios of road disturbance excitation via HILS

System Type	SWS **(m)**	% Imp. Respect to Con. Passive	% Imp. Respect to MR Passive	% Imp. Respect to CS	BA **(m/s^2)**	% Imp. Respect to Con. Passive	% Imp. Respect to MR Passive	% Imp. Respect to CS	DTL **(N)**	% Imp. Respect to Con. Passive	% Imp. Respect to MR Passive	% Imp. Respect to CS
Conventional Passive	0.0053	-	-	-	0.505	-	-	-	138.1	-	-	-
MR Passive	0.0049	7.8	-	-	0.496	1.9	-	-	134.4	2.7	-	-
CS	0.0045	15.1	8.2	-	0.467	7.5	5.8	-	120	13.1	10.7	-
RNN	0.0031	41.5	36.7	31.1	0.401	20.6	19.1	14.1	103.8	24.8	22.8	13.5

the three MR systems with the conventional passive system. These results again show that the semi-active vehicle suspension system controlled with inverse RNN control gives the best improvements in ride comfort and vehicle stability.

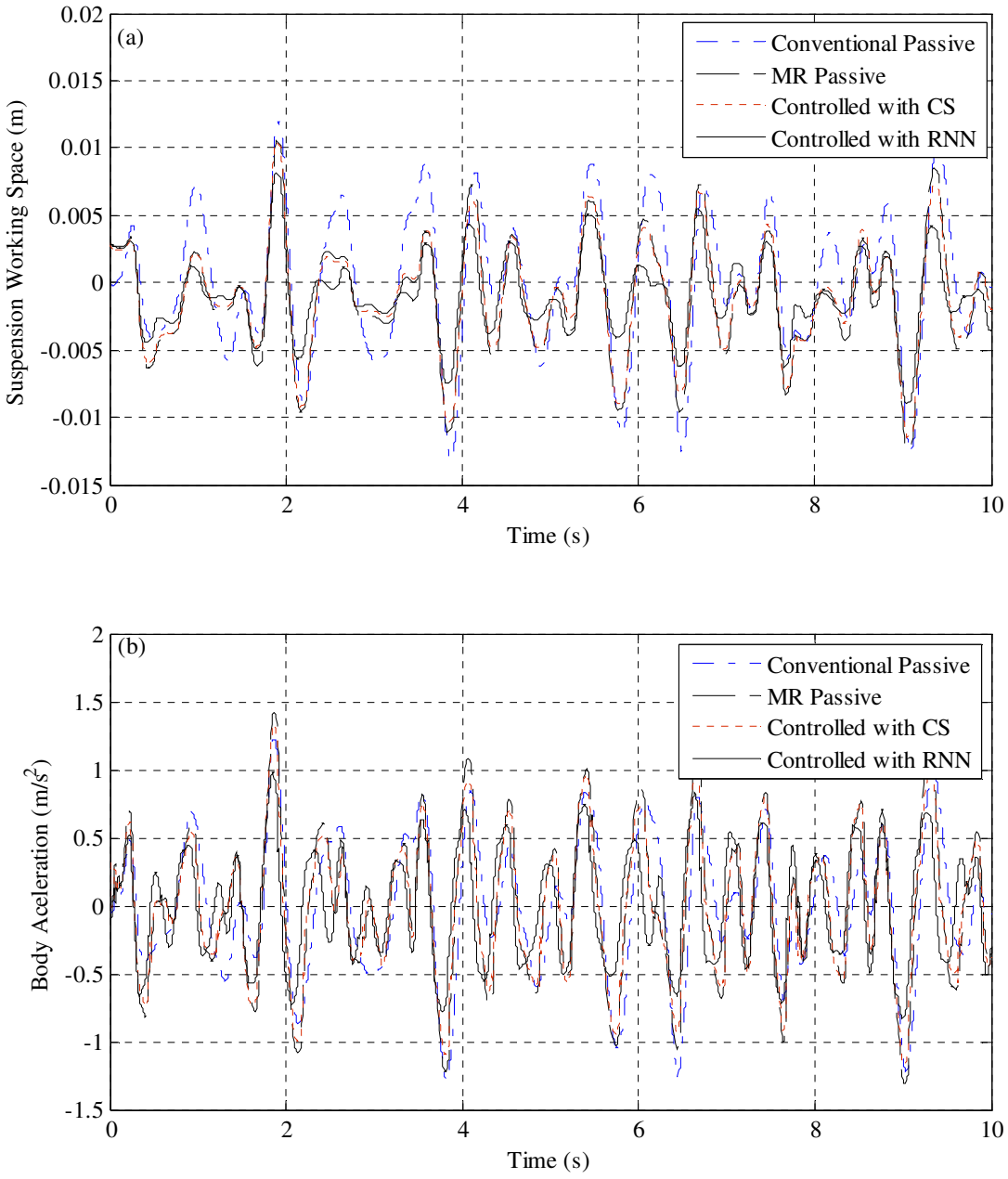

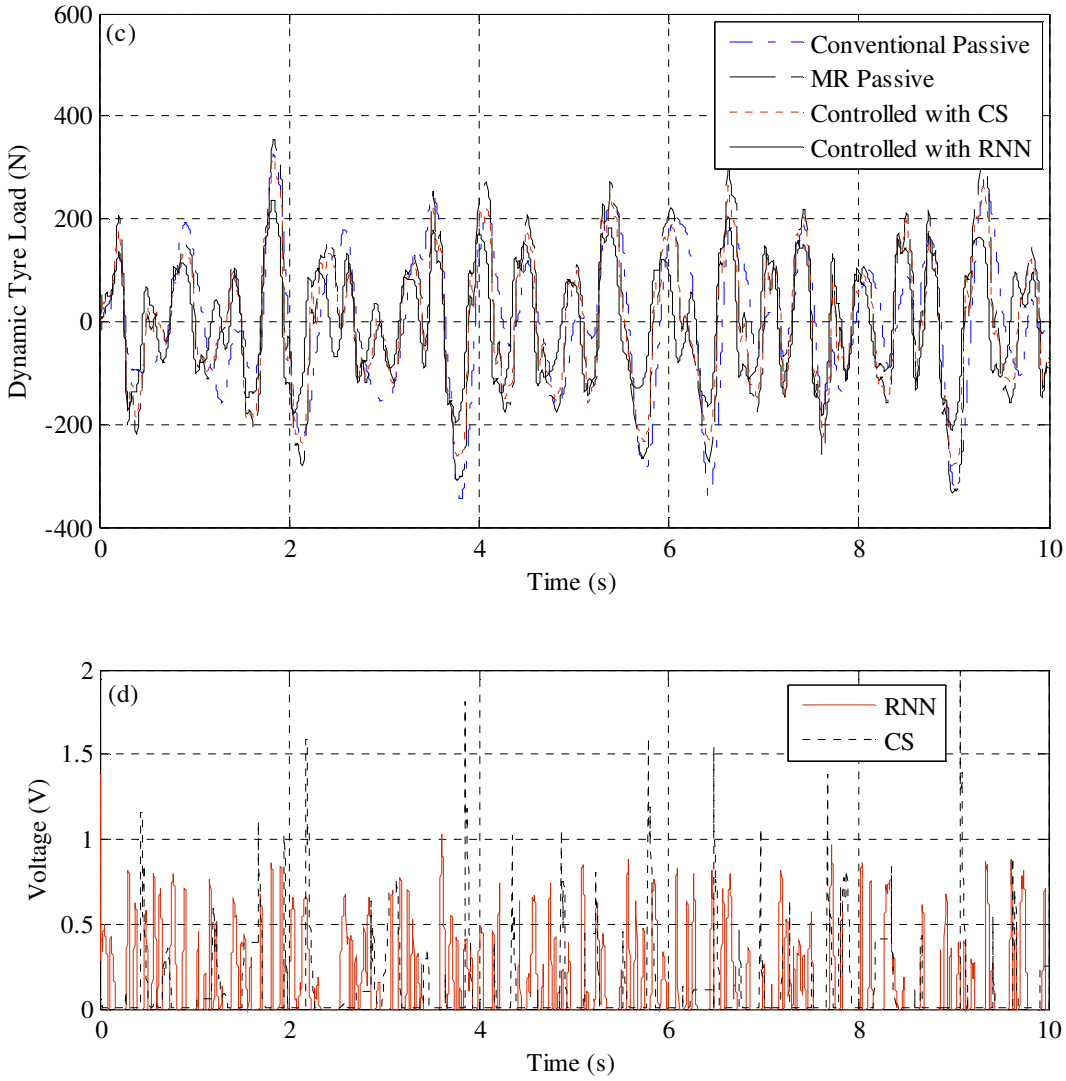

Fig. 6.10 The time history of system response to random excitation via HILS
a- SWS b- BA c- DTL d-Input Voltage

6.5.3 Study using forward RNN model to determine f_a

The suspension performance for the same input excitation used in the HILS study was redone using the neural damper model of Fig. 6.7. Figure 6.11 (a) compares the time histories of the resulting body displacement with that obtained by HILS. It is evident that there is very good agreement between the two. Figure 6.11 (b) shows that the error between the two signals is less than 0.4 %. This means that the forward neural model is a good substitute for HILS where this is not practicable,

namely for testing multi-damper suspension models i.e. half and full-vehicle models, which would necessitate two or four tensile testing machines if HILS were used.

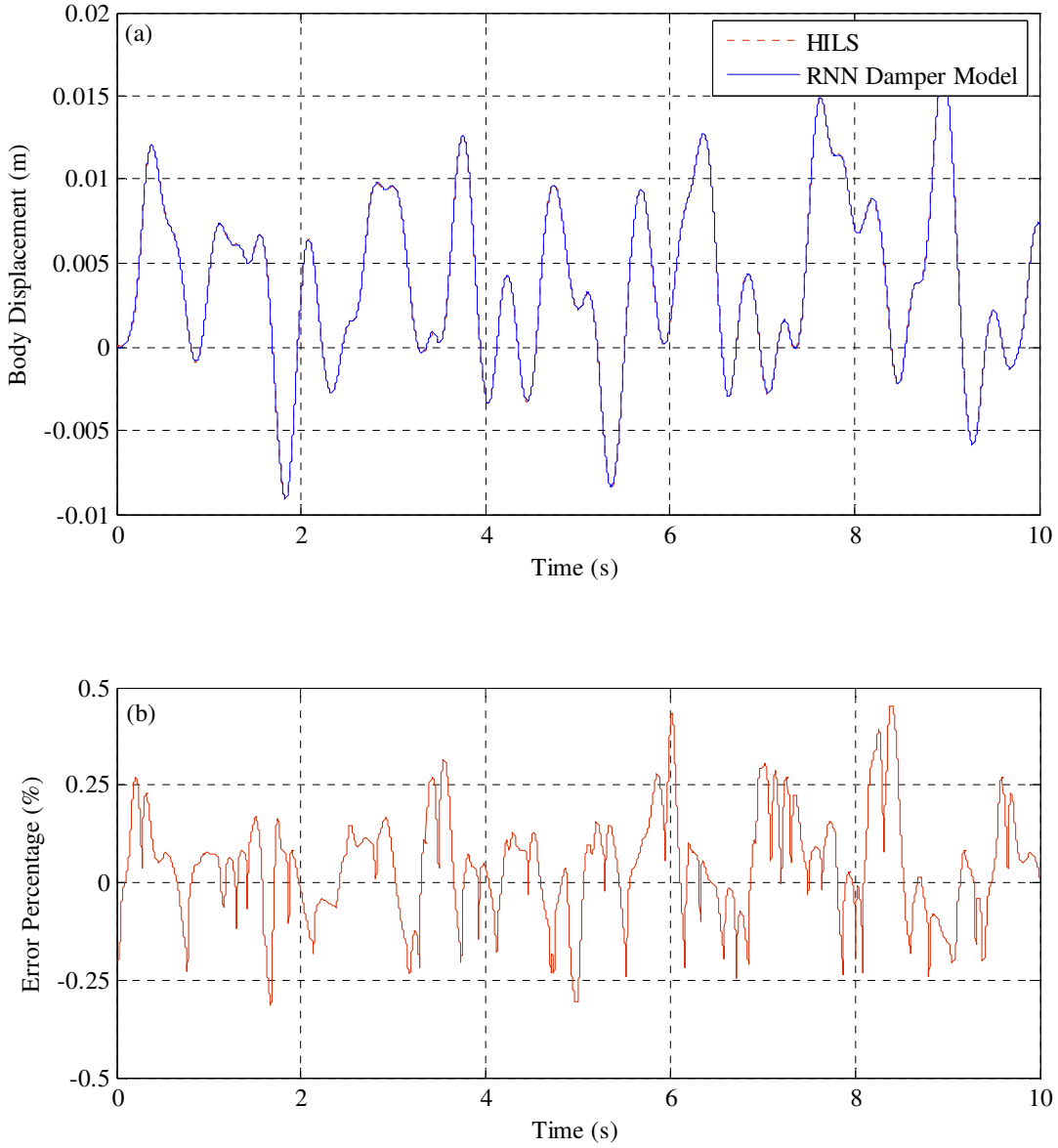

Fig. 6.11 Comparison between the performance of HILS and direct RNN model of MR damper suspension systems.

a- Body displacement b- Error Percentage

6.6 Conclusions

This paper has introduced a neural-based MR damper controller for use in conjunction with the system controller of a semi-active vehicle suspension. The performance obtained with this damper controller was compared with that obtained using a continuous state (CS) damper controller, MR passive damping, and passive damping using a conventional shock absorber. A mathematical model of a semi-active quarter vehicle suspension system using an MR damper was derived. The system controller used a sliding mode control algorithm to force the system to emulate the performance of an ideal reference system with due account of loading uncertainties being taken. Control performance criteria such as suspension working space, body acceleration and dynamic tyre load were evaluated in the time and frequency domains in order to quantify the suspension effectiveness under bump and random road disturbance. Studies using the modified Bouc-Wen model for the MR damper, as well as an actual damper fitted in a hardware-in-the-loop simulation (HILS), both showed that a damper controller based on an RNN model of the inverse MR dynamics potentially offers significantly superior ride comfort and vehicle stability over an MR damper controller based on CS control. The neural controller also produced a smoother and lower input voltage to the MR damper coil, respectively ensuring extended damper life and lower power requirement. The results also indicated that the neural controller's performance was superior even when operating outside the limits of the data used in its training. Studies performed using an RNN model of the forward dynamics of the MR damper showed that it is a reliable substitute for HILS for validating multi-damper control applications.

CHAPTER 7

Vibration Control of a Seat Suspension System using Magnetorheological Damper

Authors:

Hassan Metered, Philip Bonello and S Olutunde Oyadiji

Reformatted version of paper published in:

ASME International Design Engineering Technical Conferences & Computers and Information in Engineering Conference, IDETC/CIE 2009.
August 30 - September 2, 2009, San Diego, California, USA
Paper Number: DETC2009/CIE-86081

Abstract

A car seat's suspension system is critical to the ride comfort experience of a vehicle's driver and passengers. The use of a magnetorheological (MR) damper in a seat suspension system has been shown to offer significant benefits in this regard. In most research on seat MR dampers the control implementation was not quite appropriate for the semi-active and nonlinear hysteretic nature of the MR damper.

This paper introduces a more suitable semi-active control strategy for an MR damper used in a seat suspension, enabling more effective control. The proposed control system comprises a system controller that computes the desired damping force using a sliding mode control algorithm, and a neural-based damper controller that provides a direct estimation of the command voltage that is required to track the desired damping force. The seat suspension system is approximated by a base-excited single degree of freedom system. The proposed semi-active seat suspension is compared to a passive seat suspension for prescribed base displacements. These inputs are representative of the vibration of the sprung mass of a passive or semi-active quarter-vehicle suspension under bump or random-profile road disturbance. Control performance criteria such as seat travel distance and seat acceleration are evaluated in time and frequency domains, in order to quantify the effectiveness of proposed semi-active control system. The simulated results reveal that the use of semi-active control in the seat suspension provides a significant improvement in ride comfort.

7.1 Introduction

Seat suspension systems have a major role in offering the vehicle's driver and passengers with an adequate level of comfort. Passive suspension systems using oil dampers give system simplicity and cost reduction. However, performance limitations are unavoidable [82]. Moreover, the seat suspension system should be especially effective in the low frequency range because the seat vibration energy is concentrated at low frequency below 10 Hz [61]. Active suspensions can offer high control performance over any specified frequency range [83]. Nevertheless, active suspensions require high power requirements, sensors, and servo-valves, making them not cost-effective for seat suspensions.

Semi-active suspension systems are considered to be an effective way of resolving the drawbacks of active suspensions [9]. In general, semi-active suspension systems offer a desirable performance comparable to that achieved with active systems but without high costs. Magnetorheological (MR) dampers are semi-active devices that are becoming popular in vehicle seat suspension applications because most vehicles have the facility to provide the voltage (or current) that is required to generate a controllable variable damping force. References [25, 58-60] provide examples of research into seat suspensions with MR dampers. In most of these works [25, 58, 59] the control implementation was not quite appropriate for the semi-active and nonlinear hysteretic nature of the MR damper. For example, in [25, 59] the current required to produce the skyhook damper force was calculated on the basis of the simplified Bingham Model, which assumes that the damper force is $F_d = k_a x + c_f \dot{x} + P_{MR}$ where x is the relative displacement across the damper ends, k_a is the stiffness of the accumulator, c_f is the viscosity of the carrier fluid and P_{MR} is a controllable part that is independent of velocity and only dependent on current. This model is known to be inadequate for MR damper control purposes since it neglects nonlinearity and hysteresis in the force-velocity loop [14]. The skyhook control strategy was applied in [25, 59] to P_{MR} as follows:

$$P_{MR} = G\dot{x}_1 \quad for \quad \dot{x}_1(\dot{x}_1 - \dot{x}_2) > 0 \quad and \quad P_{MR} = 0 \quad for \quad \dot{x}_1(\dot{x}_1 - \dot{x}_2) \le 0$$

where x_1, x_2 are the displacements of the sprung and unsprung masses respectively and G is a gain. Hence, with such a control strategy there would be a passive damping component $c_f(\dot{x}_1 - \dot{x}_2)$ that would tend to increase the absolute velocity $\dot{x}_1$ of the sprung mass when $\dot{x}_1(\dot{x}_1 - \dot{x}_2) \le 0$. The addition of such a passive damping component between the sprung and unsprung masses results in a non-ideal skyhook

system [2]. In [58], the MR damper force was assumed to be a linear function of the velocity and an empirical relation was established between the approximate damping coefficient of the MR damper and the applied current. A more appropriate approach is to use a semi-active or adaptive control scheme that would enable the MR damper to accurately track the desired control force and force the system to emulate an ideal skyhook model. To date, such semi-active control schemes have been mainly used in seat suspensions containing an electrorheological damper e.g. [61, 62], although adaptive control of a seat MR damper has been recently considered [60].

This paper introduces an improved semi-active control strategy for an MR damper used in a seat suspension, enabling more effective control while retaining simplicity in implementation. Like most semi-active systems, the proposed system comprises a "system controller" that computes the desired damping force and some means of commonly the "damper controller" to produce this force. In this paper, a sliding mode control algorithm is used for the system controller since this guarantees robustness to model uncertainties e.g. (variations in sprung mass). A neural-based "damper controller" is used to provide a direct estimation of the command voltage that is required to track the desired damping force. The damper controller is trained using an experimental identification procedure. The main advantages of using a neural network damper controller over conventional damper controllers e.g. [5, 48, 49] are its robustness, extended service life of the damper and the minimal use of sensors.

Although some researchers have used a multi-degree-of-freedom model for the seat suspension [25, 61, 62, 84], most others have approximated the seat suspension

system as a base-excited single-degree-of-freedom system [60, 85-88]. This latter approach is adopted in this paper. The proposed semi-active seat suspension is compared to a passive seat suspension for prescribed base displacements. Following the work in [61, 84], representative examples for these input signals to the seat suspension base are obtained by solving separately a quarter-vehicle suspension model that excludes the seat dynamics (i.e. a two-degree-of-freedom vehicle model). These inputs are representative of the vibration of the sprung mass of a quarter vehicle suspension under bump or random-profile road disturbance. Since the quarter vehicle suspension can be either passive or semi-active, four possible seat suspension problems can be considered for any given road disturbance: (a) passive seat suspension with input disturbance calculated from a passive vehicle suspension; (b) passive seat suspension with input calculated from a semi-active vehicle suspension; (c) semi-active seat suspension with input calculated from a passive vehicle suspension; (d) semi-active seat suspension with input calculated from a semi-active vehicle suspension. It should be noted that a more accurate approach would involve consideration of the full three-degree-of-freedom model that couples the quarter-vehicle suspension with the seat suspension. However, the above described prescribed seat-base displacement method, also used by other researchers [61, 84], is considered as an adequate first approximation for the preliminary assessment of semi-active seat suspension performance. Control performance criteria such as seat travel distance (STD) and seat acceleration (SA) are assessed in time and frequency domains, under two road conditions, in order to quantify the effectiveness of proposed control system.

The rest of this paper is organized as follows: section 7.2 describes the seat suspension model. The semi-active control algorithm using MR dampers is explained in section 7.3. The results are discussed in section 7.4.

7.2 Modeling of Vehicle Seat Suspension

Figure 7.1 shows the passive and semi-active vehicle seat suspension models based on a single degree of freedom (SDOF) idealisation system. The semi-active suspension uses an MR damper. The damper is represented by a controllable MR damper force, F_a, which is adopted in this study using the modified Bouc-Wen model, shown in Fig. 7.2, of MR damper [14]. The vertical motion of the seat is described by the displacement x_s while the seat-base displacement due to road disturbance is x_b.

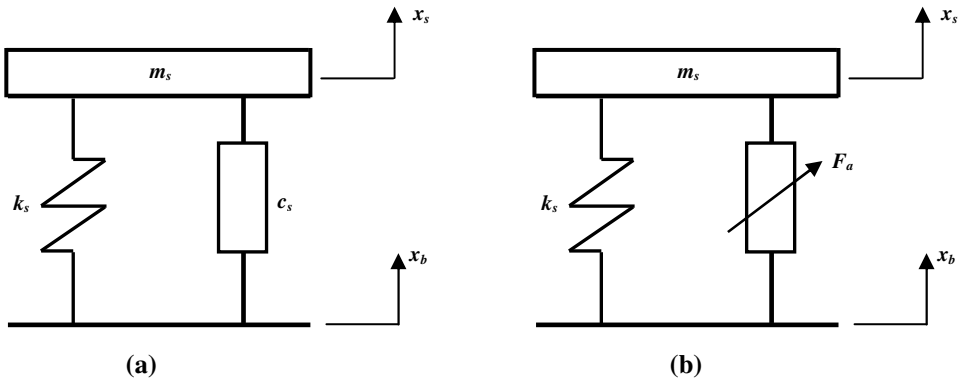

Fig. 7.1 Vehicle seat suspension model.
(a) Passive (b) Semi-active using MR damper

The sprung mass, comprising driver and seat, $m_s = 86.4\,\text{kg}$. The suspension spring constant is $k_s = 7004\,\text{N/m}$ and the passive damping coefficient is $c_s = 830\,\text{Ns/m}$ in passive seat suspension. The excitation input from the road is transmitted to the vehicle body and then causes unwanted vibrations on the driver. For simplification of the dynamic modeling, it is assumed that there exists only vertical motion of the

vehicle. Both pitching and rolling motions are ignored in this study. Therefore, the governing equation of motion of the vehicle seat suspension can be written as:

$$m_s\ddot{x}_s + k_s(x_s - x_b) + F = 0 \tag{7.1}$$

where,
$$F = \begin{cases} c_s(\dot{x}_s - \dot{x}_b), & \text{for Passive suspension} \\ F_a, & \text{for Semi - active suspension} \end{cases} \tag{7.2}$$

From the modified Bouc-Wen model of the MR damper [14], the damper force in the semi-active suspension is given by:

$$F_a = c_1(\dot{y} - \dot{x}_b) + k_1(x_s - x_b) \tag{7.3}$$

where,

$$\dot{y} = \frac{1}{c_0 + c_1}[\alpha z + c_0\dot{x}_s + c_1\dot{x}_b + k_0(x_s - y)] \tag{7.4}$$

$$\dot{z} = -\gamma|\dot{x}_s - \dot{y}||z|^{n-1}z - \beta(\dot{x}_s - \dot{y})|z|^n + A(\dot{x}_s - \dot{y}) \tag{7.5}$$

$$\alpha = \alpha(u) = \alpha_a + \alpha_b u \tag{7.6}$$

$$c_1 = c_1(u) = c_{1a} + c_{1b}u \tag{7.7}$$

$$c_0 = c_0(u) = c_{0a} + c_{0b}u \tag{7.8}$$

$$\dot{u} = -\eta(u - v) \tag{7.9}$$

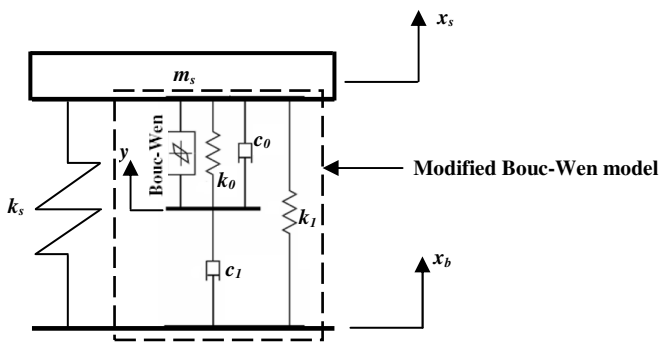

Fig. 7.2 Semi-active seat suspension incorporating Modified Bouc-Wen model

where y is the internal displacement of the MR fluid damper; u is the output of a first-order filter and v is the command voltage sent to the current driver. In this model, the accumulator stiffness is represented by k_1; the viscous damping observed at large and low velocities are represented by c_0 and c_1, respectively. k_0 is present to control the stiffness at large velocities; x_0 is used to account for the effect of the accumulator. α is the scaling value for the modified Bouc–Wen model. The scale and shape of the hysteresis loop can be adjusted by γ, β, A and n. A total of 14 model parameters are taken from [50] to characterize the MR fluid damper, see Table 7.1.

Table 7.1 Bouc-Wen model parameters for MR damper [50]

PARAMETER	VALUE	PARAMETER	VALUE
c_{0a}	784 Nsm^{-1}	α_a	12441 Nm^{-1}
c_{0b}	1803 $NsV^{-1}m^{-1}$	α_b	38430 $NV^{-1}m^{-1}$
k_0	3610 Nm^{-1}	γ	136320 m^{-2}
c_{1a}	14649 Nsm^{-1}	β	2059020 m^{-2}
c_{1b}	34622 $NsV^{-1}m^{-1}$	A	58
k_1	840 Nm^{-1}	n	2
x_0	0.0245 m	η	190 s^{-1}

7.3 Semi-active control using MR fluid dampers

Figure 7.3 describes the block diagram of a semi-active vibration control system using an MR damper. It consists of two nested controllers; a system controller and a damper controller. The system controller uses the dynamic responses of the seat suspension mathematical model to compute the desired damping force F_d according to a sliding mode control algorithm [50]. The damper controller adjusts the voltage v

applied to the damper in order to track its actual force F_a to the desired force F_d. In this paper; the damper controller is a recurrent neural network (RNN) of the inverse dynamics of an MR damper, trained using experimental data for the simulation performed in this study. The output of this damper controller is fed into the numerical model of the forward dynamics of the MR damper (the modified Bouc-Wen model).

As mentioned in the Introduction, the disturbance of the system in Fig. 7.3 is taken as a prescribed base displacement which is calculating by solving separately a two-degree-of-freedom quarter-vehicle suspension model that excludes the seat dynamics. This quarter-vehicle model could itself be either passive or semi-active.

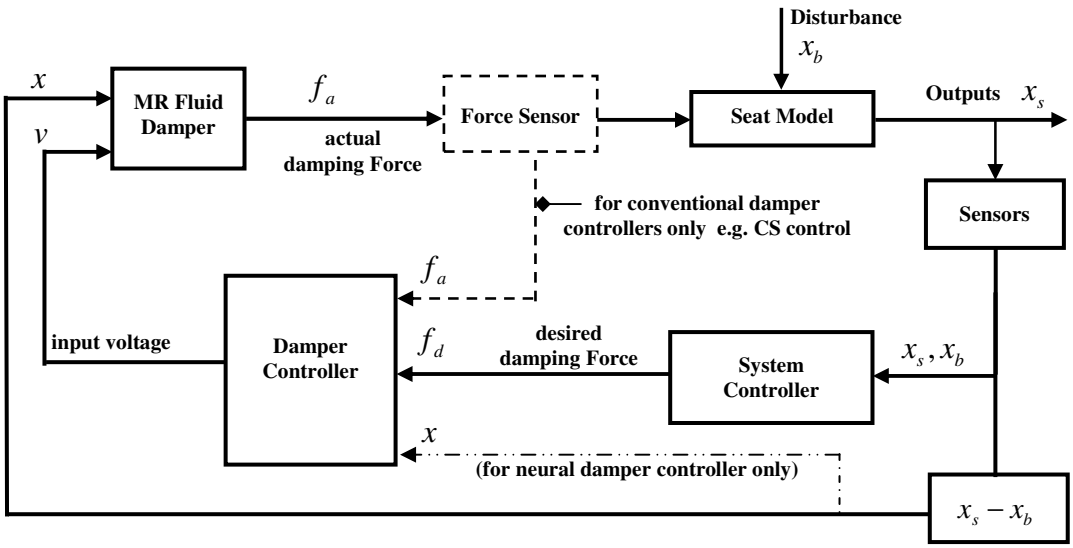

Fig. 7.3 Semi-active control system for a vehicle seat integrated with an MR damper.

7.3.1 System Controller: Sliding Mode Control

In this subsection, a brief description of the sliding mode control algorithm is introduced, taking due account of the loading uncertainties. The sliding mode control is used for the system controller. The sliding surface is defined as:

$$S = \dot{e} + \lambda e \tag{7.10}$$

where $$e = x_s - x_{ref} \tag{7.11}$$

The reference model used here is the ideal skyhook system, which has been reported to be highly effective in controlling a SDOF system [89]. The possible bound of the seat mass can be assumed as follows:

$$m_s = m_{so} + \Delta m_s \qquad \text{and} \qquad |\Delta m_s| \le 0.2 m_{so} \tag{7.12}$$

where m_{so} represents the nominal seat mass and Δm_s is the uncertain seat mass. The uncertainty ratio 0.2 is selected here for the purpose of application. The desired control force F_d can be derived as [50] and the structure of the sliding mode controller using the ideal skyhook reference model was shown in Fig 7.4. The system parameters of the MR suspension system and the ideal skyhook reference model used in this study are chosen on the basis of the conventional suspension system for a medium-sized passenger vehicle.

$$F_d = -m_{so}\left(u_o' - K' \operatorname{sgn}(S)\right) \tag{7.13}$$

$$u_o' = \left(\frac{k_s}{m_{so}}(x_s - x_b) - \lambda \dot{e} + \ddot{x}_{ref} \right) \tag{7.14}$$

$$K' = (\psi - 1)\left(|u_o'| + \frac{k_s}{m_{so}}|x_b| + \frac{k_s}{m_{so}}|x_s| \right) + \psi\varphi \tag{7.15}$$

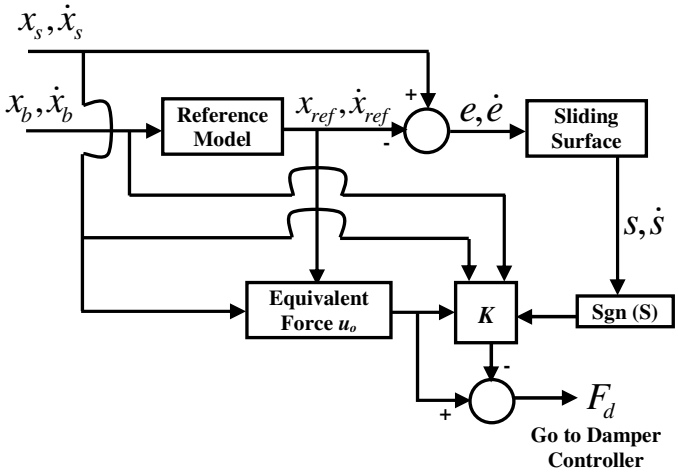

Fig. 7.4 Schematic Diagram of Sliding Mode Control Algorithm

7.3.2 Damper Controller: RNN Damper Controller

Figure 7.5 illustrates the identification scheme for the inverse RNN model. During the training phase, the network is subjected to data generated through dynamic tests with damper mounted on a tensile test machine. A full description of the experimental identification procedure will be published in a forthcoming paper [64]. The parameters of the network are then optimised to minimise the error (e_k') between the target normalized voltage (v_k') and the predicted voltage ($\hat{v}_k'$) produced by the network.

The validation test results clearly showed that the inverse RNN can reliably represent the inverse dynamic behaviour of an MR damper. The inverse RNN model was introduced as a damper controller and experimentally evaluated against some conventional types of damper controllers [5, 48, 49]. The results reveal that the inverse RNN damper controller offers superior damper control among the controllers studied in [64]. The conventional damper controllers [5, 48, 49] need to be fed with a measurement of F_a from a force sensor, as indicated in Fig. 7.3. This sensor needs to be in series with each MR fluid damper for a multi-damper system, thereby reducing system reliability and increasing its cost. The inverse RNN damper controller does not require an input from F_a, thereby dispensing with the force sensor. This controller uses instead a measure of the seat travel displacement (STD) which is already available from the sensors used by the system controller.

The architecture of the inverse RNN model is shown in Fig. 7.6. It is a three layer network with one output. The output layer has a single neuron with a linear transfer function and the hidden layers each have 18 neurons, each with a tangent-sigmoid

transfer function [73]. The network output $\hat{v}'_{k+1}$ (estimated voltage) and the vector of inputs (force ($\mathbf{f}'_k$), STD ($\mathbf{x}'_k$), voltage ($\hat{\mathbf{v}}'_k$), and their delays) to the first layer of the net is given by:

$$\mathbf{p}_k = \begin{bmatrix} \mathbf{f}'_k \\ \mathbf{x}'_k \\ \hat{\mathbf{v}}'_k \end{bmatrix}, \quad \mathbf{f}'_k = \begin{bmatrix} F'_k \\ F'_{k-1} \\ F'_{k-2} \end{bmatrix}, \quad \mathbf{x}'_k = \begin{bmatrix} x'_k \\ x'_{k-1} \\ x'_{k-2} \end{bmatrix}, \text{ and } \quad \hat{\mathbf{v}}'_k = \begin{bmatrix} \hat{v}'_k & \hat{v}'_{k-1} & \cdots & \hat{v}'_{k-5} \end{bmatrix}^{\mathrm{T}} \qquad \text{(7.16a-d)}$$

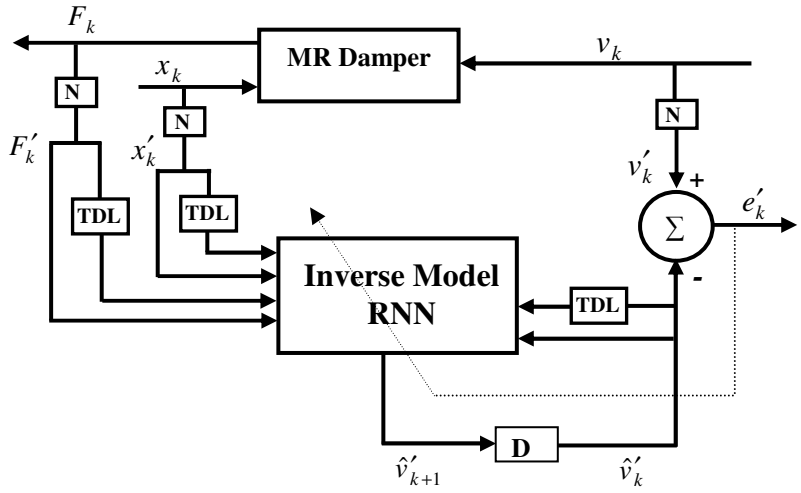

Fig. 7.5 Scheme of inverse identification of MR dampers by RNN: (D: delay by one time step; TDL: tapped delay line; N: normalisation)

The operation of the RNN damper controller is depicted in Fig. 7.7. It employs the inverse RNN model of the MR damper that used to generate the command voltage according to the desired damping force. The scheme of the system is shown in which F_{d_k} represents the desired force that the MR fluid damper should generate, and F_{a_k} represents the actual damping force that the MR damper actually produces.

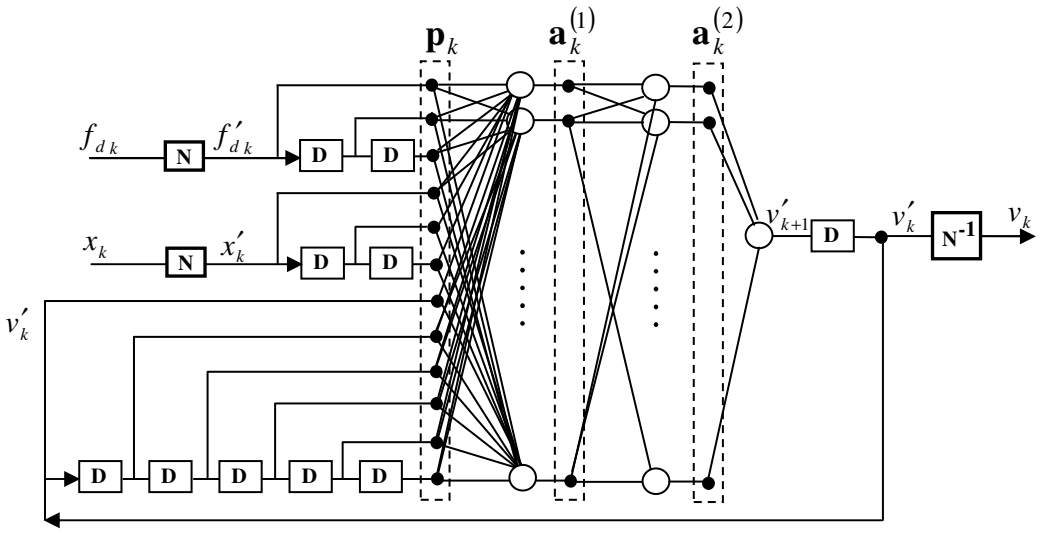

Fig. 7.6 RNN architecture for the inverse dynamic model (D: delay by one time step)

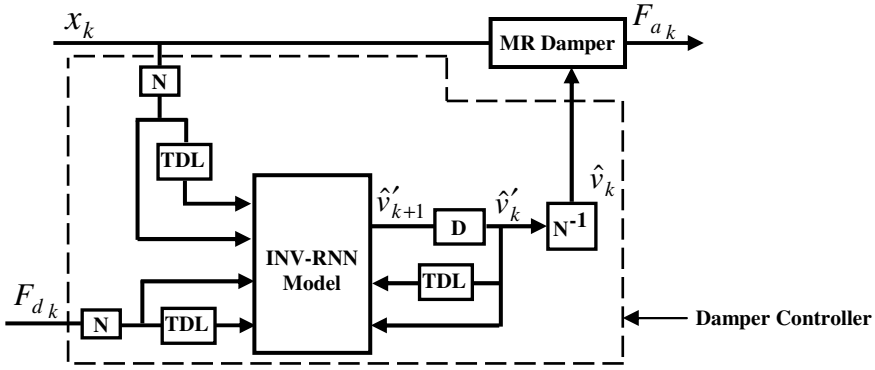

Fig. 7.7 The scheme of the controller for tracking the desired damping force via the inverse RNN model. (D: delay by one time step; TDL: tapped delay line; N: normalisation; N-1: de-normalisation)

7.4 Results and discussion

Seat travel distance and seat acceleration are the two main performance criteria in vehicle seat suspension design according to the ride comfort. All simulations were performed using Matlab/Simulink and the results for the conventional passive and semi-active seat suspension systems are compared. Figure 7.8 presents the Simulink

model for semi-active seat suspension system and no force sensor required to implement, only seat and body displacement must be measured.

Control characteristics for vibration suppression of the vehicle seat suspension systems are evaluated using two types of road excitations, which are chosen to be very similar to the real-world road bumps and classified as follows:

1- Road disturbance excitation.

The first excitation, normally used to reveal the transient response characteristic is a bump described by

$$x_r = \begin{cases} a\ \{1-\cos(\omega_r(t-0.5))\}, & \text{for} \quad 0.5 \le t \le 0.5+\dfrac{d}{V} \\ 0, & \text{otherwise} \end{cases} \tag{7.17}$$

where a is the half of the bump amplitude, in this study (a = 0.035 m) [78], $\omega_r = 2\pi V / D$, (D = 0.8 m) is the width of the bump, and V is the vehicle speed. In the bump excitation, the vehicle travels the bump with constant speed (V) of 0.856 m/s.

2- Random road excitation.

This type of road excitation [78] is used to evaluate the performance of suspension system in frequency domain with zero mean described by:

$$\dot{z} + \rho V z = V W_n \tag{7.18}$$

where W_n is white noise with intensity $2\sigma^2 \rho V$, ρ is the road irregularity parameter, and σ^2 is the covariance of road irregularity. In random road excitation, the values of road surface irregularity are selected assuming that the vehicle moves on the paved road with the constant speed (V) of 20 m/s. The values of ρ=0.45 m^{-1} and σ^2=300 mm^2 are chosen in the sense of the paved road condition.

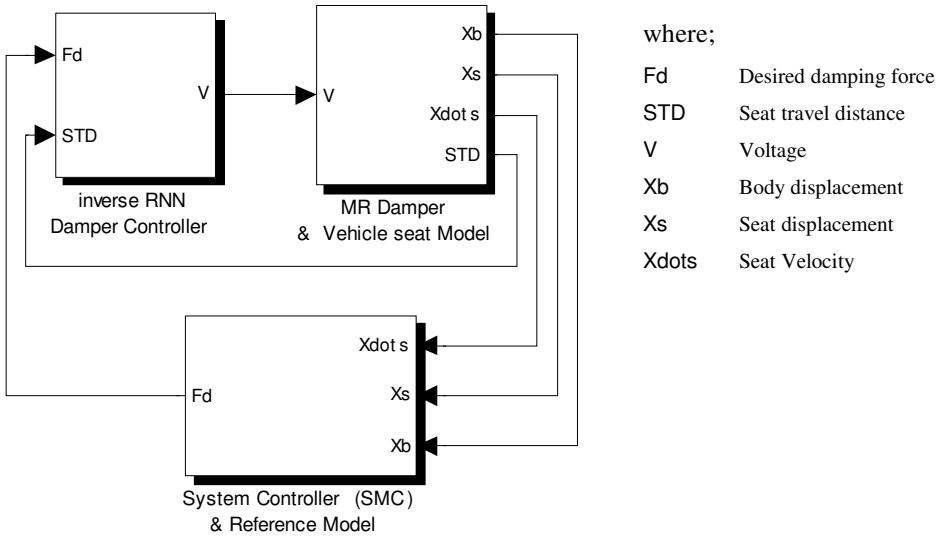

Fig. 7.8 Simulink Model of the Proposed Control System

The time history of the vehicle seat suspension system response under road bump excitation is shown in Fig. 7.9. Figure 7.9(a) introduces the body displacement, for both passive and controlled (semi-active) suspension systems according to Eq. (7.17), which describes the input disturbance of the seat system. The seat travel distance, and the seat acceleration are shown in Figs. 7.9(b, c) respectively. From this figure, the controlled vehicle suspension system included controlled seat can dissipate the energy due to bump excitation, cut down the settling time and also improve the ride comfort.

The peak-to-peak (PTP) values of the system response are presented in Table 7.2, which show that the controlled/controlled system has fewer peaks for the seat travel distance and seat acceleration among the systems examined. This system is more effective than others in improving the ride comfort. The controlled/controlled system can reduce maximum peak-to-peak of seat travel distance and seat acceleration 64.28 % and 29 %, respectively, comparing with the passive/passive system. Also, the two

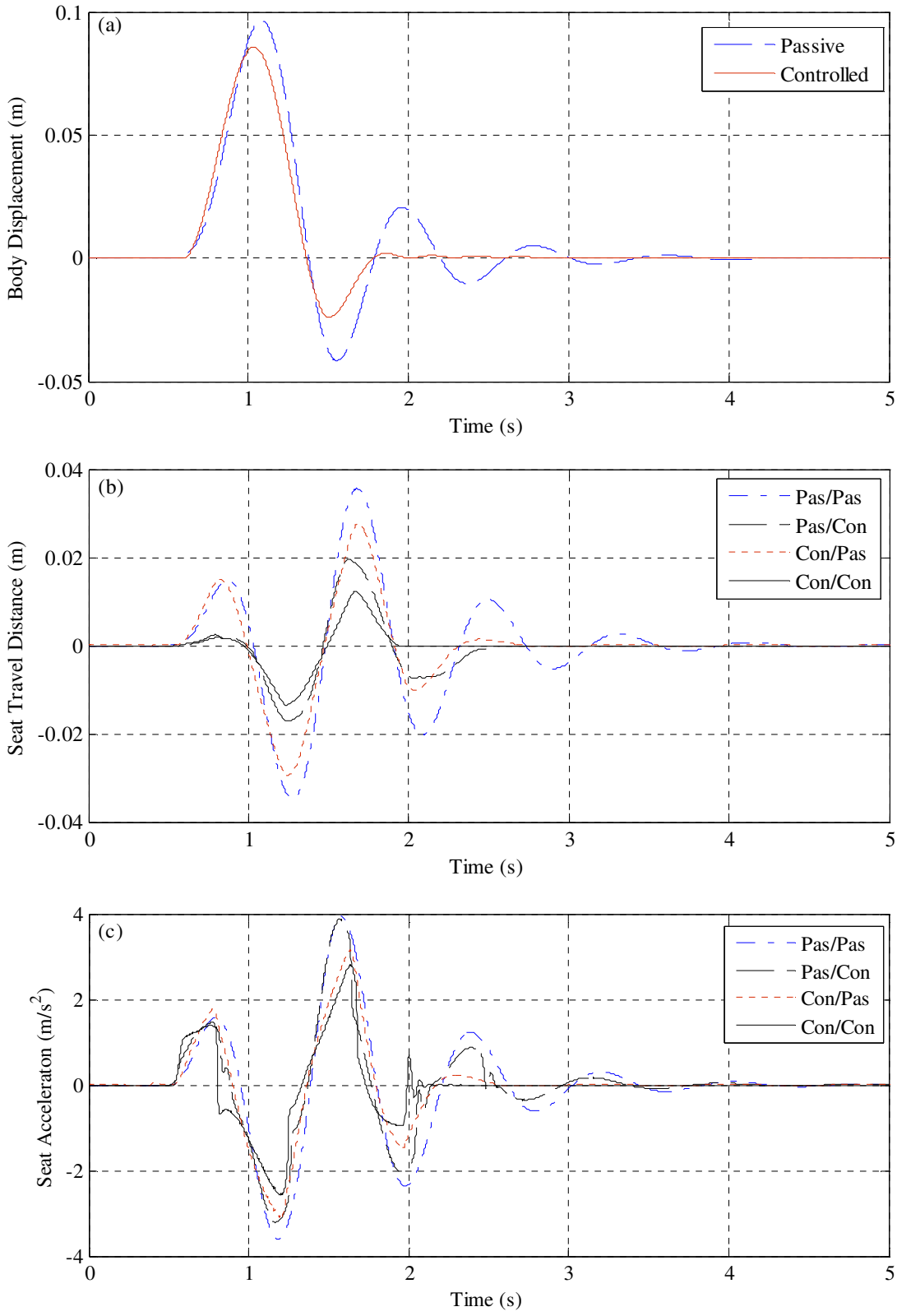

Fig. 7.9 The time history of system response under road disturbance excitation
a- Body Displacement b- Seat Travel Distance c- Seat Acceleration

where;

Pas/Pas	Passive vehicle suspension with passive seat suspension
Pas/Con	Passive vehicle suspension with controlled seat suspension
Con/Pas	Controlled vehicle suspension with passive seat suspension
Con/Con	Controlled vehicle suspension with controlled seat suspension

other systems were compared with the passive/passive system and the improvement percentages are listed in Table 7.2. The results show that the controlled/controlled MR seat suspension system can depress the peaks. Also, they prove the effectiveness of the semi-active seat suspension system.

Table 7.2 PTP values and improvement ratios of road disturbance excitation

System Type	Seat Travel Distance (**m**)	% Imp. Respect to Pas/Pas	% Imp. Respect to Pas/Con	% Imp. Respect to Con/Pas	Seat Acceleration (**m/s^2**)	% Imp. Respect to Pas/Pas	% Imp. Respect to Pas/Con	% Imp. Respect to Con/Pas
Pas/Pas	0.070	-	-	-	7.55	-	-	-
Pas/Con	0.036	48.57	-	-	7.08	6.22	-	-
Con/Pas	0.057	18.57	-	-	6.23	17.48	-	-
Con/Con	0.025	64.28	30.55	56.14	5.36	29	24.29	13.96

For the random road excitation, Figure 7.10 shows the response of the suspension system in frequency domain, where the displacement of the random signal is shown in Fig. 7.10(a), for both passive and controlled suspension systems according to Eq. (7.18), which shows the input signal of the seat suspension system. The seat travel distance, and the seat acceleration are shown in Figs. 7.10(b, c) respectively. According to this figure just like for the bump excitation, the controlled/controlled system can dissipate the energy due to the random excitation and improve the ride comfort.

The root mean square (RMS) values of the system response are presented in Table 7.3, which shows that the controlled/controlled system has a lower RMS value for the seat travel distance and seat acceleration than the other examined systems. This system is more effective than others in improving the ride comfort. The controlled/controlled system can reduce maximum RMS value of seat travel distance

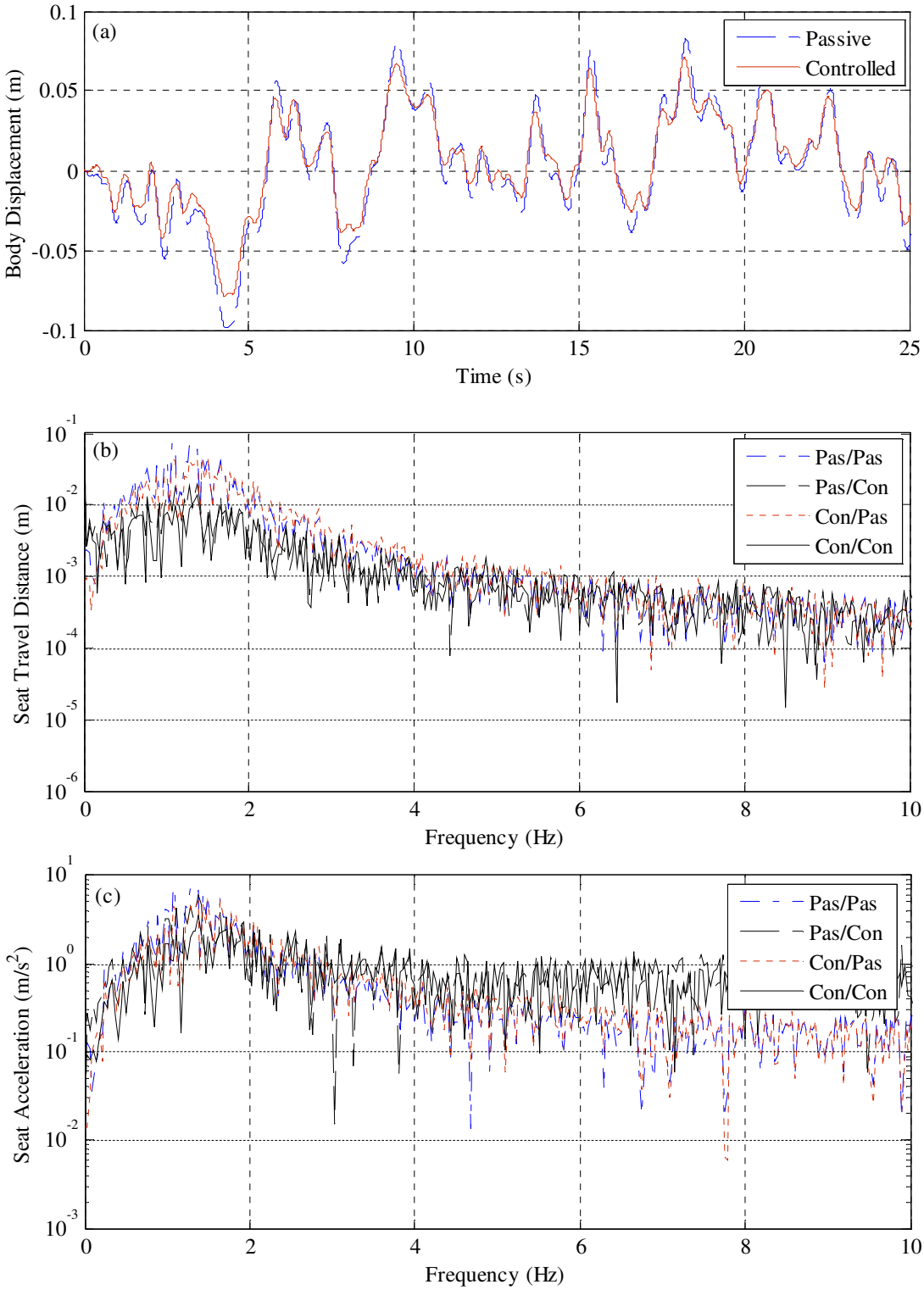

Fig. 7.10 The system response under random road excitation
a- Body Displacement b- Seat Travel Distance c- Seat Acceleration

Table 7.3 RMS values and improvement ratios of random road excitation

System Type	Seat Travel Distance (**m**)	% Imp. Respect to Pas/Pas	% Imp. Respect to Pas/Con	% Imp. Respect to Con/Pas	Seat Acceleration (**m/s^2**)	% Imp. Respect to Pas/Pas	% Imp. Respect to Pas/Con	% Imp. Respect to Con/Pas
Pas/Pas	0.0102	-	-	-	1.156	-	-	-
Pas/Con	0.0075	26.47	-	-	0.911	21.19	-	-
Con/Pas	0.0041	59.8	-	-	1.118	3.28	-	-
Con/Con	0.0033	67.64	56	19.51	0.844	26.99	7.35	24.5

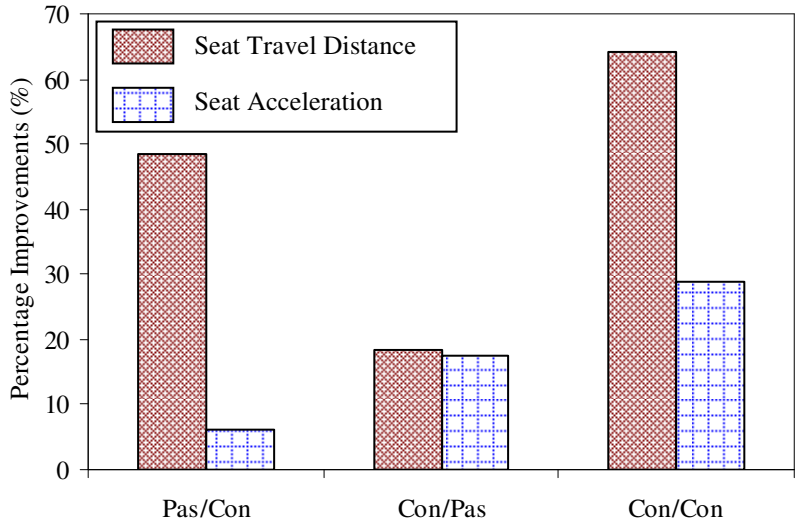

Fig. 7.11 Percentage improvements in PTP values for the controlled systems compared to passive/passive system for road disturbance excitation

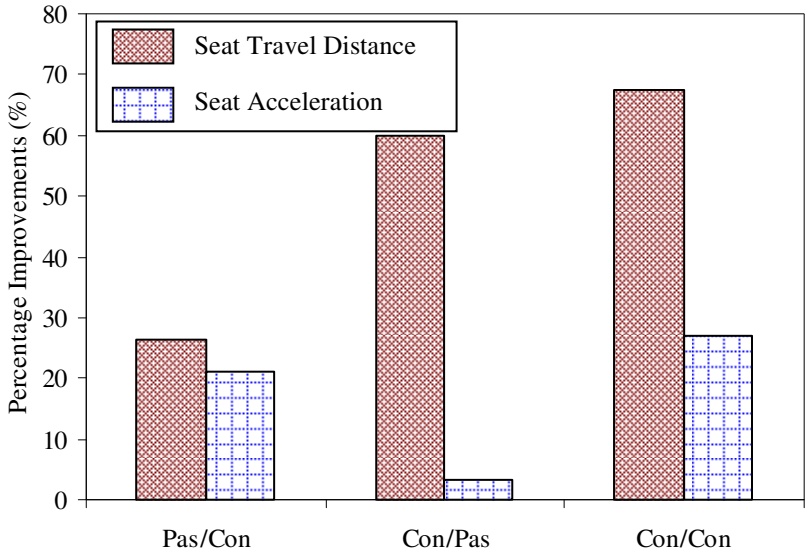

Fig. 7.12 Percentage improvements in RMS values the controlled systems compared to passive/passive system for random road excitation

and seat acceleration 67.64 % and 27 %, respectively, compared with the passive/passive system. Moreover, the two other systems were compared with the passive/passive system and the improvement percentages are listed in Table 7.3. These results again confirm that the semi-active seat suspension system improves the ride comfort and the controlled/controlled system can achieve a superior response in terms of passenger comfort. Figures 7.11 and 7.12 present a summary of the above-discussed results for the simulations performed in this study.

7.5 Concluding remarks

In this paper, a semi-active vehicle seat suspension system incorporated an MR damper was investigated and the control performance was evaluated via computer simulations. A mathematical model of the seat suspension system using an MR damper was demonstrated and then the equation of motion is derived. In order to obtain a favourable control performance of the MR vehicle seat suspension system subjected to parameter uncertainties, a sliding mode control algorithm was applied as a system controller and an inverse RNN model was implemented as a damper controller. The proposed semi-active seat suspension is compared to a passive seat suspension for prescribed base displacements. These inputs were representative of the vibration of the sprung mass of a passive or semi-active quarter-vehicle suspension under both bump and random-profile road disturbance. Comparisons were made between passive and semi-active seat suspensions for different base excitation through numerical simulations based on a SDOF seat model. Control performance criteria such as seat travel distance and seat acceleration are evaluated in time and frequency domains in order to quantify the effectiveness of the proposed semi-active vehicle seat suspension system. The simulated results reveal that the use

of semi-active control in the seat suspension offers a considerable improvement in ride comfort. The suitable selection of a damper controller (RNN) together with a properly chosen system controller (sliding mode control algorithm) will make the application of MR dampers in vehicle seat suspension systems more successful through the minimal use of sensors and the reduction of implementation cost.

CHAPTER 8

Summary, Conclusions and Recommendations

This chapter summarises the outcomes of all the research work of this thesis, highlighting important findings. It concludes with some recommendations for future work to extend this study.

8.1 Summary

The overall aims of this thesis were twofold:

- The investigation of non-parametric techniques for the identification of the nonlinear dynamics of an MR damper.
- The implementation of these techniques in the investigation of MR damper control of a vehicle suspension system. The investigation was aimed at improving ride comfort and vehicle stability with minimal reliance on the use of sensors, thereby reducing the implementation cost and increasing system reliability.

In order to meet the specific objectives listed in Section 1.2, important preparatory work was done. This included a comprehensive literature review of: i) the models of MR dampers; ii) MR damper controllers and iii) advanced control strategies suitable for system controllers in semi-active vehicle suspension systems incorporating MR damper.

A new model for studying the dynamical behaviour of an MR damper was presented. It consisted of a three dimensional interpolation using Chebyshev orthogonal polynomial functions to identify the damping force as a function of the displacement, velocity and input voltage. The identification and its validation were done in both simulation and experimentation. In the former case the data were generated by solving the modified Bouc-Wen model. In the experimental approach, the data were generated through dynamic tests with the damper mounted on a tensile testing machine.

The experimental identification of the dynamic behaviour of an MR damper through neural networks was introduced. Feed-forward and recurrent neural networks were used to model both the direct and inverse dynamics of the damper. Training and validation of the proposed neural networks were performed using the data generated through dynamic tests with the damper mounted on a tensile testing machine. The effect of the cylinder's surface temperature on both the direct and inverse dynamics of the damper was studied. The inverse recurrent neural network model was introduced as a damper controller and experimentally evaluated against alternative controllers proposed in the literature.

This thesis introduced a neural-based MR damper controller for use in conjunction with the system controller of a semi-active vehicle suspension. A mathematical model of a semi-active quarter-vehicle suspension using an MR damper was derived. The system controller was based on model-reference sliding mode control. The performance criteria were: the suspension working space (SWS); vertical body acceleration (BA); dynamic tyre load (DTL). These performance criteria were evaluated in the time and frequency domains in order to quantify the suspension effectiveness under bump and random road disturbance. These studies were performed using two alternative means of providing the damper force in the model: (a) a modified Bouc-Wen model; (b) an actual damper fitted in a hardware-in-the-loop simulation (HILS). The former method was used to study bump excitation where the large damper deflections could not be achieved by HILS. The latter method was used to illustrate the practical implementation of the control strategy. In either case the damper controller was based on an experimentally trained RNN network of the inverse dynamics of the damper. Further studies were performed using an experimental RNN model of the forward dynamics of the MR damper as a substitute for HILS.

An improved semi-active control strategy for an MR damper used in a car seat suspension was demonstrated in this study. The seat suspension system was approximated by base-excited single degree of freedom system. The proposed semi-active seat suspension was compared with a passive seat suspension for prescribed base displacements. These inputs were representative of the vibration of the sprung mass of a passive or semi-active quarter-vehicle suspension under bump or random-profile road disturbance. Performance criteria such as seat travel distance and seat

acceleration were evaluated in time and frequency domains, in order to quantify the effectiveness of proposed semi-active control system.

8.2 Conclusions

The studies reported in this thesis are intended to provide a deeper insight into the behaviour of MR dampers and their potential application in a vehicle suspension system. The outcomes of this study are expected to accelerate the implementation of these dampers in vehicle suspension systems. The main findings from this study can be summarized as follows:

1- Validation data sets representing a wide range of working conditions of the damper showed that the damper force can be approximately identified as a function of the displacement, velocity and input voltage using Chebyshev polynomial.

2- This explicit functional representation allows a rapid means of reliably estimating the damping force for any desired combination of voltage, amplitude, and frequency of the excitation.

3- Results showed that neural networks were superior to Chebyshev polynomials for modelling the MR damper and were capable of reliably representing both its direct and inverse dynamic behaviours.

4- Experimental validation tests showed that the RNN was almost as accurate as the FNN for modelling the direct dynamics of the damper. These tests also showed that the voltage output from the RNN of the inverse dynamics was

capable of commanding a damper to closely track a desired damping force signal.

5- The experimentally trained FNN and RNN models were shown to be reasonably robust against significant temperature variation.

6- For the first time, an experimental evaluation was performed on all principal alternative MR damper controllers (RNN, Heaviside Function, Signum Function and Continuous State control). The results showed that the RNN damper controller gave the best tracking of the desired damper force signal.

7- The RNN damper controller produced the smoothest input voltage to the MR damper coil, thereby ensuring low-power requirement and extended damper life. These observations, together with the RNN controller's independence of a force sensor, indicate that, among the controllers investigated, a neural-based damper controller potentially offers the most cost-effective semi-active vibration control solution.

8- The semi-active vehicle suspension system analysis showed that a damper controller based on an RNN model of the inverse MR dynamics offered significantly superior ride comfort and vehicle stability over an MR damper controller based on CS control.

9- The neural controller also produced a smoother and lower input voltage to the MR damper coil, respectively ensuring extended damper life and lower power requirement. The results also indicated that the neural controller's performance was superior even when operating outside the limits of the data used in its training.

10- Studies performed using an RNN model of the forward dynamics of the MR damper showed that it was a reliable substitute for HILS for validating multi-damper control applications.

11- The simulation results of the semi-active car seat suspension showed that the use of semi-active control offered a considerable improvement in the rider's comfort.

8.3 Recommendations for Future Work

The research performed in this study has significantly contributed to the implementation of MR dampers in semi-active vehicle suspension systems. However, two limitations of the present work are identified. Firstly, the car seat suspension in Chapter 7 was modelled as a SDOF system subjected to *prescribed* base displacements. Hence, its influence on (i.e. coupling with) the dynamics of the vehicle suspension was neglected. Secondly, with regard to the vehicle suspension, this was modelled as a quarter-vehicle model. Hence pitching and rolling were not considered. Quantifying these motions allows a better assessment of both the rider's comfort and the stability of the vehicle. Hence, the following suggestions are made for developing the work in this thesis:

1- Extension of the semi-active 2-DOF Quarter car model, introduced in Chapter 6, to a multiple-degree-of-freedom (3 or 4-DOF) system incorporating seat dynamics.
2- Solving a semi-active "half car" suspension model using the inverse RNN damper controller to evaluate improvement in the pitch motion.

3- Solving the semi-active full car model using the inverse RNN damper controller to evaluate the improvement in all performance criteria, especially roll motion.

In addition to the above, another interesting area of research is a deeper investigation into the generality of the observation made at the end of Section 5.4 and in reference [23]. There it was observed that, although the inverse RNN model gave an unsatisfactory prediction of the voltage, the predicted voltage still produced a highly satisfactory representation of the desired force. This observed behaviour was consistent throughout this research and was the basis of the proven success of the inverse RNN controller in Chapters 6 and 7.

REFERENCES

[1] **Carlson, J. D. & Weiss, K. D.**
A growing attraction to magnetic fluids
1994, Machine design 66 (August) 61–66.

[2] **Lam, A. H. & Liao, H. W.**
Semi-active control of automotive suspension systems with magneto-rheological dampers
2003, International Journal of Vehicle Design, Volume: 33, pp 50-75.

[3] **Karkoub, M. A. & Zribi, M.**
Active/semi-active suspension control using magnetorheological actuators
2006, International Journal of Systems Science, Volume: 37 (1), pp 35-44.

[4] **Liao, W. H. & Wang, D. H.**
Semi-active vibration control of train suspension systems via magnetorheological dampers
2003, Intelligent Material Systems and Structures, Volume: 14, pp 161-172.

[5] **Dyke, S. J., Spencer, B. F. Jr., Sain, M. K. & Carlson, J. D.**
Modelling and control of magnetorheological dampers for seismic response reduction
1996, Journal of Smart Materials and Structures, Volume: 5, pp 565-576.

[6] **Bani-Hani, K. A. & Sheban, M. A.**
Semi-active neuro-control for base-isolation system using magneto-rheological (MR) dampers
2006, Earthquake Engineering and Structural Dynamics, Volume: 35, pp 1119-1144.

[7] **Gillespie, T. D.**
Fundamentals of Vehicle Dynamics
1992, Warrendale, PA, USA: Society of Automotive Engineers.

[8] **Rajamani, R.**
Vehicle Dynamics and Control
2006, New York, NY, USA: Springer Science & Business Media.

[9] **Karnopp, D. , Crosby, M. J., & Harwood, R. A.**
Vibration control using semi-active force generators
1974, ASME Journal of Engineering for Industry, Volume: 96, pp 619-26.

[10] **Yi, K. & Song, B. S.**
A new adaptive skyhook control of vehicle semi-active suspensions
1999, Proceedings of the Institution of Mechanical Engineers, Part D: Journal of Automobile Engineering, Volume: 213 (3), pp 293-303.

[11] **Lee, H. S. & Choi, B. S.**
Control and response characteristics of a magnetorheological fluid damper for passenger vehicles
2000, Intelligent Material Systems and Structures, Volume: 11, pp 80-87.

[12] **Chooi, W. W. and Oyadiji, S. O.**
Mathematical Modelling, Analysis and Design of Magnetorheological (MR) Dampers 2009, ASME Journal of Vibration and Acoustics, Volume: 131, 061002-10 pages.

[13] **Simon, D. & Ahmadian, M.**
Vehicle evaluation of the performance of magnetorheological dampers for heavy truck suspensions
2001, ASME Journal of Vibration and Acoustics, Volume: 123, pp 365-375.

[14] **Spencer, B. F. Jr., Dyke, S. J., Sain, M. K. & Carlson, J. D.**
Phenomenological model for magnetorheological dampers
1997, Journal of Engineering Mechanics, Volume: 123, pp 230–238.

[15] **Winslow, W. M.**
Method and means for translating electrical impulses into mechanical force
1947, U.S. Patent 2,417,850.

[16] **Winslow, W. M.**
Induced fibration of suspensions
1949, Journal of applied physics, Volume: 20, pp 1137-1140.

[17] **Weiss, K. D. & Nixon, D. A.**
Viscoelastic properties of magneto- and electrorheological fluids
1994, Journal of Intelligent Material Systems and Structures, Volume: 5, pp 772-775.

[18] **Fernando, D., Goncalves, J. H. K., & Mehdi, A.**
A review of the state of the art in magnetorheological fluid technologies – Part I: MR fluid and MR fluid models
2006, the Shock and Vibration Digest, Volume: 38, (3), pp 203–219.

[19] **Wang, J. & Meng, G.**
Magnetorheological fluid devices: principles, characteristics and applications in mechanical engineering
2001, Proceedings of the Institution of Mechanical Engineers; Part B; Journal of Engineering Manufacture Volume: 215 (3) pp 165- 174.

[20] **Carlson J. D., Catanzarite, D. M., & Clair, K. A.**
Commercial magnetorheological fluid devices
1995, Proceedings of the 5th International Conference on ER Fluids, MR Fluids and Associated Technology, Sheffield, UK. 10 - 14 July.

[21] **Dyke, S. J.**
Acceleration feedback control strategies for active and semi-active control systems: modeling, algorithm development, and experimental verification
1996, PhD Thesis, Department of Civil and Geological Sciences, Notre Dame, Indiana.

[22] **Marin, L., Nicolae, C. P., Cornel, V., & Ladislau, N. V.**
Investigations of a magnetorheological fluid damper
2004, IEEE Transactions on Magnetics, Volume: 40, (2), pp 469-472.

[23] **Wang, D. H., & Liao, W. H.**
Modeling and control of magnetorheological fluid dampers using neural networks
2005, Journal of Smart Materials and Structures, Volume: 14, pp 111-126.

[24] **Lord Corporation Website**
http://www.lord.com

[25] **Choi, S. B., Nam, M. H., & Lee, B. K.**
Vibration control of a MR seat damper for commercial vehicles
2000, Journal of Intelligent Material Systems and Structures, Vol. 11 (12), pp 936-944.

[26] **Yu, M., Dong, X. M., Choi, B. S., & Liao, C. R.**
Human simulated intelligent control of vehicle suspension system with MR dampers
2009, Journal of Sound and Vibration, Volume: 319 (3-5), pp 753-767.

[27] **Smyth, A., Masri, S., Kosmatopoulos, E., Chassiakos, A., & Caughey, T.**
Development of adaptive modeling techniques for non-linear hysteretic systems
2002, International Journal of Non-Linear Mechanics, Volume: 37, pp 1435–1451.

[28] **Stanway, R., Sproston, J.L. & Stevens, N.G**
Non-linear modelling of an electrorheological vibration damper
1987, Journal of Electrostatics, Volume: 20 (2), pp 167–184.

[29] **Wen, Y. K.**
Method of random vibration of hysteretic systems
1976, Journal of Engineering Mechanics, Volume: 102 (2), pp 249–263.

[30] **Kwok, N. M., Ha, Q. P., Nguyen, M. T., Li, J., & Samali, B.**
Bouc–Wen model parameter identification for a MR fluid damper using computationally efficient GA
2007, ISA transactions, Volume: 46, pp 167–179.

[31] **Giuclea, M., Sireteanu, T., Stancioiu, T., & Stammers, C. W.**
Model parameter identification for vehicle vibration control with magnetorheological dampers using computational intelligence methods
2004, Proceedings of the Institution of Mechanical Engineers, Part I: Journal of Systems and Control Engineering, Volume: 218 (7), pp 569-581.

[32] **Choi, B. S. & Lee, K. S.**
A hysteresis model for the field-dependent damping force of a magnetorheological damper
2001, Journal of Sound and Vibration, Volume: 245 (2), pp 375-383.

[33] **Hudha, k., Jamaluddin, H., Samin, P. M., & Rahman, R. A.**
Non-parametric linearised data driven modelling and force tracking control of a magnetorheological damper
2008, International Journal of Vehicle Design, Volume: 46 (2), pp 250-269.

[34] **Masri, S. F. & Caughey, T. K.**
A nonparametric identification technique for nonlinear dynamic problems
1979, Journal of Applied Mechanics, Volume: 46, pp 433-447.

[35] **Ehrgott, R. C. & Masri, S. F.**
Modeling the oscillatory dynamic behavior of electrorheological materials in shear
1992, Journal of Smart Materials and Structures, Volume: 1, pp 275-285.

[36] **Gavin, H. P., Hanson, R. D., & Filisko, F. E.**
Electrorheological dampers, Part II: Testing and modeling.
1996, Journal of Applied Mechanics, Volume: 63 (3), pp 676-682.

[37] **Oyadiji, S. O. & Sarafianos, P.**
Characterization and comparison of the dynamical properties of conventional and electrorheological fluid shock absorbers
2003, International Journal of Vehicle Design, Volume: 33 (1-3), pp 251-278.

[38] **Chang, C. C. & Roschke, P.**
Neural network modeling of a magnetorheological damper
1998, Journal of Intelligent Material Systems and Structural, Volume: 9, pp 755–764.

[39] **Zhang, J. & Roschke, P.**
Neural network simulation of magnetorheological damper behavior
1998, Proceedings of International Conference on Vibration Engineering, August, 6-9, Dalian, China.

[40] **Xia, P. Q.**
An inverse model of MR damper using optimal neural network and system identification
2003, Journal of Sound and Vibration, Volume: 266 (5), pp 1009-1023.

[41] **C.C. Chang, L. Zhou,**
Neural network emulation of inverse dynamics for a magnetorheological damper
2002, Journal of Structural Engineering, Volume: 128 (2), pp 231–239.

[42] **Du, H., Lam, J., & Zhang, N.**
Modeling of a magnetorheological damper by evolving radial basis function networks
2006, Engineering Applications of Artificial Intelligence, Volume: 19 (8), pp 869–881.

[43] **Schurter, K., and Roschke, P.**
Fuzzy modeling of a magnetorheological damper using ANFIS
2000, Proceedings of the IEEE International Conference on Fuzzy Systems, pp 122–127.

[44] **Sadok, S., Khaled, C., Lotfi, M., Marc, T. & Asma, K.**
An innovative magnetorheological damper for automotive suspension: from design to experimental characterization
2005, Smart Materials and Structural, Volume: 14, pp 811–822.

[45] **Olatunbosun, O. A. & Dunn, J. W.**
An evaluation of the effect of suspension nonlinearities on vehicle ride
1992, Proceeding of the second International Conference on Vehicle Comfort, Bologna, Italy.

[46] **Yao, G. Z. Yap, F. F., Chen, G., Li, W. H., & Yeo, S. H.**
MR damper and its application for semi-active control of vehicle suspension system
2002, Mechatronics, Volume: 12 (7), pp 963-973.

[47] **Ahmadian, M. & Pare, C.A.**
A quarter-car experimental analysis of alternative semiactive control methods
2000, Intelligent Material Systems and Structures, Volume: 11 (8), pp 604–612.

[48] **Wang, D. H. & Liao, W. H.**
Semi-active controllers for magnetorheological fluid dampers
2005, Journal of Intelligent Material Systems and Structural, Volume: 16 (11-12), pp 983–993.

[49] **Sims, N. D., Stanway, R., Peel, D. J., & Bullough, W. A.**
Controllable viscous damping: an experimental study of an electrorheological long-stroke damper under proportional feedback control
1999, Journal of Smart Materials and Structures, Volume: 8, pp 601-615.

[50] **Lai, C. Y. & Liao, H. W.**
Vibration Control of a Suspension System via a Magnetorheological Fluid Damper
2002, Journal of Vibration and Control, Volume: 8 (4), pp 527-547.

[51] **Du, H., Sze, K. Y., & Lam, J.**
Semi-active H_∞ control of vehicle suspension with magnetorheological dampers
2005, Journal of Sound and Vibration, Volume: 283, pp 981–996.

[52] **Choi, B. S., Lee, H. S., & Park, Y. P.**
H_∞ control performance of a full-vehicle suspension featuring magnetorheological dampers
2002, Vehicle System Dynamics, Volume: 38, pp 341-360.

[53] **Guo, D. L., Hu., Y. H., & Yi, J. Q.**
Neural network control for a semi-active vehicle suspension with a magnetorheological damper
2004, Journal of Vibration and Control, Volume: 10 (3), pp 461-471.

[54] **Zribi, M. & Karkoub, M. A.**
Robust control of a car suspension system using magnetorheological dampers
2004, Journal of Vibration and Control, Volume: 10 (4), pp 507-524.

[55] **Shen, Y., Golnaraghi, M. F., & Heppler, G. R.**
Semi-active vibration control schemes for suspension systems using magnetorheological dampers
2006, Journal of Vibration and Control, Volume: 12 (1), pp 3-24.

[56] **YU, M., Liao, C. R., Chen, W. M., & Huang, S. L.**
Study on MR semi-active suspension system and its road testing
2006, Intelligent Material Systems and Structures, Volume: 17 (8-9), pp 801–806.

[57] **Gawronski, W. K.**
Advanced Structural Dynamics and Active Control of Structures
2004, Springer-Verlag, New York, Inc.

[58] **Lee, Y., & Jeon, D.**
A study on the vibration attenuation of a driver seat using an MR fluid damper
2002, Journal of Intelligent Material Systems and Structures, Vol. 13 (7-8), pp 437-441.

[59] **Han, Y. M., Nam, M. H., Han, S. S., Lee, H. G., & Choi, S. B.**
Vibration control evaluation of a commercial vehicle featuring MR seat damper
2002, Journal of Intelligent Material Systems and Structures, Vol. 13 (9), pp 575-579.

[60] **Song, X., Ahmadian, M., Southward, S., & Miller, L.**
Parametric study of nonlinear adaptive control algorithm with magneto-rheological suspension systems
2007, Communications in Nonlinear Science and Numerical Simulation, Vol. 12, pp 584-607.

[61] Choi, S. B., & Nan, Y. M.
Vibration control of electrorheological seat suspension with human-body model using sliding mode control
2007, Journal of Sound and Vibration, Vol. 303, pp. 391-404.

[62] Choi, S. B., Choi, J. H., Lee, Y. S., & Han, M. S.
Vibration control of an ER seat suspension for a commercial vehicle
2003, Journal of Dynamic Systems, Measurement, and Control, Vol. 125, pp 60-68.

[63] Metered, H., Bonello, P., & Oyadiji, S. O.
Nonparametric identification modeling of magnetorheological damper using Chebyshev polynomials fits
2009, SAE International Journal of Passenger Cars - Mechanical Systems, Vol. 2 (1), pp 1125-1135.

[64] Metered, H., Bonello, P., & Oyadiji, S. O.
The experimental identification of magnetorheological dampers and evaluation of their controllers
2010, Mechanical systems and signal processing, Volume: 24 (4), pp 976–994.

[65] Metered, H., Bonello, P., & Oyadiji, S. O.
An investigation into the use of neural networks for the semi-active control of a magnetorheologically damped vehicle suspension
2010, Proceedings of the Institution of Mechanical Engineers, Part D: Journal of Automobile Engineering, Volume: 224 (7), pp 829–848.

[66] Metered, H., Bonello, P., & Oyadiji, S. O.
Vibration control of a seat suspension system using magnetorheological damper
2009, ASME International Design Engineering Technical Conferences & Computers and Information in Engineering Conference, San Diego, California, USA (paper no. DETC2009-86081), 30 August - 2 September.

[67] Wereley, N. M., Pang, L., & Kamath G. M.
Idealized hysteresis modeling of electrorheological and magnetorheological dampers
1998, Journal of Intelligent Material Systems and Structural, Volume: 9 (8), pp 642–649.

[68] Dominguez, A., Sedaghati, R., & Stiharu, I.
A new dynamic hysteresis model for magnetorheological dampers
2006, Journal of Smart Materials and Structures, Volume: 15, pp 1179-1189.

[69] **Li, W. H., Yao, G. Z., Chen, G., Yao, S. H., & Yap, F. F.**
Testing and steady state modeling of a linear MR damper under sinusoidal loading
2000, Journal of Smart Materials and Structures, Volume: 9, pp 95-102.

[70] **F. A. Rodrigues, F. Thouverez, C. Gibert, & L. Jezequel**
Chebyshev polynomials fits for efficient analysis of finite length squeeze film damped rotors
2003, Journal of Engineering for Gas Turbines and Power, Volume: 125, pp 175-183.

[71] **Liu, Y., Gordaninejad, F., Evrensel, C. A., Dogruer, U., Yeo, M. S., Karakas, E. S., & Fuchs, A.**
Temperature Dependent Skyhook Control of HMMWV Suspension using a Failsafe Magnetorheological Damper
2003, Damper, SPIE Annual International Symposium on Smart Structures and Materials, Volume: 5054, 332–340.

[72] **Batterbee, D. & Sims, N. D.**
Temperature Sensitive Controller Performance of MR Dampers
2009, Journal of Intelligent Material Systems and Structural, Volume: 20 (3), pp 297–309.

[73] **D.H. Demuth, M., Beale & M. Hagan**
Neural network toolbox user's guide,
2007, The MathWorks Inc.

[74] **Choi, B. S. & Sung, K. G.**
Vibration control of magnetorheological damper system subjected to parameter variations
2008, International Journal of Vehicle Design, Volume: 46, pp 94–110.

[75] **Choi, S. B., Choi, Y. T. , & Park, D. W.**
A sliding mode control of a full-car electrorheological suspension system via hardware in-the-loop simulation
2000, Dynamic Systems, Measurement, and Control, Volume: 122, pp 114-121.

[76] **Tu, S. & Akc, H.**
A study of random vibration characteristics of the quarter-car model
2005, Journal of Sound and Vibration, Volume: 282, pp 111–124.

[77] **Li, X., Zhao, X-P., & Chen, J.**
Sliding mode control for torque ripple reduction of an electric power steering system based on a reference model
2008, Proceedings of the Institution of Mechanical Engineers, Part D: Journal of Automobile Engineering, Volume: 222, pp 2283–2290.

[78] **Choi, S. B., Zhu, W. Q., & Kim, W. K.**
Vibration control of a semi-active suspension featuring electrorheological fluid dampers
2000, Journal of Sound and Vibration, Volume: 234, pp 537-546.

[79] **Fischer, D. & Isermann, R.**
Mechatronic semi-active and active vehicle suspensions
2004, Control Engineering Practice, Volume: 12 (11), pp 1353-1367.

[80] **Sammier, D., Sename, O., & Dugard, L.**
Skyhook and H∞ Control of Semi-active Suspensions: Some Practical Aspects
2003, Vehicle System Dynamics, Volume: 39, pp 279–308.

[81] **Choi, S. B. & Han, S. S.**
H∞ control of electrorheological suspension system subjected to parameter uncertainties
2003, Mechatronics, Volume: 13, pp 639–657.

[82] **Rakheja, S., Afework, Y., & Sankar, S.**
An analytical and experimental investigation of the driver-seat-suspension system
1994, Vehicle System Dynamics, Vol. 23, pp. 501-524.

[83] **Stein, G. J.**
A driver's seat with suspension of electro-pneumatic type
1997, Journal of Vibration and Acoustics, Vol. 119 (2), pp. 230–235.

[84] **Han,Y. M., Jung, J. Y., Choi, S. B., Choi, Y. T., & Wereley, N. M.,**
Ride Quality Investigation of an Electrorheological Seat Suspension to Minimize Human Body Vibrations
2006, Proceedings of the Institution of Mechanical Engineers, Part D: Journal of Automobile Engineering, Volume: 220, pp 139–150.

[85] **Guclu, R., & Gulez, K.**
Neural network control of seat vibrations of a nonlinear full vehicle model using PMSM
2008, Mathematical and Computer Modelling, Vol. 47, pp. 1356–1371.

[86] **Guclu, R.**
Fuzzy logic control of seat vibrations of a nonlinear full vehicle model
2005, Nonlinear Dynamics, Vol. 40, pp. 21-34.

[87] **Hostens, I., Deprez, K. & Ramon, H.**
An improved design of air suspension for seats of mobile agricultural machines
2004, Journal of Sound and Vibration, Vol. 276, pp. 141-156.

[88] Zuo, L., & Nayfeh, S.

Structured H_2 optimization of vehicle suspensions based on multi-wheel models

2003, Vehicle System Dynamics, Vol. 40 (5), pp. 351-371.

[89] Ahmadian, M.

On the isolation properties of semi-active dampers

1999, Journal of Vibration and Control, Vol. 5, pp. 217-232.

APPENDIX A

Particular Chebyshev polynomials of the first kind:

$$T_0(x) = 1$$

$$T_1(x) = x$$

$$T_2(x) = 2x^2 - 1$$

$$T_3(x) = 4x^3 - 3x$$

$$T_4(x) = 8x^4 - 8x^2 + 1$$

$$T_{n+1}(x) = 2xT_n(x) - T_{n-1}(x)$$

APPENDIX B

Brief Introduction to Neural Networks

Neural networks are composed of simple elements operating in parallel. These elements are inspired by biological nervous systems. As in nature, the network function is determined largely by the connections between elements. Neural networks can perform a particular function by adjusting the values of the connections (weights) between elements during the training phase.

Generally, neural networks are adjusted or trained so that a particular input leads to a specific target output. The network is adjusted, based on a comparison of the output and the target, as shown in Fig. B.1, until the network output matches the target. Typically many such input/target pairs are required to train a network.

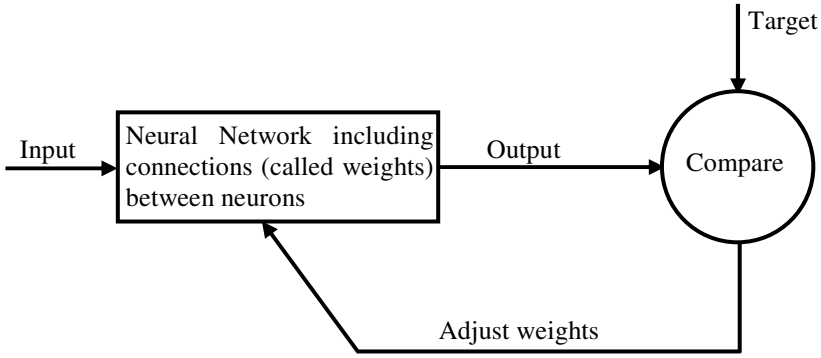

Fig. B.1 Simplified block diagram of neural network identification [73]

Nowadays neural networks can be trained to solve difficult problems that are not easy for conventional computers or human beings [73]. These problems cover pattern recognition, identification, classification, speech, vision, and control systems [73]. Further details are available from the "Neural Network Toolbox 5, User's Guide [73]" published by "The MathWorks".